Ferrierite-Catalysed Branching of Unsaturated Fatty Acids

Gekatalyseerde Vertakking van Onverzadigde Vetzuren door Ferrieriet

(met een samenvatting in het Nederlands)

Proefschrift

ter verkrijging van de graad van doctor aan de Universiteit Utrecht
op gezag van de rector magnificus, prof. dr. G.J. van der Zwaan,
ingevolge het besluit van het college voor promoties in het openbaar te verdedigen
op woensdag 9 december 2015 des ochtends te 10.30 uur

door

Sophie Claude Catherine Wiedemann-Tollington

geboren op 4 oktober 1966 te Parijs, Frankrijk

Promotor: Prof. dr. ir. B.M. Weckhuysen

Copromotor: Dr. P.C.A. Bruijnincx

This thesis was accomplished with financial support from CRODA.

“Nature uses only the longest threads to weave her patterns,

so that each small piece of her fabric

reveals the organization of the entire tapestry.”

Richard P. Feynman (1918 - 1988)

Cover drawing by François Tollington and cover design by Joseph Stewart

ISBN: 978-94-6233-165-5

Printed by: Gildeprint - The Netherlands

Table of Contents

Chapter 1

General Introduction

Abstract

Vegetable oils and animal fats are important and established raw materials for the production of chemicals and ingredients. From its origin more than 150 years ago, the oleochemical industry has grown in scale and diversity to become an important branch of the chemical industry. With increasing emphasis on renewable and sustainable industrial practices, oleochemistry has gained a new momentum as a means to develop alternatives to fossil-derived products. This Chapter reviews the role of catalysis and catalyst development in the production of isostearic acid, as an example of recent research in oleochemistry. Starting with a brief history of the oleochemical industry, we trace the development of isostearic acid and other branched fatty acids. The special properties of isostearic acid are illustrated through its use in applications inaccessible to commodity fatty acids. Finally, we present the latest developments in heterogeneous catalysis for isostearic acid production, and specifically the step-change in yields and selectivities recently achieved with ferrierite, a medium pore zeolite. The objective of this PhD Thesis is to gain a deeper understanding of the relationship between structure and performance of this special molecular sieve, in order to design more effective catalysts for the branching reaction, thereby opening up significant new markets and applications for renewable and sustainable ingredients.

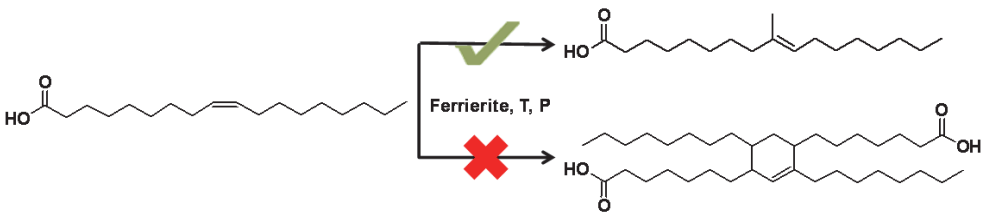

This Chapter is based on the manuscript: S.C.C. Wiedemann, P.C.A. Bruijnincx, B.M. Weckhuysen, in *Chemicals and Fuels from Bio-based Building Blocks* (eds. F. Cavani, F. Basile, S. Albonetti, A. Gandini) Wiley-VCH, Weinheim, accepted for publication.

1.1. World Production of Fats and Oils

The total world production of the major oils and fats in 2014 is estimated at around 207 million metric tonnes [1-2], of which palm, soybean and rapeseed together account for two-thirds (**Figure 1.1**). Animal fats (tallow, lard, butter and fish) contribute around 12.5% of the total, and speciality vegetable oils such as corn, linseed and castor oil, constitute 2.6%. The annual growth rate in production of the major vegetable oils, over the period 2010 to 2014, is around 4.2%.

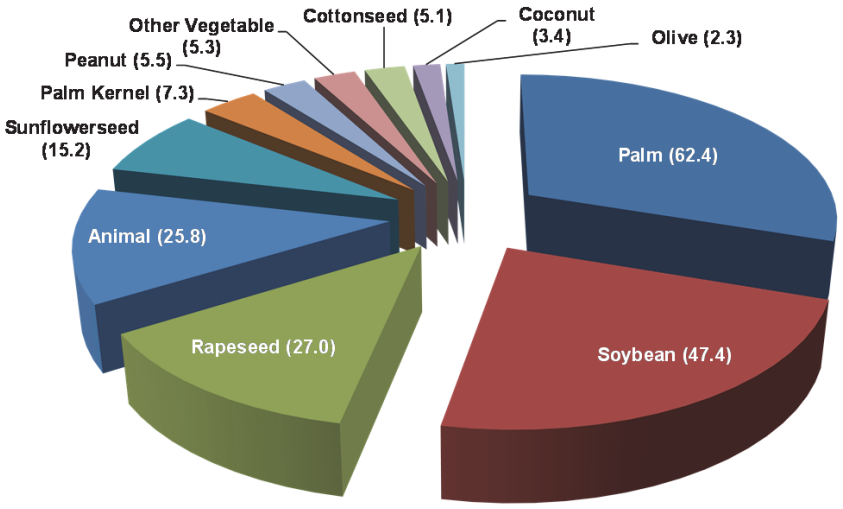

Figure 1.1: World production of major vegetable oils and fats in 2014 (million metric tonnes) [1,2].

In 2011, it was estimated that around 70-75% of the global production of oils and fats was consumed in human nutrition, with the remainder going into animal feed, biofuels and oleochemicals [3]. In recent years, fuel uses, biodiesel production in particular, and co-generation in power stations have increased the non-food demand for vegetable oils. Their large-scale use for fuel and energy is, however, generally uneconomic in the absence of financial incentives. The on-going debate on the use of food-grade vegetable oils in both industrial applications and for fuels production has an impact on the assessment of the net environmental and sustainability benefits of (bio-based) raw material choices in these sectors. The focal point of these discussions has been biodiesel and power generation since, compared to chemical and industrial uses, these have the potential to consume vast amounts of natural resources. A dramatic illustration of the potential problems was seen in 2006-2007, when riots in Mexico over a growing shortage of the food staple corn tortillas,

were blamed on the rapidly rising demand for corn ethanol created by the USA biofuels industry [4].

Recognition that food-grade vegetable oils alone cannot economically or practically meet a significant part of the demand for vehicle fuels has led to research into second and third generation biofuels based on abundant alternative feedstocks, such as lignocellulosic biomass, and municipal and agricultural waste streams. Biodiesel producers have also adapted their processes to handle tallow, used cooking oil, yellow greases and other lipid streams not suitable for human consumption. Alternative lipid sources such as algae are also under intense investigation [5], both for fuels and chemicals production.

1.2. Biorefining and Related Concepts

The use of natural and agricultural feedstocks for the production of chemicals has grown rapidly in recent years, and has led to the development of integrated “bio-refinery” concepts [6] as a way to achieve the scale and economics to compete with current mineral and petrochemical routes. A parallel strategy has been to adapt existing mineral oil refinery infrastructure, so that the bio-based feedstocks can be used directly, or with limited modification, in the downstream refinery operations. The development of supporting technologies, and the relative prices of mineral sources and agricultural commodities, will determine the rate at which this transformation occurs. A perspective on opportunities for biobased chemicals production in the Port of Rotterdam, for instance, estimated that 10-15% of the fossil oil-based bulk chemicals could be substituted by bio-based equivalents within 10 years [7].

Sugars, starches, and other carbohydrates can be converted to small molecules with high functionality, making them good starting points for the production of bio-based monomers and chemicals. Some commercial examples of biobased chemical production include (poly-)ethylene from sugar cane ethanol (Braskem [8]), (poly-)lactic acid from corn sugar (NatureWorks [9]), 1,3-propanediol from fermentation of corn syrup (Dupont [10]), succinic acid from fermentation of various sugars (Bioamber [11]) and methanol from glycerol and biogas (BioMCN [12]). Economically feasible alternative feedstocks are available for glycols, iso-propanol, acetone and methyl ethyl ketone, and production processes already exist or are in advanced stages of development [7].

By contrast, oils and fats have long carbon chains and limited functionality, making them more suited to the production of hydrocarbon-rich chemicals and products. The already well-established oleochemical industry deals with such conversions and can be considered as biorefineries, in which crude vegetable oils and animal fats are used as raw materials for a diverse range of chemicals [13]; indeed, the origins of the industry can be traced back to the French scientist Michel

Eugene Chevreul (1786-1889), following the publication of his pioneering research *Recherches chimiques sur les corps gras d'origine animale* in 1823 [14]. The sector has continued to develop, however, and current lipid research in Europe focuses mainly on functionalisation of vegetable oils and their derivatives, especially to the double bond, for the production of speciality chemicals and monomers. Enzymatic and fermentation processes are also developing alongside more traditional chemical routes [15-22]. Furthermore, developments in crop breeding technology have a growing importance in industrial oleochemistry, opening up the possibility for new and improved oilseed varieties with more tailored compositions, in an economically viable way [23]; previously, oleochemical feedstocks were intrinsically linked to food production, and were rarely developed solely for the production of chemicals and industrial products.

The renaissance in oleochemistry is not confined to academia, and important industrial developments are notable in the last decade: In the USA, Elevance Renewable Sciences [24] has pioneered the use of metathesis to produce a range of speciality chemicals, ingredients and feedstocks based on vegetable oils, many of which are novel. In Europe, Novamont [25] is combining both oleochemistry and carbohydrate chemistry in the development of biodegradable polymers for packaging materials, within a broad and highly integrated biorefinery concept; in this example, the unsaturated vegetable oils are subjected to a catalysed oxidative cleavage reaction in the presence of hydrogen peroxide, forming mono- and di-functional acids, which can be considered the basic (lipid-derived) platform chemicals.

In summary, the future of oleochemistry looks bright; in addition to growth of the traditional oleochemical products, driven in part by improving economics versus mineral oil-based chemicals, developments in raw materials, process technologies and in the combination with other plant-based materials promise to further expand the utilisation of oils and fats in industrial products.

1.3. Sustainability of Oils and Fats for Industrial Applications

In 2005, production of palm oil overtook soybean oil to gain pole position as the major vegetable oil source. In 2014 palm accounted for 62 million metric tonnes, versus 47 million tonnes for soybean oil. The rapid rise of palm oil production can be attributed to both economic and agronomic factors; palm oil yields (including the palm kernel oil) are around 5 metric tonnes/hectare/year (predicted to rise in the short term to more than 6 metric tonnes/hectare/year), compared to 0.7 for rapeseed and 0.4 for soybean [26] (In this comparison, it is important to add that soybeans contain only 20% of oil, and are grown primarily for their protein-rich meal). Palm oil is therefore the most efficient of the major vegetable oil crops in terms of land use.

This rapid growth has come with an environmental price tag; unchecked deforestation, destruction of natural habitats (e.g. of the orang-utan), and air pollution from burning of rain forests are major concerns in the palm oil industry. However, due to the work of the certification body RSPO (Round Table on Sustainable Palm Oil [27]) and the intervention of activist groups such as Greenpeace, there is a strong momentum in the European oil and fat industry towards the development of sustainable palm oil supply chains. Major multinational food producers, such as Unilever, Nestlé and P&G, are committed to sourcing palm oil from sustainable production sites, allowing the oil to be traced back to the individual mills. With this development, and well-publicised commitments from the multinationals, the primacy of palm in the oils and fats industry looks assured for years to come.

Several Malaysian and Indonesian palm producers have purchased European oleochemical companies in recent years, and others have set up distribution networks to supply the European market. As a result, imported palm streams have, to a large extent, displaced animal fats as the key oleochemical raw material. These vertically integrated producers are now moving further down the supply chain into the production of fatty alcohols, speciality chemicals and surfactants [28]. This has parallels with the growth of the petrochemical industry during the post-war years, in which oil producers moved downstream to convert the crude oil fractions into value-added chemicals and products, mitigating the volatility in oil price and helping to stabilise profits.

Producers of other major oil crops are developing their own criteria for sustainability relevant for the conditions and geographies where they are grown: schemes such as the German RedCert certification scheme [29] and ISCC (International Sustainability and Carbon Certification [30]) have been set up to support the development and monitoring of sustainable supply chains. Imported crude vegetable oils, such as soybean and canola, have additional supply chain complexities to meet the consumer demand in Europe for traceable non-GM (Genetically Modified) oils. Although current EU rules allow genetically modified crops to be grown anywhere within the European Union after approval by the European Food and Safety Authority (EFSA), and the oils of GM crops can be imported for industrial *and* food use, consumer-related markets may demand a non-GM option.

Both fuel and industrial producers target by-products from vegetable oil refining as raw materials; acid oils, fatty acid distillates and similar. However, these streams have a limited availability. They are typically about 5% of the total vegetable oil refinery output, and there are established applications in oleochemicals, animal feed and others with which any new use must compete. The reality for vegetable oil refining is that very little of the output is a genuine “waste stream”, when that is defined as a stream with zero or negative value - indeed some by-products have a higher value than the incoming crude oil, and thus positively contribute to the economics of the refinery. By-products are generally indexed in value to the crude

vegetable oil, which they may substitute when the difference in price is sufficient to overcome the extra costs to purify or process them further. Tall oil provides an interesting example of such a lipid by-product and is obtained from the Kraft or sulphate process for paper pulp production from pine wood. It is used exclusively for industrial purposes, and consists of a complex mixture of about 50% fatty acids, 40% rosin acids and 10% unsaponifiable fraction, which are separately purified and sold in a wide range of applications [31].

The use of oils and fats for industrial applications has thus been growing steadily over recent years, at a faster rate than in human nutrition. Furthermore, vegetable oils experience a growing share of the industrial and chemicals sector through substitution of traditionally mineral oil-based chemicals and products, as a sustainable source of hydrocarbon-rich feedstock.

The development of green chemistry and biorefinery concepts also give a new momentum to the field of oleochemistry. In this Chapter, we give a short introduction to the modern oleochemical industry, and illustrate the renewed interest in oils and fats chemistry with recent research in the catalytic isomerisation of linear fatty acids to branched acids - 'isostearic acid'. The history of isostearic acid production, and current routes to branched fatty acids (natural and fossil-derived), are discussed. The special properties of isostearic acid are illustrated through its use in applications and processes inaccessible to conventional fatty acids. Finally, the latest developments in zeolite catalysis for its selective manufacture are presented.

1.4. Fatty Acids

Whereas food and food production uses predominantly refined oils and fats, fatty acids are the major raw materials for the production of chemicals and industrial products (excluding direct fuel and biodiesel uses). World consumption and production of fatty acids in 2011 was estimated at 6.0 million tonnes (excluding production of fatty alcohols), expected to rise to 7.0 million tonnes by 2016. Western Europe consumes 1.5 million tonnes (including 170 thousand tonnes of tall oil fatty acids), but produces only 0.9 million tonnes, the balance being mainly palm-based import streams from South-East Asia [32]. Soaps, chemicals, surfactants, lubricants and coatings are some of the important applications of fatty acids; in general, their growth follows GDP growth in the region of consumption, reflecting the broad range of end-use industries.

Several processes are described for the hydrolysis ("splitting") of fats and oils into fatty acids and glycerol [33], including enzymatic splitting using lipases, but the dominant commercial process is high-pressure continuous splitting, known as the Colgate-Emery Process; water is contacted in counter-current flow with the oil or fat at around 250 °C and 50 bar pressure, in a mass ratio of ~ 2:1 fat:water, for

residence times of 1-3 h. The resulting hydrolysis of the oil or fat to fatty acids and glycerol is almost complete, with yields of up to 99% of the theoretical value. The dilute glycerol stream (10-15 wt%) can be purified and concentrated to 85-99 wt% by evaporation and distillation, and is used in many industrial, consumer and food products.

The crude fatty acids can then be subjected to a variety of downstream physical processes, such as:

- Distillation: The crude fatty acids are purified by distillation, to remove odour, colour, impurities and volatile components.
- Crystallisation: Saturated acids can be separated from unsaturated acids by crystallisation; using processes based on solvents, water/surfactants or simply cooling the fatty acids and pressing out the liquid fraction ("dry fractionation"). Commercial grade oleic acid is made by all of these methods, starting from fatty acids derived from tallow fat or palm oil.
- Fractionation: The term 'fractionation' in the oleochemical industry refers to a distillation process in which fatty acids are separated based on the boiling point of the different chain lengths. For example, coconut fatty acids, which consist of carbon chains from C8-C18, are fractionated into a C8-C10 fatty acid cut, which has a high value as a raw material for lubricants, cosmetics and food supplements, and a C12-C18 fatty acid cut which is suitable for soaps and detergents, for example.

In addition to physical processes, chemical modifications, such as hydrogenation, esterification, amidation, ethoxylation and polymerisation, are all currently performed on an industrial scale (**Figure 1.2**).

1.5. Polymerisation of Fatty Acids

1.5.1. Thermal Polymerisation

Thermal polymerisation of vegetable oils to produce bodied (thickened) oils was practiced from the beginning of the 20th century, but in the 1940's attention turned to polymerisation of unsaturated fatty acids and their monoesters for use in the manufacture of polymers [34]. The investigations of Bradley and Johnston [35] and subsequent publications showed that the main products from thermal polymerisation of fatty methyl esters were dimeric, and that the structures formed were determined mainly by the degree of unsaturation of the starting material. Johnston hydrogenated the resulting oligomers to polyhydric fatty alcohols using a copper chromite catalyst [36].

The un-catalysed thermal polymerisation of unsaturated fatty acids was performed industrially by Emery Industries in the USA from 1948. Tall Oil Fatty Acids

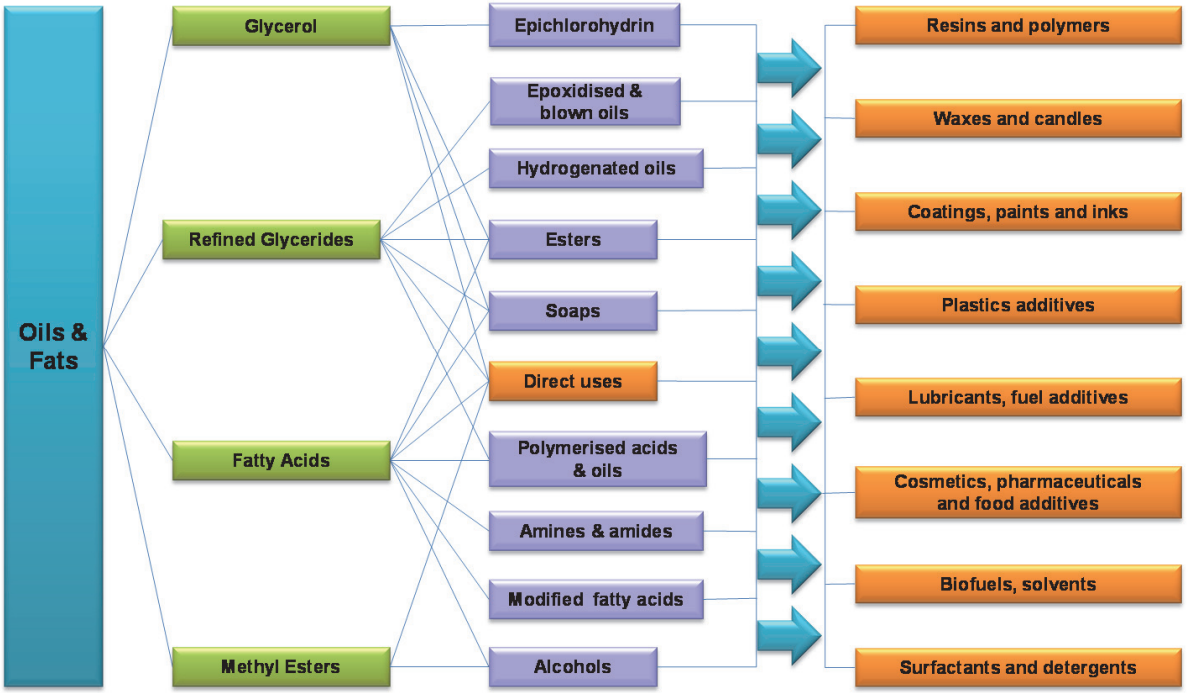

Figure 1.2: Schematic overview of the different conversion routes of oils and fats, and the applications of the oleochemicals derived from them; the "modified fatty acids" group includes e.g. conjugated, branched, hydroxylated and hydrogenated fatty acids.

(TOFA), a by-product of paper production, was the preferred feedstock, being highly unsaturated and therefore sufficiently reactive. The dimer acids were used in the production of polyamide resins for inks and adhesives. However, a process for polymerisation of unsaturated fatty acids, and their purification and use in making synthetic resins with improved properties, was described as early as 1935 [37].

1.5.2. Clay-catalysed Polymerisation

A step change in fatty acid polymerisation was achieved in 1957, when Barrett, Goebel and Myers developed a clay-catalysed process based on swelling Montmorillonite-rich smectite clays (**Scheme 1.1**) [38-39].

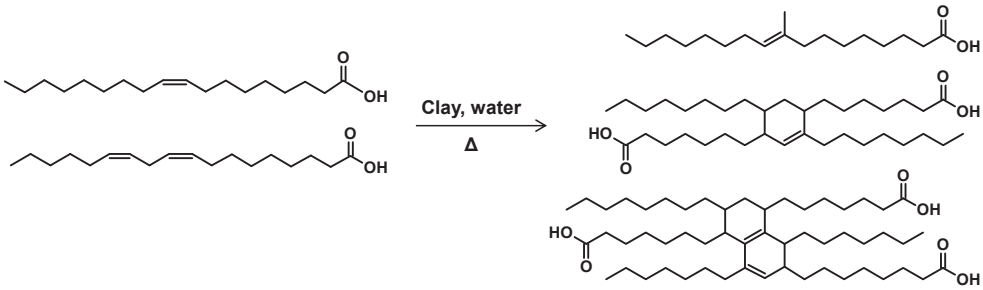

Scheme 1.1: Clay-catalysed polymerisation of commercial oleic acid, which contains mainly linoleic acid in addition to oleic acid. The reaction product is a complex mixture of branched (monomeric) oleic acid, C36 dimeric acids and C54 trimeric acids (typical structures are shown for each fraction; note that all fractions contain many isomers).

There are several key advantages of this process over thermal polymerisation, namely:

- Reaction times are shorter, and polymerisation temperatures lower.
- A wider range of feedstocks can be used; the clay-catalysed process can polymerise both polyunsaturated and predominantly monounsaturated fatty acids, such as tallow oleic acid.
- Better control is achieved over the ratio of dimeric to trimeric and higher fatty acids, with less dependence on the feedstock composition, due to the constrained reaction sites within the clay interlayers.
- Reaction products with lighter colours are achieved.

A further advantage of the catalysed process over the thermal one was the quality of the “monomer acids”, i.e. the non-polymerised fraction of the feed. In the thermal process, it consisted mainly of inert and unreacted fatty acids. However, a different monomer composition was observed in the clay-catalysed process; the monomeric fraction was not characterised in detail until the 1970’s, when McMahon identified it to be rich in methyl-branched saturated and unsaturated acids [40]. Haase, in the late 1980’s further characterised the hydrogenated branched fraction,

dividing it into mono- and multiple methyl-branched fatty acids [41]. These methyl-branched isomers, once purified and hydrogenated, became the commercial product now better known as isostearic acid.

In later improvements to the clay-catalysed process, certain alkali and alkaline-earth metal salts were shown to modify the clay interlayer distances and therefore provide a means to fine-tune the process towards higher polymerised fatty acid yields [42]. The modern process includes downstream modifications to the polymerised acids, such as hydrogenation, and further purification of the polymerised acids into dimeric (>98%) and trimeric (>80%) fractions. Derivatives, such as the diol and the diamine, are also commercially available.

1.6. Isostearic Acid

During the first decades of the clay-catalysed process, monomer acids were distilled off from the more valuable polymerised fraction and sold as cost-effective fatty acids for a range of applications. Later, the branched acids were hydrogenated and purified by solvent separation from the saturated straight-chain acids, to form what became known as isostearic acid, commonly abbreviated to ISAC (**Figure 1.3**). The first commercial ISAC was produced by Emery Industries, most likely based on the patented process described by Peters in 1957 [43].

It took time for the unique properties of isostearic acid to be fully appreciated, and for markets and applications to be developed; the relatively high production costs meant that performance benefits had to be demonstrated versus cheaper liquid fatty acids such as tallow oleic acid, rapeseed and tall oil fatty acids (themselves feedstocks for the isomerisation/polymerisation process). Furthermore, the process could be steered towards isostearic acid only to a limited extent, effectively linking isostearic acid production to polymerised fatty acid demand.

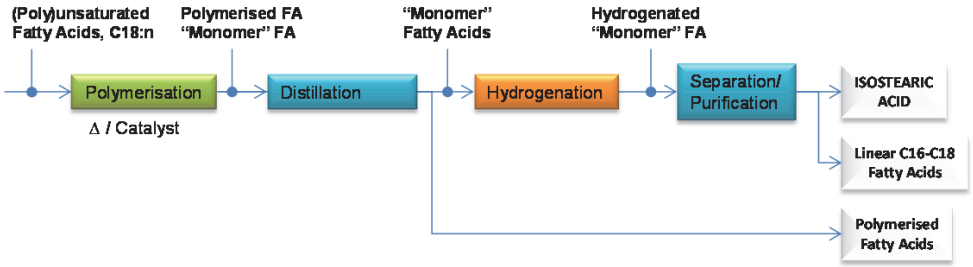

Figure 1.3: Current process for production of isostearic acid and polymerised fatty acids.

Despite these practical hurdles, the use of isostearic acid has grown steadily to the point where it can no longer be considered as a “co-product”, but as a high-

value functional oleochemical in its own right. The properties of isostearic acid are unique within the class of vegetable-derived fatty acids, allowing it to be used in applications where the technical performance of commodity fatty acids is insufficient, thus expanding the use of renewable resources in industrial and consumer applications.

1.7. Other Branched Chain Fatty Acids

1.7.1. Natural

C20-chain fatty acids with monomethyl branching at the iso- (ω-1) and anteiso- (ω-2) positions are the major constituents of fatty acids bonded to the surface of human hair and mammalian fur [44]. Similar branched structures are found in the milk fat of cows (and other mammals), constituting about 2% of the total fatty acids [45]. Iso- and anteiso-fatty acids with carbon chain lengths of C4-C15, in the form of wax esters, are major components of lanolin (purified sheep wool grease). Lanolin is a complex mix of lipid components, comprising esters and alcohols as the major fractions [46].

Branched chain fatty acids with methyl groups present on all positions along the alkyl chain have furthermore been isolated from bacteria, although only in minor amounts [47]. Dembitsky presented a comprehensive survey of naturally-occurring neo-acids (in this definition, “neo” refers to an alkyl chain terminating with a *tert*-butyl group, which differs from the definition for synthetic branched acids covered in section 1.7.2). The sources identified include plants, fungi, algae, marine invertebrates and microorganisms [48].

Although interesting, and in many cases serving important biological functions, most of these sources of natural branched lipids are not sufficiently abundant, accessible or concentrated to provide a viable feedstock source for industrial scale production. Lanolin is a notable exception; it is purified, separated into different fractions and further functionalised, and represents an important speciality lipid with applications in cosmetics, pharmaceuticals and industrial products.

1.7.2. Petrochemical

Most of the branched alcohols, acids and other branched derivatives are currently provided by the petrochemical industry, using ethylene, propylene, paraffin and (linear and branched) olefins as hydrocarbon sources. Coal and natural gas, current feedstocks for Fischer-Tropsch processes, can also be considered as raw materials.

Branched acids from petrochemical sources generally have shorter carbon chains and more and/or longer chain branching compared to isostearic acid. The main commercial route to synthetic branched acids is by carboxylation of olefins, using a modified oxo (carbonylation) process (**Scheme 1.2**). The olefins themselves are derived from a variety of petrochemical routes, and can be branched or linear, internal or terminal (alpha olefins). Alternatively, though less common, oxo alcohols can be oxidised under basic conditions to the corresponding acids.

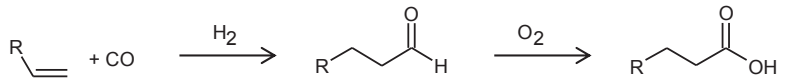

Scheme 1.2: Production of "oxo" acids using hydroformylation and oxidation; R is a branched or linear alkyl chain.

ExxonMobil's "neoacids" are produced commercially by a modified oxo process (Koch-Haaf) and are highly branched [49]. In the presence of a strong acid catalyst, the protonated olefins can rearrange to the more stable tertiary carbocation, which after carbonylation and addition of water yields a tertiary carboxylic acid group (**Scheme 1.3**). This "neo" structure results in high steric hindrance, which in turn imparts excellent thermal and hydrolytic stability to derivatives. Momentive Specialty Chemicals produce the Versatic™ acid 10 (Neodecanoic acid) by a similar route. The most important oxo-derived acids have total carbon C9-C11 chains, and are used as intermediates in the production of e.g. PVC stabilisers, organic peroxide initiators and metal salt-based catalysts.

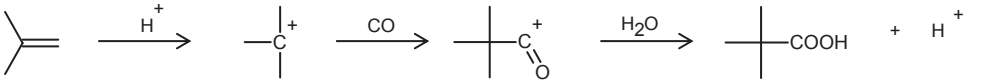

Scheme 1.3: Production of neopentanoic acid from isobutene via the two-stage Koch reaction.

Closer in structure to ISAC are the C16-C18 "isostearic" acids of Nissan Chemical (Fineoxocol® tradename), also derived from an oxo process via oxidation of the corresponding alcohol - a highly branched and a less branched alternative are offered. Due to the absence of linear fatty acids, and relatively highly branched structures, the pourpoints of these synthetic acids are very low (below -30 °C). The published applications of the Fineoxocol® acids are similar to those of ISAC.

Paraffin waxes (linear and branched) can be oxidised with air directly to fatty acids at about 110-130 °C in the presence of cobalt or manganese salts. This route was particularly prevalent in Russia and former Eastern Europe, where an ample supply of the wax was available from the petroleum refineries. However, it is a free radical oxidation which produces a complex mixture of products including linear and branched acids, esters, aldehydes and ketones, and isolation of the branched fatty

acids requires an expensive work-up process [50]. Production of fatty acids by this route is now of relatively minor importance.

Some specific branched-chain alcohols use similar synthetic routes to the acids, and can be considered alternatives to isostearyl alcohol, the hydrogenated derivative of ISAC, and an important personal care ingredient. Shell's Neodol® 67 process, developed for the detergent market in collaboration with Procter & Gamble, produces lightly branched C16-C17 fatty alcohols, structurally close to isostearyl alcohol (**Figure 1.4**). Notably, the process uses a medium pore zeolite with uni-dimensional channels of ~ 0.4-0.7 nm (hydrogen-form ferrierites being preferred) to isomerise linear internal olefins to predominantly (mono-) methyl-branched olefins [51], which are then selectively hydroformylated to the primary alcohol (**Figure 1.4**). The alcohols, when ethoxylated and/or sulphated, form detergent actives with excellent properties; advantages cited include excellent cold water solubility (despite the longer alkyl chain length compared to conventional detergent surfactants), good tolerance to calcium salts ("hard water"), acceptable biodegradability and superior surface activity [52].

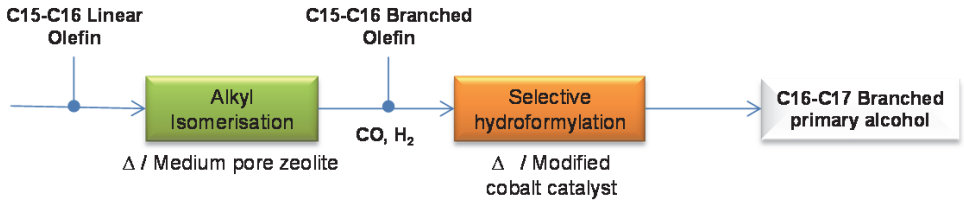

Figure 1.4: Production of C16-C17 branched primary alcohols (Neodol® 67) from C15-C16 linear olefins.

It is anticipated that the possible growth in Fischer-Tropsch synthesis processes will yield alternative sources of lightly-branched olefins from wax cracking, as potential raw material sources for the Neodol® 67-type products.

Guerbet alcohols are produced from linear alcohols at high temperature, and in the presence of a base and a hydrogen transfer catalyst (copper or Raney nickel). The four-step synthesis route involves oxidation to the aldehyde, aldol condensation, dehydration and finally hydrogenation to form the branched alcohol (**Scheme 1.4**). The branching is exclusively on the beta position, and of chain length smaller by two carbons than the parent alcohol. This structure gives a significant depression in melting point, making them useful fatty materials for cosmetics and homecare products, a.o. [53]. The corresponding acids can be formed by oxidation of the aldehyde; one of the most important commercial synthetic acids, 2-ethylhexanoic acid, is produced in this way starting from 1-butanal.

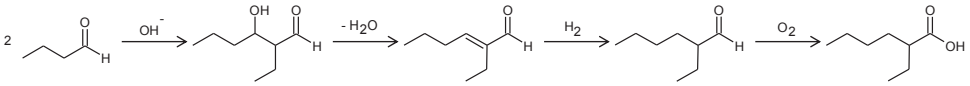

Scheme 1.4: Production of 2-ethylhexanoic acid via the aldol condensation of butanal.

Biermann et al. have reviewed a range of (mainly) preparative synthesis routes to branched acids, starting from natural (linear) unsaturated fatty acids and methyl esters [54]. Radical additions, Friedel-Crafts alkylations, transition metal-catalysed additions and zeolite-induced skeletal isomerisation are covered in detail.

1.8. Properties of Isostearic Acid

Kinsman has collated and reviewed the physical properties of isostearic acid and other branched-chain acids [55]. This work is further expanded in a book chapter dedicated to branched fatty acids, in [56]. More recently, Ngo has measured a number of important physical properties of ISAC (and some of its esters), produced by a zeolite-catalysed route [57].

In most cases, isostearic acid exhibits properties, which combine the “best” features of oleic acid (*cis*-9-octadecenoic acid, OA) and stearic acid (octadecanoic acid). Some of the key attributes for industrial and consumer applications are discussed below.

1.8.1. Thermal and Oxidative Stability

ISAC is comparable in thermal and oxidative stability to stearic acid: this makes it well-suited to applications where long shelf-life and/or elevated usage temperatures are required. Data from the Kinsman work [55] is illustrative; in an oxygen absorption test performed at 60 °C, ISAC was stable up to 100 days, while commercial grade oleic acid only reached 1-7 days and technical grade stearic acid (with a residual unsaturation given by the iodine value of 5 g I_2/100 g) 25 days. Similarly, Ngo compared the oxidative stability of the methyl ester of purified ISAC with soybean oil methyl esters at 110 °C; the ISAC fatty acid methyl esters were 18 times more stable relative to the soybean fatty acid methyl esters by this test [57].

1.8.2. Low-temperature Liquidity

Liquidity at low temperature is a required property for fatty acid-based ingredients used in outdoor and refrigerated environments, especially in markets such as lubricants. More generally, a liquid fatty acid is easier to store, transport, process and formulate.

When purified to remove most of the linear saturated fatty acids, ISAC has good cold-flow properties, comparable to oleic acid; this is carried over into derivatives such as esters. The branching pattern of oleic acid isomerised using a zeolite, shows a skewed distribution around the midpoint [58]. This midpoint methyl-branching gives the maximum melting point depression, as confirmed by the study of Cason on C19-chain mono-methyl-branched fatty acids in which the branching position was systematically varied [59]; it is, however, the complex isomeric mix which accounts for the liquidity in commercial ISAC, since the study of Cason indicates that the pure isomers are all solid at room temperature.

An additional feature in commercial ISAC is the presence of multiple(methyl)branched species, which when purified by solvent crystallisation reach melting points as low as -54 °C [41]; by comparison, a eutectic mixture of (unsaturated) oleic and linoleic fatty acids has a melting point of about -10 °C [60].

1.8.3. Solubility

Derivatives of isostearic acid show improved solubility across a range of solvent types and polarities compared to the analogous stearic acid derivatives, which makes them easier to formulate and apply in industrial and consumer products. For example, the isostearate salts of zinc and lead were tested in 12 solvents of broadly different polarities, and were shown to be compatible with more solvents than either the oleate or stearate analogues [61]. In aqueous solution, the sodium soap of isostearic acid has a solubility of ~15 wt% in water at room temperature, comparable to sodium oleate, whereas sodium stearate is only soluble to ~1 wt% [61].

1.8.4. Biodegradability

In general, the inclusion of an alkyl branch in the hydrocarbon chain of a fatty molecule hinders its biodegradability; hence it is important to establish the impact, when ISAC and its derivatives are to be developed for use in environmentally sensitive applications.

Commercial isostearic acid has been tested for biodegradability according to OECD Guideline 301 B (Ready Biodegradability: CO_2 Evolution Test), and the results published on the website of the European Chemicals Agency [62] in support of REACH registration. Isostearic acid is confirmed to be “readily biodegradable” in this test, meeting the criteria of at least 60% conversion to CO_2 in a 28 day period.

Ngo has studied the biodegradation of isostearic acid produced by the ferrierite-catalysed isomerisation of high-purity oleic acid [63]. Three strains of *Pseudomonas* bacteria were selected, and all were able to metabolise the ISAC to a good extent, while new linear and/or branched-chain fatty acids were formed as products of partial degradation. The results are not directly comparable to the OECD

301B test, but confirm that isostearic acid can be readily utilised by bacteria as a carbon source, and is thus suitable for use in environmentally sensitive applications where losses and spills could occur.

For a more comprehensive review of the physical properties of natural and synthetic branched acids, the reader is directed to the review of Kinsman [55].

1.9. Applications of Isostearic Acid

Due to the (currently) relatively high costs of production and purification, ISAC is used in more demanding applications where the properties listed above are particularly valued. Lubricants, cosmetics/personal care ingredients and a wide range of industrial applications are important markets for ISAC, and these are discussed in more detail below (**Table 1.1**).

Table 1.1: Overview of the major markets and applications of ISAC and its derivatives, based on patent and published literature.

Markets	Applications	Key properties	Ref.
Lubricants	Metal-working, Gear oils, 2-/4-stroke engines Friction modifiers	Lubricity Liquidity Oxidative & thermal stability Low toxicity Biodegradability Dispersing	[66-74]
Cosmetic & personal care	Skin & hair care Colour cosmetic Sun cream Toiletries	Liquidity Odour & colour stability Skin feel, substantivity Water resistance Dispersing & emulsifying	[75-82]
Industrials	Textile softening	Rewettability	[83]
	Metal paste	Dispersing	[84]
	Paper sizing	Water resistance Lubricity	[89]

1.9.1. Lubricants

Currently, bio-lubricants constitute only a minor part of the total lubricant market, estimated as approximately 3% in the EU in 2012 [64]), although with a moderately positive legislative climate this share is expected to double by 2020. Wagner has stated that vegetable-derived lubricants have the *technical* potential to substitute over

90% of the mineral oil-based lubricants currently in use [65]. However, the considerable cost gap between mineral and vegetable oils must reduce further to encourage switching, and some inherent functional weaknesses need to be overcome. ISAC has great potential here, addressing key concerns around oxidative/thermal stability and low-temperature properties, which are commonly cited as stumbling blocks to further development of vegetable-based lubricants. Esters of ISAC are used as components of base oils for the production of synthetic lubricants and greases. In addition to their inherent low toxicity and good biodegradability [66], they exhibit high flashpoints, low pour points and good application properties. Important base oils include polyol ISAC esters based on pentaerythritol [67], trimethylol propane (TMP) [68] and neopentyl glycol (NPG). In some cases, the purified ISAC can be substituted by the monomer acids, when the application is tolerant of the slightly inferior low-temperature properties and stability.

Important applications within the broad classification of lubricants include metal-working fluids, industrial gear oils [69], 2- and 4-stroke automotive engines [70], hydraulic fluids [71], greases and textile lubricants. ISAC-derived amines and amides are also used as friction modifiers in transmission fluids [72-73]). For a recent survey of synthetic lubricant esters, see [74].

1.9.2. Cosmetics and Personal Care

ISAC and derivatives are important raw materials in the production of a.o. emollients and emulsifiers for cosmetic and skin care products. ISAC esters have similar physical properties to those of unsaturated fatty acids like oleic acid, but with the important benefit of superior odour and colour stability (and sometimes additional desirable sensory properties). ISAC can form permeable lipid films on the skin, increasing moisture transport and supporting the penetration of other ingredients through the *stratum corneum* -making them useful carriers for active ingredients [75].

ISAC esters of light alcohols give a light emolliency, with no oiliness or stickiness. The capryl ester is reported to give similar sensory properties to cyclomethicones (cyclic polydimethylsiloxane polymers currently used in skincare and haircare products as a carrier and delivery system for active ingredients [76]). ISAC can be partially esterified to produce non-ionic emulsifiers (e.g. polyglycerol, sorbitan or polyethylene glycol esters). When fully esterified, they are emollient oils; depending on the structure and functionality of the alcohol/polyol used, a wide range of physical and sensory properties can be achieved, from light oils (e.g. isopropyl isostearate) to viscous, highly skin substantive and water-repellent liquid waxes (e.g. pentaerythritol tetraisostearate).

ISAC and derivatives are used to disperse metal oxides in sunscreen products [77, 78], and inorganic pigments in colour cosmetics [79]. High molecular weight

isostearate esters based on e.g. oligomers of glycerol and pentaerythritol, are highly substantive, hydrolysis-resistant, and function to enhance gloss in e.g. lipsticks [80].

ISAC and derivatives are also used in hair conditioners, shampoos [81] and colourants, hand soaps, shaving products, deodorants and nail polish removers. Thickening agents based on ISAC have also been reported (e.g. polyoxyalkylene ethers of glycerin or 1,2-propanediol, esterified with isostearic acid [82]).

1.9.3. Other Industrials

ISAC and derivatives are used in a very broad range of other markets and applications, including (production of) textiles, paper, plastics additives, surfactants and detergents. Some examples are given below as an illustration of their scope of application.

Cationic surfactants, in particular quaternary nitrogen-containing ones, such as Evonik's Rewoquat® W 325 PG [bis-(isostearic acid amidoethyl)-N-polyethoxy-N-methyl ammonium methosulfate] are used in industrial textile softening [83]. The isostearic hydrophobe gives superior re-wetting of certain fabrics, i.e. it conditions and softens the fabric without excessively water-proofing it. This property has a clear analogy with the use of isostearic derivatives in topical skin care products, which permit the formation of protective yet water-permeable films.

ISAC provides a functional coating for metal and mineral particles used as fillers or pigments in polymer-based products such as plastics and paints; the carboxylic acid group binds to the particle surface, while the fatty chain allows solubilisation in the polymer matrix; e.g. alumina (surface modification of alumina hydrate with liquid fatty acids [84]). In the form of organo-titanate esters, this compatibilising coating has broad application (inorganic-organic composites and methods of reacting the same with organo-titanium compounds [85]), improving dispersion of the inorganic particles leading to lower melt viscosity, higher filler loadings and improved physical/mechanical properties in polymer systems. ISAC also provides a de-dusting coating for aluminium powder, for use a.o. in aqueous slurry explosives [86].

In laundry detergents, formulations containing cationic ISAC derivatives impart anti-static properties to fabrics (isostearic acid, acrylamide cationic polymers [87], N-alkylisostearamides as antistatic agents [88]). Alkyl ketene dimers based on isostearic acid-rich fatty acids are used in the paper industry as sizing agents, with improved properties for ink-jet printing [89]. In PVC production, isostearate metal salts (such as zinc, calcium and tin) are components of liquid stabilizer packages, while esters of ISAC can be used as plasticizers. Polyamide ink resins using ISAC as chain stoppers are claimed to show reduced blooming [90].

1.10. Selective Routes to the Production of Isostearic Acid

As shown above, ISAC has unique properties within the general class of fatty acids, due to its lightly branched structure. These properties are exploited in a variety of more demanding markets and applications, where commodity liquid vegetable fatty acids are unsuitable or inferior. Its current commercial production is linked to that of polymerised fatty acids (**Scheme 1.1**). This has several disadvantages, which hinder its further development, namely:

- ISAC co-production with polymerised fatty acids requires a constant balancing of supply and demand; this limits in any case the supply growth rate to that of the polymer acids;
- Purification of ISAC requires multi-step separation processes, which makes the end product costly to produce;
- The clay-catalysed process offers limited scope to increase the yield of ISAC, and modifications to the process in this direction usually impact the quality of the polymerised acid fraction; and
- Synthetic routes to branched fatty acids exist, but they are based on non-sustainable petrochemical sources, and/or produce acids or alcohols with substantially different properties.

Therefore, there is a need for a more direct and cost-effective synthesis of ISAC, which would decouple supply from polymerised fatty acid production and allow its unique properties to be fully exploited.

1.10.1. Optimisation of the Clay-catalysed Process

As mentioned in section 1.5.2, the current commercial process for production of ISAC uses a swelling clay in which skeletal isomerisation of the unsaturated fatty acids competes with oligomerisation. For both products, the main reaction mechanism is believed to go via the same carbocation intermediate [91]. As a result, complete decoupling of these reactions cannot be achieved by optimisation of the process conditions alone, and the catalyst system must be modified.

Oligomerisation has been found to be favoured by swelling of the clay using water and/or cations (e.g. Li^{+}), with an increase in oligomer yields from 35 to 55 wt% [92]. Although Brønsted acid sites (tetrahedral sites with Al^{3+} substitution of Si^{4+}) were confirmed as active sites, high yields require the *simultaneous* presence of octahedral sites (e.g. substitution of Si^{4+} by Mg^{2+}); binding of the carboxylic groups to the latter is believed to prevent poisoning of the tetrahedral sites [93]. Conversely, addition of a small amount of Brønsted acid (e.g. phosphoric acid) as co-catalyst significantly increases yields of the isomerised monomeric fatty acids (from 30 to 50 wt%) [92].

1.10.2. Zeolite-catalysed Branching in the Petroleum Industry

The replacement of the clay catalyst by a zeolite holds considerable promise for the decoupling of the two competing pathways. Their shape-selective properties are well known in the refining and petrochemical industry [94-95] and have also been exploited for biomass conversion [96-97]. The limited space of their intracrystalline volume inhibits the transition state formation from bimolecular reactions, suppressing di- and oligomeric fatty acids. Another advantage of zeolites for the OA skeletal isomerisation is the ability to tailor their acidity, in terms of type (Brønsted/Lewis), density and strength [98].

Shape selectivity effects have been widely studied for the skeletal isomerisation of butene to isobutene catalysed by zeolites and molecular sieves [95, 99-101]. This reaction was heavily studied up to the nineties, in order to meet the expected increasing demand in isobutene for the production of methyl *tert*-butyl ether. Since the USA ban of this additive, the intermediate needs are restricted to the methacrylate, poly-isobutene and butyl rubber markets. High yields in isobutene require narrow-pore molecular sieves with 10-membered ring (MR) channels, such as MeAPO-11 [102], SAPO-11 [103-104], Theta-1 [105] and ZSM-22 (both TON, one-dimensional) [106], ZSM-23 (MTT, one-dimensional) [107] and ZSM-35 (FER) [108]. The three-dimensional 10-MR ZSM-5 (MFI) shows higher butene conversion but a much lower selectivity to isobutene; this is attributed to its larger void volume (from somewhat larger channels and their intersection) [107, 109-110]. On the other hand, the 10-MR channels (3.1 x 7.5 Å) of heulandite (HEU) are believed to be too narrow for isobutene diffusion [100]. The best overall performance (activity, selectivity and stability) is achieved with ferrierite; this zeolite has a pore structure, made from the perpendicular crossing of one-dimensional 10-MR channels (4.2 x 5.4 Å) with one-dimensional 8-MR channels (3.4 x 4.7 Å); its moderately strong acidity is also thought to contribute to the low level of oligomerisation and cracking reactions [99, 101]. Therefore, since its discovery by Shell, ferrierite has been widely adopted by industry for the isomerisation of small olefins (e.g. ISOMPLUS® technology from Lyondell/CDtech [111-112] and is commercially available (e.g. from Tosoh Corporation and Zeolyst international).

The Pt/zeolite-based hydro-isomerisation of long chain *n*-alkanes (> C7) for the upgrade of petroleum fractions to high-grades fuels and lubricants is another reaction of relevance, known for its specific shape selectivity [95, 112]. It has been the research focus of a number of groups, leading to a detailed understanding of the molecular mechanism [113-115]. High selectivity to branching requires an “ideal” bi-functional catalyst with an optimised ratio between Pt sites for dehydrogenation/hydrogenation reactions, and acid sites for the isomerisation [114, 116]. The formation of multiple-branched alkanes, precursors of cracking, is again limited by the use of one-dimensional narrow molecular sieves with 10-MR channels,

including SAPO-11, ZSM-22, ZSM-23. Conversely, significant cracking has been observed with zeolites with larger pores (Beta and USY) [117]. Besides the intermediate state selectivity, the use of the one-dimensional medium pore zeolites also results in a specific methyl branching pattern that varies as a function of the *n*-alkane chain length. Product diffusion shape selectivity has been invoked to explain this observation [118-120]. Alternatively, the specific branching pattern has also been attributed to pore mouth and key-lock catalysis, involving van der Waals interactions between the external surface and the long chain alkanes [121-123]. Similar results, although less marked, have been described for the hydro-isomerisation of *n*-paraffins in the liquid phase [124]. Latest developments in zeolite engineering to enhance the external surface (and the number of pore mouths) while preserving its acidity, have resulted in significant increase of the desired branched alkanes yields: for example, hierarchical zeolites obtained by desilication in alkaline medium followed by acid washing [125], as well as by demetallation [126], have recently been reported.

1.10.3. Zeolite-catalysed Branching of Fatty Acids

The examples listed above suggest that zeolites could also represent a promising route to selective production of branched unsaturated fatty acids (BUFA) in high yields, and have inspired several research groups to study the alkyl isomerisation of OA. Focus has initially been on molecular sieves with large-size channels, a choice motivated possibly because of the bulkiness of the BUFA compared to the isobutene and branched alkanes. Most of the information available is contained in patents, and BUFA yields are often difficult to compare due to the limited analytical information provided on product composition. For example, in some cases the chemical analysis data presented suggest significant purification. **Table 1.2** below summarises the key developments.

The first example of zeolite catalysis for OA conversion to BUFA, dates from 1997 [127]. The patent discloses the use of molecular sieves, such as protonated mordenite, with large-sized channels (12-MR, 6.5 x 7.0 Å) and linear pore structures. Reactions were carried out for 6 h at 280-300 °C with 4-8% catalyst loading. Addition of a small amount of water was shown to promote the conversion to BUFA, postulated to be due to the conversion of Lewis acid sites into Brønsted ones; this conclusion was drawn based on experiments using zeolite with Si/Al = 7.5 and Si/Al = 9.5.

On the contrary, calcination of the catalyst for 2 h at 600 °C led to a significant decrease in BUFA yields, confirming the key role of Brønsted acidity. A direct comparison with the clay-catalysed process demonstrated the superior selectivity of the protonated mordenite to monomeric acids, although the temperature used for the clay-catalysed reaction was lower (240 °C) and the solidification point characterising the zeolite-derived product differed significantly from commercial isostearic.

Table 1.2: Literature overview for the selective OA alkyl isomerisation in presence of zeolites and mesoporous materials.

Year	Type	Largest channels	Si/Al	Cat. (wt%)[a]	Reaction parameters	Catalytic testing	References
1997	Mordenite	12-MR (One-dim.)	7.5 9.5	8	Water 280-300 °C 6 h	BUFA yields > 60%; Better than with: clay, USY, ZSM-5	[127]
1997	Mordenite, Omega, L-Type	12-MR (One-dim.)	10	2.5	No water 265 °C 4 h	BUFA yields > 50% with flat crystals	[128-129]
2004	Beta Beta/ Pd or Pt	12-MR (Three-dim.)	12.5	10	No water 250 °C 5 h	OA conversion up to 50%; range of feedstocks; large fraction of multiple branching	[132-133]
2007	Beta	12-MR (Three-dim.)	13.5[b]	3	Water 250 °C 4 h	Conversion > 65%	[134]
2004	MAS-5	Meso-porous	25	10	No water 250 °C 5 h	Conversion > 60%; More efficient filtration; Slower deactivation	[135-136]
2007	Ferrierite	10-MR (Two-dim.)	8.5 27.5	2.5	Water 250 °C 6 h	Conversion > 95%; BUFA yields > 70%	[59, 137]
2012	Ferrierite/ TPP	10-MR (Two-dim.)	8.5	5	Water 280 °C 6 h	Conversion > 95%; BUFA yields > 75%; Lower oligomer yields	[137]
2014	Ferrierite	10-MR (Two-dim.)	8.5	5	Water 260 °C 4 h	10 recycles with: Conversion: 90-99%; BUFA yields: 75-85%	[139]

a: Relative to the feedstock.
b: Calcination at 450 instead of 550 °C.

Zeolite USY (Si/Al = 3), and to a minor extent ZSM-5 (Si/Al = 7), gave lower BUFA yields under similar conditions, confirming the importance of the microstructure and/or its acidity.

The same year, the potential of one-dimensional zeolites with linear large-sized channels (mordenite, omega and L-type) was confirmed by Roberts et al. [128-129]. Reactions were carried out for 4 h with 1-5% catalyst loading without addition of water. Optimum temperature around 265 °C and minimum Si/Al ratios of 10 were disclosed. Further improvements were obtained by crystal morphology manipulation, such as flat-plate crystals with the pores along the shortest dimension (L/D > 10, where L is the crystallite diameter and D is the crystallite thickness); for both mordenite (hexagonal discs) and L-type zeolites (circular plates), BUFA yields above 50 wt% could be reached with 2.5% loading.

In 2004, large pore zeolites (> 6 Å) were claimed to promote OA conversion to BUFA [130-131]. Reactions were carried out for 5 h at 250 °C with a high catalyst loading (10%). OA conversions of (up to) 50% were disclosed using Beta zeolite (three-dimensional, BEA) with Si/Al = 12.5. The oligomeric fraction is not reported in the product composition and the comparative example is based on mordenite with very high acidity (Si/Al below 10), so the claim cannot be deduced based on the data provided. The patent discloses the application of H-Beta zeolite for a wide range of unsaturated fatty acid sources (a.o. tallow oleic acid, erucic acid), while up to this point most studies used only high purity oleic acid. Zhang et al. also described a “one-pot” process of isomerisation followed by hydrogenation, catalysed by Pt or Pd supported on Beta. In addition, intermediate state shape selectivity was used to explain the observed branching pattern [132-133]: The large pore size results in both ethyl- and methyl-branched fatty acids, while medium pore size limits the branching to methyl. Compared to the clay-catalysed process, the large pore zeolites increase the fraction of multiple-branched fatty acids; quaternary carbon atoms, indicative of geminal, doubly alkyl-substituted ISAC, were not detected in the analysis by ^{13}C NMR, however.

OA conversion to BUFA in the presence of Beta zeolite could again be improved by the addition of a small amount of water (as earlier with the mordenite), and by optimising the zeolite calcination temperature [134]. A compromise between template removal and preservation of the strong Brønsted sites was found at 450 °C instead of 550 °C (conversion of 67% versus 46% after 5 h at 250 °C for Si/Al = 13.5 and a loading of 3%).

Zhang at al. also disclosed the use of mesoporous sieves (MAS-5, Si/Al = 25) for OA conversion to BUFA [135-136]. After 5 h reaction at 250 °C with 10% catalyst loading, a conversion of up to 60% was achieved. Such structures are believed to further enhance acid site accessibility to the large fatty acid molecules. Again, no details of the oligomeric fraction are reported in the product composition, and its potential increase due to the larger external surface cannot be ruled out. On the other

hand, filtration of such mesoporous sieves from the reaction mixture left little residue in the spent catalyst, and deactivation was less marked (OA conversion only decreased from 60 to 44% upon re-use after filtration, acetone washing and drying).

1.10.4. Ferrierite - A breakthrough in Fatty Acid Isomerisation

In 2007, Ngo et al. reported a step change in both OA conversion (> 95%) and selectivity towards BUFA (> 70%) with protonated zeolites from the ferrierite group [58]. Two commercial ferrierite catalysts ex Tosoh (Si/Al = 8.5, H-Fer-K) and Zeolyst (Si/Al = 27.5, H-Fer-NH_4) were used, the former activated by HCl exchange and the later by calcination at 500 °C. A number of co-catalysts were tested, of which water was found to be the most effective. Reactions were carried out for 6 h at 250 °C with a catalyst loading of 2.5-5%. Comparative examples with clay (2.5 h at 250 °C with a 4.3% loading) and protonated mordenite (Si/Al ~ 9, 6 h at 250 °C with a 2.5% loading) clearly confirmed the superiority of ferrierite. This zeolite, however, was found to suffer from deactivation and could not be reused directly.

Later, the ferrierite selectivity towards the monomeric fraction was further improved by the addition of a small amount of a bulky Lewis base as promoter, e.g. 2.5% (relative to the catalyst) of triphenylphosphine (TPP) [137]. It is believed that such a base interacts with the non-shape-selective acidic sites on the external zeolite surface. However, this method did not allow the complete suppression of residual oligomers, and significantly slowed down the reaction; the temperature was increased to 280 °C to compensate for this effect. TPP also promoted reaction selectivity with mordenite.

Picolinyl esters of the hydrogenated BUFA were analysed by GC x GC-TOF-MS. Ngo et al. reported that ferrierite and mordenite gave different branching fingerprints (both type and number of isomers differed). These results are in line with earlier findings of Zhang et al. [132-133]. Surprisingly, when analysing the picolinyl esters of the BUFA, only 30 isomers were counted in the distillate from ferrierite catalysis [138]; this is hardly higher than the 28 species found after hydrogenation [137], suggesting a preferred configuration for the unsaturations.

Recently, Ngo et al. proposed a series of protocols to regenerate the spent ferrierite, allowing for 10 to 20 times re-use. After an initial solvent washing, the first method involves a laborious acid treatment that consumes a large amount of water [137]. The second procedure alternates a number of heat (110 to 260 °C) and acid treatments (after 5-6 cycles) [139]. The focus of this study was on regeneration and no details were reported on the deactivation mechanisms themselves.

The examples described above clearly show that zeolites hold considerable promise for the selective manufacture of ISAC. The patent literature bears witness to the research efforts of the oleochemical industry in searching for the ideal microstructure. Inspired from the development of zeolites in the refining and

petrochemical industry in the 1990's, catalytic testing initially targeted the microstructures with medium to large channels. Ferrierite, extensively researched for its superior activity and stability in the isomerisation of butene to isobutene, has only recently been tested in the skeletal isomerisation of OA. In this reaction, it has been shown to give complete conversion, and high selectivity to the BUFA, representing a major improvement over previously-tested zeolites. However, the mechanisms and origins of the deactivation are not well understood, and although the key role of the microstructure has been highlighted, there is no clear understanding of the role of acidity.

1.11. Ferrierite - Shape Selectivity and Acidity

Ferrierite, as all zeolites, is a microporous crystalline material with an alumino-silicate framework of the orthorhombic type [140-141]. This zeolite, with structure code FER, is characterised by a two-dimensional channel system. Based on its largest channel made of 10 T atoms (4.2 x 5.4 Å), it belongs to the medium-pore zeolites. The 10-membered (10-MR) channels [001] perpendicularly cross 8-MR channels ([010], 3.5 x 4.8 Å); the latter also includes spherical cavities of 6 to 7 Å in size with 6- and 5-MR windows. This is illustrated in **Figure 1.5**.

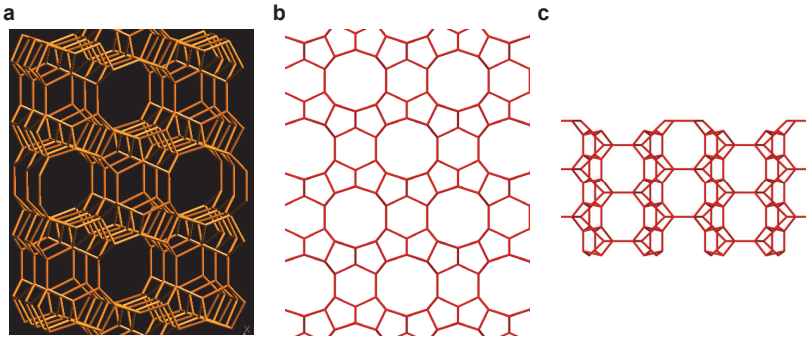

Figure 1.5: (a) Framework structure of zeolite FER [142] with its pore system viewed along the **(b)** [001] and the **(c)** [010] directions.

This specific micropore system confers to ferrierite a number of catalytic properties. As mentioned previously, transition-state shape selectivity plays a key role in the skeletal isomerisation of OA, by constraining the carbocation and inhibiting oligomerisation. Bulky multiple-branched fatty acids, prone to cracking, are also suppressed by the same space limitation.

However, the bulky fatty acid molecules have limited access to the micropore volume, especially to the smaller 8-MR channels. The external surface is thus

expected to significantly influence their interaction with the catalyst material [95, 143], and the product composition could be controlled by other types of selectivities [95]:

- Reactant selectivity: Milder external acid sites can catalyse geometrical isomerisation of the double bond in OA to elaidic acid (*trans*-9-octadecenoic acid, EA), which has a smaller kinetic diameter and may preferentially enter the micropores. Similar discrimination between the geometrical isomers has already been reported for selective hydrogenation of the methyl esters of OA and EA by Pt/ZSM5 [144].
- Product selectivity: The product will not readily undergo successive branching reactions, as re-entry into the catalyst pores is severely hindered by the alkyl branch.
- Pore mouth and key-lock catalysis: These models have been introduced to explain the product distribution observed for the Pt/zeolite-based hydro-isomerisation of long chain n-alkanes (> C7) mentioned in 10.2. The pore mouth catalysis assumes entry of the molecule to optimize the van der Waals interaction, followed by branching at the pore mouth (and thus close to the chain end) to enable desorption. In the key-lock configuration, the two ends of the long carbon chain enter two adjacent pores, resulting in a bimodal distribution of the branching. These models cannot strictly apply, as the position of the double bond in the oleic acid molecule determines the initial location of the carbocation. However, the asymmetry of the fatty acid i.e. the low polarity of the carbon chain and the polar carboxylic acid head group, must control the interaction between fatty acids and external surface of the crystallites. Therefore, an approach followed by channel entry similar to that assumed by the pore mouth model, is relevant to the alkyl isomerisation of OA, especially if OA has been isomerized to EA.

Another key catalytic property of zeolites used in acid-catalysed reactions, is that their acidity can be tailored to the specificity of each particular reaction. Earlier studies have shown that catalysis of OA alkyl isomerisation requires Brønsted acidity [92, 100, 101, 127, 134]. The substitution in some neutral $SiO_{4/2}$ tetrahedrons of the tetravalent silicon by the trivalent aluminium, results in a number of $AlO_{4/2}$ tetrahedrons that are negatively charged. Subsequent neutralisation by protons leads to bridging hydroxyls connecting silicon and aluminium, endowing the material with its Brønsted acidity (**Figure 1.6a**) [98].

However, the Si/Al ratio only indicates a maximum concentration of such active species, as aluminium can also be found as three other species, with Lewis acidity of varying strength [98]:

- Silanol groups (terminal hydroxyls, **Figure 1.6b**) are located at the crystal surface, possibly within some framework defects.
- Extra framework aluminium (EFAl, **Figure 1.6c**) may be octa-, penta-, tetra- or tri-coordinated; they are part of species which may be neutral or cationic, and monomeric or oligomeric.

- Coordinatively unsaturated aluminium (**Figure 1.6d**) are made of tri-coordinated Si^+ closely located to tri-coordinated aluminium.

These Lewis sites are formed to differing extents during synthesis and/or post-treatment (e.g. calcination, steaming, de-alumination). One of the roles of water used as co-catalyst in the isomerisation reaction is in the modification of these Lewis acid sites, and their potential presence should be considered for the reaction under investigation in this PhD Thesis.

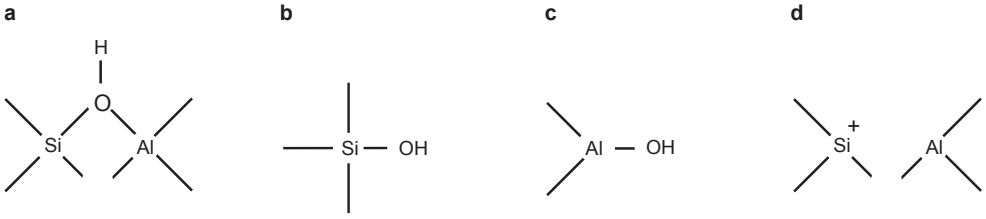

Figure 1.6: Overview of different acid sites found in zeolites: **(a)** Brønsted acid site; **(b)** silanol group; **(c)** aluminol group; and **(d)** defect site originating from the removal of a bridging hydroxyl group.

1.12. Scope and Outline of the PhD Thesis

In this PhD Thesis, the catalytic skeletal isomerisation of oleic acid (OA) with ferrierite zeolites has been investigated. The overall goal is to increase our understanding of the key mechanisms responsible for the superior activity and selectivity of zeolite ferrierite in this reaction, and its limitations. More precisely, this study aims to understand the relation between structure and performance, in order to further improve the selectivity, activity and robustness of ferrierite and thus providing guidelines for the design of an optimal catalytic process for the industrial scale production of isostearic acid (ISAC), a unique and valuable fatty acid. The new perspective brought by this research work is in the combination of the catalytic testing with a detailed study of the catalyst - down to the level of an individual zeolite crystal - before and after reaction, using a very wide range of analytical tools, from more established to state-of-the-art techniques. Spectroscopy, from IR to UV and including fluorescence, played a key role in unveiling the mechanisms. The experimental work utilised both commercial and model catalysts on a range of scales from 2 L to 10 mL.

Chapter 1 reviews the role of catalysis and catalyst development in the production of isostearic acid, as an example of recent research in oleochemistry. Starting with a brief history of the oleochemical industry, we trace the development of isostearic acid and other branched fatty acids. The special properties of isostearic acid are illustrated through its use in applications inaccessible to other fatty acids. Finally, we present the latest developments in zeolite catalysis; the step-change in

yields and selectivities achieved by these new routes, illustrates the potential that proper catalyst design can bring to open up significant new markets and applications for oleochemicals.

In **Chapter 2**, the formation and nature of coke (precursor) species has been studied during the skeletal isomerisation of oleic acid catalysed by protonated ferrierite, in the presence and absence of a triphenylphosphine promoter. UV-Vis and FT-IR spectroscopic analyses of the spent catalyst materials, complemented by NMR and mass spectrometry of the coke deposits extracted after HF dissolution, provide new insights into the deactivation mechanisms.

Chapter 3 studies the deactivation of protonated ferrierite during the skeletal isomerisation of OA using large zeolite crystals as model catalyst, in order to seek additional evidence supporting the concept of pore mouth catalysis, suggested by the findings of the previous Chapter. UV-Vis micro-spectroscopy has been used to compare bulk with local electronic spectra in order to determine the nature of the carbonaceous deposits formed on the large zeolite crystals. Finally, a combination of wide-field and confocal fluorescence microscopy enabled us to determine the 3-D location of the carbonaceous deposits on a number of ferrierite crystals.

Despite the limitation of the reaction to the pore mouth, protonated ferrierite shows superior activity and selectivity in the liquid-phase isomerisation of linear unsaturated fatty acids to (mono)branched-chain unsaturated fatty acids, (Mo)BUFA. **Chapter 4** presents a detailed investigation of the relationship between ferrierite acidity and performance. Five commercial catalysts have been studied, to understand how differences in morphology and acidity, including type, strength, location and accessibility of the acid sites, can explain the often unexpected results of catalytic testing.

Chapter 5 summarises the main conclusions from the previous chapters and, based on these learnings, proposes some potential future directions for exploration, including as a first example some initial results from catalyst modification inspired by the pore mouth concept.

Acknowledgements

Hans Ridderikhoff, Hans Vreeswijk, Dr. Bas Wels (all from Croda) and Peter Tollington (Cargill) are acknowledged for their helpful comments. Thanks also to Zoran Ristanović (Utrecht University) for providing Figure 1.5.

References

[1] www.ers.usda.gov/data-products/oil-crops-yearbook.aspx, USDA Crop Yearbook, Table 47.

[2] Oil World Monthly, ISTA Mielke GmbH (2015) March 27th.

[3] M. P. Malveda, M. Blagoev, C. Funada, www.ihs.com/chemical, CEH Industry Overview, IHS report 220.5000 (2012) April.

[4] National Geographical News (2010) October 28th.

[5] A.L. Ahmad, N.H. Mat Yasin, C.J.C. Derek, J.K. Lim, Renew. Sust. Energ. Rev., 15 (2011) 584.

[6] *Biorefineries - Industrial Processes and Products* (eds. B. Kamm, P.R. Gruber, M. Kamm) Wiley-VCH Verlag, Weinheim (2005).

[7] J. van Haveren, E.L. Scott, J. Sanders, Biofuels, Bioprod. Bioref., 2 (2008) 41.

[8] www.braskem.com.br.

[9] www.natureworksllc.com.

[10] www.duponttateandlyle.com/zemea.

[11] www.bio-amber.com.

[12] www.biomcn.eu.

[13] *Fatty acids in industry: processes, properties, derivatives, applications* (eds. R.W. Johnson, E. Fritz) Marcel Dekker Inc., New York (1989).

[14] M.E. Cheuvreul in *Recherches chimiques sur les corps gras d'origine animale*, P. Levrault, Paris (1823).

[15] M.A.R. Meier, J.O. Metzger, U.S. Schubert, Chem. Soc. Rev., 36 (2007) 1788.

[16] J.O. Metzger, M.A.R. Meier, Eur. J. Lipid Sci. Technol., 110 (2008) 787.

[17] J.O. Metzger, Eur. J. Lipid Sci. Technol., 111 (2009) 865.

[18] B. Arno, J. Pérez Gomes, Eur. J. Lipid Sci. Technol., 112 (2010) 31.

[19] J.O Metzger, M.A.R. Meier., Eur. J. Lipid Sci. Technol., 113 (2011) 1.

[20] U. Biermann, U. Bornscheuer, M.A.R. Meier, J.O. Metzger, H.J. Schäfer, Angew. Chem. Int. Ed., 50 (2011) 3854.

[21] J.O. Metzger, M.A.R. Meier, Eur. J. Lipid Sci. Technol., 114 (2012) 1.

[22] J.O. Metzger, M.A.R. Meier, Eur. J. Lipid Sci. Technol., 116 (2014) 1.

[23] www.techcrops.com.

[24] www.elevance.com.

[25] www.novamont.com.

[26] www.palmoilandfood.eu/en/palm-oil-production.

[27] www.rspo.org.

[28] K.K. Peng, The Chemical Engineer, 880 (2014) 40.

[29] www.redcert.org.

[30] www.iscc-system.org.

[31] M. W. Formo, in *Bailey's Industrial Oil and Fat Products* (eds. D. Swern) John Wiley & Sons Inc., New York, Vol. 2 (1982) pp 384.

[32] M.P. Malveda, M. Blagoev, C. Funada, his.com/chemical, CEH Industry Overview, IHS report 6575000, 2012, July.

[33] N.O.V. Sonntag, in *Fatty acids in industry: processes, properties, derivatives, applications* (eds. R.W. Johnson, E. Fritz) Marcel Dekker Inc., New York (1989) pp 23-72.

[34] K.S. Mackley, in *Fatty acids - their chemistry and physical properties*, Interscience Publishers Inc., New York (1947) pp 328-332.

[35] T.F. Bradley, W.B. Johnston, Ind. Eng. Chem., 32, (1940) 802.
[36] W.B. Johnston, US Patent 2347562 (1944) to American Cyanamid Co.
[37] A. Hill, E.E. Walker, GB Patent 428864 (1935) to ICI Ltd.
[38] F.O. Barrett, C.G. Goebel, R.M. Peters, US Patent 2793219 (1957) to Emery Industries, Inc.
[39] F.O. Barrett, C.G. Goebel, R.M. Peters, US Patent 2793220 (1957) to Emery Industries, Inc.
[40] D.H. McMahon, E. P. Crowell. J. Am. Oil Chem. Soc., 51 (1974) 522.
[41] K.D. Haase, A.J. Heynen, N.L.M. Laane, Lipid/Fett, 91 (1989) 350.
[42] F.O. Barrett, C.G. Goebel, L.D. Myers, US Patent 2955121 (1960) to Emery Industries, Inc.
[43] R.M. Peters, US Patent 2812342 (1957) to Emery Industries, Inc.
[44] J.F.D. Liljeblad, E. Tyrode, E. Thormann, A. Dublanchet, G. Luengo, C. M. Johnson, M.W. Rutland, Phys. Chem. Chem. Phys., 16 (2014) 17869.
[45] R.R. Ran-Ressler, S.E. Bae, P. Lawrence, D.H. Wang and J.T. Brenna, Brit. J. Nutr. (2014) 1.
[46] F.D. Gunstone, Chem. Phys. Lipids, 65 (1993) 155.
[47] N. Polgar, in *Topics in Lipid Chemistry* (eds. F.D. Gunstone), Logos Press, London, Vol. 2 (1971) pp 207.
[48] V.M. Dembitsky, Lipids 41.4 (2006) 309.
[49] M. Fefer, J. Am. Oil Chem. Soc., 55 (1978) A342.
[50] B. Fells, in *Anionic Surfactants: Organic Chemistry* (eds. H.W. Stache), Marcel Dekker Inc., New York, Vol. 156 (1995) pp 29-30.
[51] L. Kravetz, Brendan Dermot Murray, D.M. Singleton, US Patent 5849960 (1998) to Shell Oil company.
[52] J.J. Scheibel, in *Handbook of Detergents, Part F: Production*, (eds. U. Zoller, P. Sosis) CRC Press, Boca Raton, Vol. 142 (2009) pp 129-130.
[53] A.J. Olenick, R.E. Bilbo, Soap Cosmet. Chem. Spe., 63 (1987) 52.
[54] U. Biermann, J.O. Metzger, Eur. J. Lipid Sci. Technol., 110 (2008) 805.
[55] D.V. Kinsman, J. Am. Oil Chem. Soc., 56 (1979) 823A.
[56] D.V. Kinsman, in *Fatty acids in industry: processes, properties, derivatives, applications* (eds. R.W. Johnson, E. Fritz) Marcel Dekker Inc., New York (1989) pp 237-255.
[57] H.L. Ngo, R.O. Dunn, B. Sharma, T.A. Foglia, Eur. J. Lipid Sci. Technol., 113 (2011) 180.
[58] H.L. Ngo, A. Nunez, W. Lin, T.A. Foglia, Eur. J. Lipid Sci. Technol., 108 (2007) 214.
[59] J. Cason, W.R. Winans, J. Org. Chem., 15 (1950) 139.
[60] H.W. Stewart, D.H. Wheeler, Oil & Soap, 18 (1941) 69.
[61] D.V. Kinsman, in *Fatty acids in industry: processes, properties, derivatives, applications* (eds. R.W. Johnson, E. Fritz) Marcel Dekker Inc., New York (1989) pp 245-247.
[62] www.Echa.europa.eu.
[63] H.L. Ngo, R.D. Ashby, A. Nuñez., J. Am. Oil Chem. Soc., 89 (2012) 1885.
[64] D. On, Formule Verte, 10 (2012) 22.
[65] H. Wagner, R. Luther, T. Mang., Appl. Catal. A: General, 221 (2001) 429.
[66] R.J. Hartley, C.B. Duncan, G.M. Tiffany, US Patent 5880075 (1999) to Exxon Chemical Patents Inc.
[67] B.J. Beimesch, N.E. Schnur, C.J. Hughes, US Patent 4477383 (1984) to National Distillers and Chemical Corporation.

[68] G. Leleu, P. Bedague, B. Sillion, US Patent 4061581 (1977) to Institut Francais Du Petrole, Rhone Progil.
[69] T. Okada, S. Hara, European Patent 2133405 (2009) to Idemitsu Kosan Co., Ltd.
[70] L.R. Svarcas, M.S. Brenner, T.A. Nau, WO Patent 2006004806 (2006) to Lubrizol Corp.
[71] T.F. Bunemann, A. D. Kardol, A.C. de Mooij, US Patent 20040075079 (2004) to Unichema Chemie B.V.
[72] P.E. Adams, J.H. Bush, S. Lahiri, C.D. Tipton, European Patent 1534805 (2005) to The Lubrizol Corporation.
[73] J.A. Buitrago, M. Shiga, T. Shiroi, H. Takayama, European Patent 1803796 (2009) to Chevron Oronite Company LLC, Chevron Texaco Japan Ltd.
[74] S. Boyde, S.J. Randles, in *Esters. Synthetics, Mineral Oils, and Bio-Based Lubricants: Chemistry and Technology* (eds. L.R. Rudnick) CRC Press, Boca Raton (2013) pp 51.
[75] W. Vetter, I. Wegner, Chromatographia, 70 (2009) 157.
[76] A.W. Fogel, US Patent 6126951 (2000) to Bernel Chemical Company, Inc.
[77] K. Yagi, N. Kanda, European Patent 2455061 (2012) to Tayca Corporation.
[78] J.R. Strobridge, US Patent 5041281 (1991) to Amway Corporation.
[79] T. Ehara, K. Yamaguchi European Patent 1958612 (2014) to The Nisshin OilliO Group, Ltd.
[80] R.B. Hutchison, L.R. Mores, US Patent 3890358 (1975) to Emery Industries Inc.
[81] K. Hutcheson, R. Flemington, M.A. Gomolka, US Patent 3590122 (1971) to Colgate Palmolive Company.
[82] R. Huettinger, U. Holtschmidt, US Patent 4614622 (1986) to Th. Goldschmidt AG
[83] www.evonik.com.
[84] P.V. Bonsignore, US Patent 4283316 (1981) to Aluminum Company of America.
[85] S.J. Monte, P.F. Bruins, US Patent 4098758 (1978) to Kenrich Petrochemicals, Inc.
[86] T.J. Kondis, R. Rolles, US Patent 3781177 (1973) to Aluminum Company of America
[87] R.A. Bauman, R.C. Pierce, US Patent 4418011 (1983) to Colgate-Palmolive Company.
[88] R.A. Bauman, US Patent 4497715 (1985) to Colgate-Palmolive Company.
[89] O Malmstrom et al., US Patent 20010054491 (2001) to Raisio Chemicals Ltd.
[90] D.A. Van Beek, US Patent 5138027 (1992) to Henkel Corporation.
[91] R. Brütting, G. Spiteller, Fat Sci. Technol., 96 (1994) 361.
[92] Y. Nakano, T.A. Foglia, H. Kohashi, T. Perlstein, S. Serota, J. Am. Oil Chem. Soc., 62 (1985) 888.
[93] R.M. Koster, M. Bogert, B. de Leeuw, E.K. Poels, A. Bliek, J. Mol. Catal. A: Chemical, 134 (1998) 159.
[94] F.R. Ribeiro, F. Alvarez, C. Henriques, F. Lemos, J.M. Lopes, M.F. Ribeiro, J. Mol. Catal. A: Chemical, 96 (1995) 245.
[95] T.F. Degnan, J. Catal., 216 (2003) 32.
[96] G. Perot, M. Guisnet, J. Mol. Catal., 61 (1990) 173.
[97] J. Jae, G.A. Tompsett, A.J. Foster, K.D. Hammond, S.M. Auerbach, R.F. Lobo, G.W. Huber, J. Catal., 279 (2011) 257.
[98] M. Hunger, in *Zeolites and Catalysis, Synthesis, Reactions and Applications* (eds. J. Čejka, A. Corma and S. Zones) Wiley-VCH, Weinheim (2010) pp 493-546.
[99] A.C. Butler, C.P. Nicolaides, Catal. Today, 18 (1993) 443.
[100] J. Houžvička, V. Ponec, Catal. Rev. Sci. Eng., 39 (1997) 319.
[101] S. van Donk, J.H. Bitter, K.P. de Jong, Appl. Catal. A: General, 212 (2001) 97.
[102] L.H. Gielgens, I.H.E. Veenstra, V. Ponec, M.J. Haanepen, and J.H.C. van Hooff, Catal. Lett., 32, (1995) 195.

[103] J. Houžvička and V. Ponec, Appl. Catal. A: General, 145, (1996) 95.
[104] G. J. Gajda, US Patent 5132484 (1992) to UOP.
[105] S.A.I. Barri, D.W. Walker, R. Tahir, European Patent 247802 (1987) to BP Company.
[106] R. Byggningsbacka, N. Kumar, L.E. Lindfors, J. Catal., 178 (1998) 611.
[107] C. O'Young, R.J. Pellet, D.G. Casey, J.R. Ugolini, R.A. Sawicki, J. Catal., 151 (1995) 467.
[108] P. Granvallet, K.P. de Jong, A.G.T.G. Kortbeek, B. Kraushaar-Czarnetzki, H.H. Mooiweer, European Patent 0501577 (1992) to Shell.
[109] R G. Seo, H.S. Jeong, S.B. Hong, H.S. Uh, Catal. Lett., 36 (1996) 249.
[110] J. Houžvička, R. Klik, L. Kubelkova, V. Ponec, Appl. Catal. A: General, 150 (1997) 101.
[111] T.F. Degnan, Top. Catal., 13 (2000) 349.
[112] W. Vermeiren, J.P. Gilson, Top. Catal., 52 (2009) 1131.
[113] J. Weitkamp, P.A. Jacobs, J.A. Martens, Appl. Catal., 8 (1983) 123.
[114] S. Ernst, R. Kumar, M. Neuber, J. Weitkamp, Stud. Surf. Sci. Catal., 39 (1987) 531.
[115] W. Huybrechts, G. Vanbutsele, K.J. Houthoofd, F. Bertinchamps, C.S.L. Narasimhan, E.M. Giagneaux, J.W. Thybaut, G.B. Marin, J.F.M. Denayer, G.V. Baron, P.A. Jacobs, J.A. Martens, Catal. Lett., 100, (2005) 235.
[116] M. Guisnet, Catal. Today, 218 (2013) 123.
[117] H. Deldari, Appl. Catal. A: General, 293 (2005) 1.
[118] T.L.M. Maesen, M. Schenk, T.J.H. Vlugt, J.P. de Jonge, B. Smit, J. Catal., 188 (1999) 403.
[119] G. Sastre, A. Chica, A. Corma, J. Catal., 195 (2000) 227.
[120] T.L.M. Maesen, R.Krishna, J.M. van Baten, B. Smit, S. Calero, J.M. Castillo Sanchez, J. Catal., 256 (2008) 95.
[121] M.C. Claude, J.A. Martens, J. Catal., 190 (2000) 39.
[122] M.C. Claude, G. Vanbutsele, J.A. Martens, J. Catal., 203 (2001) 213.
[123] J.A. Martens, G. Vanbutsele, P.A. Jacobs, J. Denayer, R. Ocackoglu, G. Baron, J.A.M. Arroyo, J. Thybaut, G.B. Marin, Catal. Today, 65 (2001) 111.
[124] J.A. Munoz Arroyo, G.G. Martens, G.F. Froment, G.B. Marin, P.A. Jacobs, J.A. Martens, Appl. Catal. A: General, 192 (2000) 9.
[125] J.A. Martens, D. Verboekend, K. Thomas, G. Vanbutsele, J.P. Gilson, J. Pérez-Ramírez, ChemSusChem., 6 (2013) 421.
[126] J.A. Martens, D. Verboekend, K. Thomas, G. Vanbutsele, J. Pérez-Ramírez, J.P. Gilson, Catal. Today, 218 (2013) 135.
[127] H. Abe, Y. Matsumura, Y. Sakuma, T. Tomifuji, US Patent 5677473 (1997), to Kao Corporation.
[128] W.R. Hodgson, C.M. Lok, G. Roberts, W.T. Koetsier, European Patent 0774451 (1997) to Unichema Chemie B.V.
[129] W.R. Hodgson, W.T. Koetsier, C.M. Lok, G. Roberts, US Patent 5856539 (1999) to Unichema Chemie B.V.
[130] S. Zhang, Z. Zhang, D. Steichen, US Patent 6831184 (2004) to Akzo Nobel N.V.
[131] Z. Zhang, S. Zhang, US Patent 7098353 (2006) to Akzo Nobel N.V.
[132] C. Zhang, M. Dery, S. Zhang, D. Steichen, J. Surf. Deterg., 7 (2004) 211.
[133] S. Zhang, Z. Zhang, US Patent 6723862 (2004), to Akzo Nobel N.V.
[134] S. Zhang, Z.C. Zhang, Catal. Lett., 115 (2007) 3.
[135] L.Ha, J.Mao, J. Zhou, Z.C. Zhang, S. Zhang, Appl. Catal. A: General, 356 (2009) 52.
[136] S. Zhang, Z. Zhang, European Patent 1490171 (2004) to Akzo Nobel N.V.
[137] H.L. Ngo, E. Hoh, T.A. Foglia, Eur. J. Lipid Sci. Technol., 114 (2012) 213.
[138] H.L. Ngo, R.O. Dunn, E. Hoh, Eur. J. Lipid Sci. Technol., 115 (2013) 676.

[139] H.L. Ngo, Eur. J. Lipid Sci. Technol., 116 (2014) 645.
[140] P.A. Vaughan, Acta Cryst., 21 (1966) 983.
[141] B.K. Smith, Am. Mineral., 71 (1986) 989.
[142] www.iza-structure.org/databases.
[143] J.P. Gilson and E.G. Derouane, J. Catal., 88 (1984) 538.
[144] A. Philippaerts, S. Paulussen, S. Turner, O. Lebedev, G. Van Tendeloo, H. Poelman, M. Bulut, F. De Clippel, P. Smeets, B. Sels, P. Jacobs, J. Catal., 270 (2010) 172.

Chapter 2

Skeletal Isomerisation of Oleic Acid over Ferrierite in the Presence and Absence of Triphenylphosphine: Pore Mouth Catalysis and Related Deactivation Mechanisms

Abstract

The formation and nature of coke (precursor) species have been studied during the skeletal isomerisation of oleic acid catalysed by protonated ferrierite (H-FER), in the presence and absence of a triphenyl phosphine promoter. UV-Vis and FT-IR spectroscopic analyses of the spent H-FER catalyst materials, complemented by NMR and mass spectrometry of the "coke" deposits extracted after HF dissolution, provide new insights into the deactivation mechanisms. Initial high catalyst activity and selectivity are quickly lost, despite conservation of the framework integrity, as a result of severe deactivation. Pore blockage is detected very early in the reaction, and only the pore mouth is actively employed. Additionally, polyenylic carbocations formed by hydrogen transfer reactions, poison the active sites; they are considered to be the precursors to traces of condensed aromatics detected in the spent catalyst. Dodecyl benzene is the major "coke" constituent, and its precursor probably also competes for the active sites.

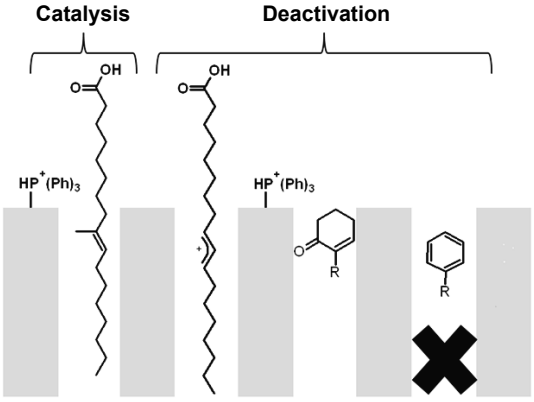

This Chapter is based on the manuscript: S.C.C. Wiedemann, J.A. Stewart, F. Soulimani, T. van Bergen-Brenkman, S. Langelaar, B. Wels, P. de Peinder, P.C.A. Bruijnincx, B.M. Weckhuysen, J. Catal., 316 (2014) 24 (DOI:10.1016/j.jcat.2014.04.018).

2.1. Introduction

As discussed in Chapter 1, branched-chain unsaturated fatty acids (BUFA) derived from natural vegetable oil sources are raw materials of great interest within the lubricant, surfactant and cosmetic markets, as they remain liquid after hydrogenation and have superior oxidative stability compared to unsaturated (liquid) fatty acids. Furthermore, they have useful interfacial properties and are compatible with a wide range of organic compounds. Some key applications include friction modifiers for fuel and lubricant oils, dispersants for pigments and metal powders, and emulsifiers for topical skin care products. The current commercial process for making BUFA is coupled to the production of oligomeric fatty acids, and maximum mass yields are limited to ca. 50%. Clays, such as montmorillonite, are typically used as catalyst in this process [1, 2].

Decoupling of the skeletal isomerisation and oligomerisation production processes is highly desired yet challenging, as both reaction pathways go through the same carbocation intermediates. The use of zeolites as solid acids holds considerable promise in this respect, as discrimination between these two competing pathways could possibly be achieved by making use of their properties as shape-selective catalysts.

Table 2.1 summarises the main product classes that are obtained after a zeolite-catalysed skeletal isomerisation of a commercial oleic acid (OA), which mainly consists of *cis*-9-octadecenoic acid (**1**). Cis/trans isomerisation of the double bond to elaidic acid (**5**) occurs readily in the presence of acidic sites, and is an important early-stage reaction. Besides the desired BUFA (**4**), a small amount of (alkyl-branched) γ-lactones (**6**) are formed as a result of double-bond migration followed by lactonisation [3]. Other monomeric components include traces of stearic (**2**), and linoleic (**3**) acids, which are derived from the starting material and from hydrogen transfer reactions [4]. Higher molecular weight compounds include oligomerised fatty acids (dimeric C36 (**7**) and higher oligomers), as well as monoestolides (**8**) and polyestolides formed by reaction of a carboxylic group and an activated doubled bond [5].

The selective production of BUFA from OA has been investigated by several groups, using medium- to large-pore molecular sieves, amongst others mordenite (MOR) [6], L-type (LTL) [7-8], Beta (BEA) [9] and mesoporous zeolites (MAS-5) [10] and has been reviewed in Chapter 1 (section 1.10). Recently, a step change in both OA conversion (> 95%) and selectivity towards BUFA (> 70%) has been achieved by Ngo and co-workers using commercial, protonated ferrierite catalysts [11]. Selectivity towards the monomeric fraction could be further improved by the use of a bulky Lewis base as promoter, e.g. triphenylphosphine (TPP) [12]. It is believed that such a base interacts with the non-shape-selective acidic sites on the external zeolite surface. The size of the Lewis base prevents it from entering the zeolite framework

Table 2.1: Reactants and main products for the zeolite-catalysed skeletal isomerisation of OA.

Feedstock: Oleic Acid (OA) Priolene™ 6936
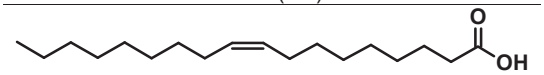
(**1**) oleic acid (*cis*-9-octadecenoic acid), 92.2 wt%
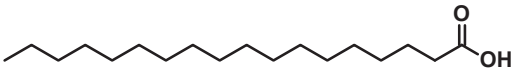
(**2**) stearic acid (octadecanoic acid), 1.7 wt%
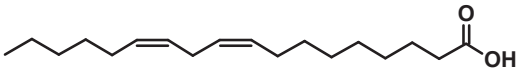
(**3**) linoleic acid (*cis,cis*-9,12-octadecadienoic acid), 3.2 wt%
Crude monomeric fraction
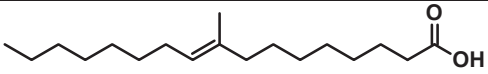
(**4**) alkyl-branched isomer of oleic acid (BUFA) [a]
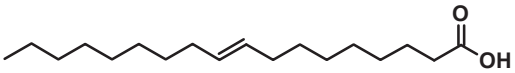
(**5**) elaidic acid (*trans*-9-octadecenoic acid) [a]
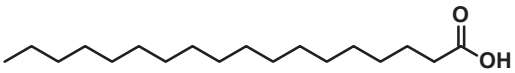
(**2**) stearic acid (octadecanoic acid)
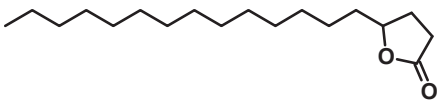
(**6**) γ-stearolactone (5-tetradecyloxolan-2-one) [b]
Crude oligomeric fraction
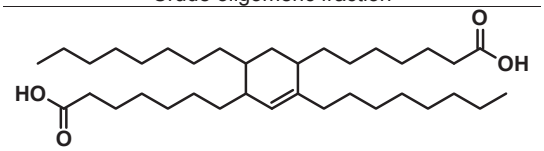
(**7**) isomer of C36 dimer acid [a]
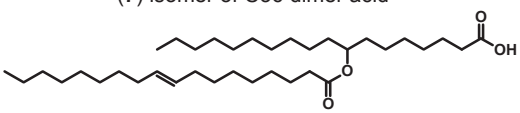
(**8**) (mono)estolide of oleic acid [a]

a: Compounds (**4**), (**5**), (**7**) and (**8**) are typical isomers of the indicated species.
b: Alkyl-branched isomers of (**6**) are also identified.

and interacting with shape-selective active sites within the channels or, as will be shown here, in the pore mouths.

Protonated ferrierite (H-FER) thus seems to have an optimal structure and acidity for the skeletal isomerisation of OA. The framework of this medium-pore zeolite has been described in Chapter 1 (section 1.11). Compared to other 10-MR zeolites, ferrierite has a low ratio of Lewis to Brønsted sites [13]. Its acidity has been characterised in detail using FT-IR spectroscopy and five distinct Brønsted acidic sites could be assigned, i.e. hydroxyl groups in 10-MR channels (20% of Si(OH)Al), at intersections between 10- and 8-MR channels (50% of Si(OH)Al), in the 8-MR channels, and finally in the 6-MR and 5-MR-windowed cavities [14]. However, overall acidity depends strongly on the accessibility of those sites [15]. FT-IR studies using bulky probe molecules also showed that the external surface of protonated ferrierite has terminal silanols (some with significant Brønsted acidity), as well as Lewis acid sites, but no bridging hydroxyl groups [16].

As ferrierite is much more expensive than the montmorillonite clay used in the current isomerisation process, catalyst stability and the possibility to re-use and/or regenerate the catalyst are key to the economic viability of BUFA production. While no studies have dealt with the details of ferrierite deactivation in BUFA production, the deactivation of zeolite materials in general has been extensively studied and the possible mechanisms have been reviewed [17-18]. For the skeletal isomerisation of OA, loss of activity or selectivity could be caused by build-up of organic deposits due to simple deposition (fouling), or by deposition after transformation (“coking”). An alternative mechanism is the poisoning of active sites by strong chemisorption of species. Finally, chemical and structural alterations could result from e.g. dealumination and/or collapse of zeolite framework. High activity and selectivity with ferrierite in the skeletal isomerisation of OA could only be obtained with the fresh catalyst, and direct reuse did not seem to be successful [11]. Later, successive solvent and acidic washings of the spent catalyst were reported to allow up to ten re-uses without significant loss of activity and selectivity [12]. This result suggests that chemical or structural alterations of the zeolite are not the cause of deactivation. However, the actual deactivation mechanism was not discussed, and the combination of solvent and hydrochloric acid washing would be difficult to implement in an oleochemical production plant. Efficient catalyst recycling procedures first require a thorough understanding of the deactivation process, i.e. the alteration of the catalytic properties of the ferrierite during the reaction of interest. To date, such a study has not been reported for the zeolite-catalysed skeletal isomerisation of OA; only the poisoning of Beta (H-BEA) zeolite by a carboxylic acid group has previously been described, by comparing the reaction of 1-octadecene to OA in the absence of water [19].

On the other hand, considerable research has been devoted to the deactivation of ferrierite in the skeletal isomerisation of butene [20]. The catalyst is

known for its poor initial selectivity to isobutene, and its high selectivity and stability at higher times-on-stream (TOS). Process parameters (especially reaction temperature) were found to affect both the amount and nature of the coke [21]. Composition of coke (including slightly condensed aromatics with methyl substituents) and location (at the intersection of the 8- and 10-MR channels) were determined, and a reaction pathway was proposed to explain the high selectivity to isobutene of the coked rather than fresh catalyst (only 10% of the pore volume is accessible at maximum selectivity) [22]. Additionally, concentration and strength of Brønsted acid sites were found to affect coke formation as well as selectivity; indeed, higher isobutene selectivity and lower coking were observed with lower acid site density [23]. Coke nature, location, rate and mode of formation have been further investigated by various spectroscopies. Of these, in-situ FT-IR spectroscopy gave much valuable information. When combined with a tapered element oscillating microbalance (TEOM), both vacant Brønsted acid groups and coking could be monitored as a function of TOS [24]. FT-IR was also used to confirm accessibility of Brønsted sites of spent ferrierite following deuteroacetonitrile (CD_3CN) adsorption [25-26], and played a key role in the elucidation of the complex mechanism supporting increased selectivity at high TOS [26]. Although carried out in the gas-phase at a higher temperature and with molecules of much smaller diameter, these studies provide important clues for our research.

In this Chapter, we present a detailed study of the deactivation pathways of H-FER zeolite materials during the skeletal isomerisation of OA, with the aim to provide pointers to ultimately improve its stability and to establish methods for its complete regeneration. OA and its methyl ester were reacted in a lab-scale batch reactor using conditions optimised by Ngo et al. [12] in the presence and absence of triphenylphosphine. The nature of the “coke” and its rate of formation were studied (amongst others) by a combination of UV-Vis and FT-IR spectroscopy. These findings were complemented by an analysis of the “coke” extract after HF dissolution of the spent H-FER zeolite materials. The causes for the activity loss could thus be systematically investigated, and reaction mechanisms explaining the deactivation proposed.

2.2. Experimental

2.2.1. Chemicals and Catalyst Materials

OA with tradename Priolene™ 6936 (92.2% C18:1 (**1**), 3.2% C18:2 (**3**), 0.2 C18:3 and 3.7% saturated fatty acids (mainly C18 (**2**)) and the methyl ester of OA (AV < 0.10 mg KOH/g, MO), were obtained from Croda. Triphenylphosphine (TPP, 99%) was obtained from Aldrich Chemicals. The zeolite material K^+-Ferrierite (HSZ-

720KOA) with a Si/Al ratio of 8.9, originates from Tosoh Corporation. K^+-Ferrierite was activated prior to catalyst testing by conversion to its protonated form, further denoted as H-FER, using an ion-exchange procedure with hydrochloric acid (HCl, 1 M) at room temperature (RT) [27], before air drying for three days at RT. The particle size distribution of H-FER is characterised by a median of 15 µm (Chapter 4, section 4.2.3). PtO_2 was purchased from Sigma Aldrich (Pt 80-85% and surface area ≥ 75 m^2/g).

2.2.2. Catalyst Testing, Sampling and Catalyst Recovery

The key parameters for all experiments (Exp.) are summarised in **Table 2.2**. Catalyst testing was carried out in an RC1 high-pressure stainless steel reactor (1.8 L) from Mettler Toledo, using the following amounts: 1000 g OA or its methyl ester MO, 50.0 g H-FER, 3.75 g TPP and 10.0 g demineralised water (or/and methanol). After purging with nitrogen 3 times, the reactor was pressurised to about 1 bar and heated under mechanical stirring (400 rpm) to (a maximum of) 260 °C at a rate of 6 °C/min, resulting in a pressure of about 11 bar. Reaction temperature was typically held for 6 h (unless otherwise stated), before the mixture was cooled to 80 °C and filtered under nitrogen for a minimum of 4 h. Spent catalyst from experiment 15 was collected and re-used in experiment 16 after acetone washing; for practical reasons, the catalyst loading was reduced to 1.5 wt% and the promoter was omitted in both runs 15 and 16.

Table 2.2: Overview of the 16 experiments for the skeletal isomerisation over H-FER in the presence and absence of TPP, with different feeds; reaction temperature of 260 °C.

Exp.	Feed type	H-FER loading (wt% on feed)	Additive	TPP loading (wt% on feed)	Reaction time (h)
1	OA	5	H_2O	0	0.5
2	OA	5	H_2O	0	1
3	OA	5	H_2O	0	2
4	OA	5	H_2O	0	6
5	OA	5	H_2O	0	12
6	OA	5	H_2O	0.375	0 [a]
7	OA	5	H_2O	0.375	0.5
8	OA	5	H_2O	0.375	2
9	OA	5	H_2O	0.375	6
10	*OA*	5	H_2O	0.375	12
11	OA + 3% C18:2 (**3**)	5	H_2O	0.375	6
12	OA + 9% C18:2 (**3**)	5	H_2O	0.375	6
13	MO	5	CH_3OH	0.375	6
14	MO	5	CH_3OH/H_2O [b]	0.375	6
15	OA	1.5	H_2O	0	6
16 [c]	OA	1.5	H_2O	0	6

a: Two minutes at reaction temperature.
b: Weight ratio CH_3OH/H_2O = 3.5.
c: Spent catalyst from Exp. 15 after filtration and acetone washing.

Because of the large differences in molecular weight of the different components in the crude reaction mixture, its composition was determined in two steps. First, the oligomer concentration in the crude reaction mixture was determined by high temperature GC (HT-GC). The monomeric fraction was separated from the oligomers by distillation at a temperature of 260 °C under a pressure of < 1 mbar. Subsequently, to reduce chemical complexity and facilitate analyses, a small amount of the collected monomeric fraction was diluted in ethyl acetate (40 mg/mL), hydrogenated at RT for 45 min using 40 mg Adam's catalyst (PtO_2 reduced in situ, hydrogen flow of 50 mL/min) and subjected to GC analyses.

Oleic acid ((**1**), with an initial mass fraction $X_{C18:1,0}$), linoleic acid ((**3**), $X_{C18:2,0}$) and linolenic acid ($X_{C18:3,0}$), are considered as the reactive components of OA; positional and cis/trans isomers are implicitly included in the simplified nomenclature. Their mass conversion ($y_{,t}$) was determined by quantification of the mass fraction of stearic acid ((**2**), $x_{C18,t}$) in the hydrogenated monomer fraction as a function of time *t*. The onset of the reaction (t = 0) is designated as the time when the reaction mixture reaches the temperature setpoint of 260 °C. A correction is made for the distillation yield of the monomeric species ($y_{M,t}$) as determined by HT-GC, and for the initial mass fraction of unreactive species, i.e. stearic acid ($X_{C18,0}$). The mass conversion of all unsaturated components, subsequently referred to simply as "conversion", is then given by:

$$y_t = 1 - \frac{[(x_{C18,t} + x_{C18:1,t}) \times y_{M,t} - x_{C18,0}]}{[x_{C18:1,0} + x_{C18:2,0} + x_{C18:3,0}]} \quad \text{(E 2.1)}$$

Note that due to the closely similar molecular weights of these molecules, mole and mass conversions can be considered almost equivalent.

The selectivity towards BUFA ($s_{B,t}$) is derived from the mass fraction of all hydrogenated BUFA ($x_{B,t}$) in the hydrogenated monomer fraction. Again, a correction was made for the distillation yield of the monomeric species ($y_{M,t}$):

$$s_{B,t} = \frac{[x_{B,t} \times y_{M,t}]}{[(x_{C18:1,0} + x_{C18:2,0} + x_{C18:3,0}) \times y_t]} \quad \text{(E 2.2)}$$

30 g of H-FER catalyst cake from each isomerisation reaction was transferred into a 500 mL Erlenmeyer flask and suspended in 100 mL of acetone. After stirring for about 2 h at room temperature, the mixture was filtered (0.2 µm polytetrafluoroethylene -PTFE- filter), using an extra 100 mL of solvent to rinse. The operation was repeated until no dry mass was detected following evaporation of the filtrate, after which the spent catalyst was air-dried for 24 h. The yield of spent catalyst after this washing series varied from 44 to 49 wt% (of the original cake). The white colour of the fresh H-FER turned to light grey after reaction in the absence of

TPP and remained light grey after washing. On the contrary, all spent catalysts from reactions involving TPP were characterised by a more yellow colouration (both before and after washing).

Spent catalyst from one selected experiment (entry 9 in **Table 2.2**) was calcined in air at 500 °C for 12 h [11]. For three selected experiments (4, 9 and 12, **Table 2.2**), 300 mg of acetone-washed spent catalyst was dissolved in hydrofluoric acid (HF) and the acidic solution extracted using dichloromethane. After neutralisation with calcium carbonate, addition of diethyl ether (10 mL) and filtration, the organic fraction was dried at reduced pressure (20 mbar) at 40 °C, leaving a greenish and odorous residue

2.2.3. Analytical Methods

The composition of the crude reaction mixtures was determined using High-Temperature GC (HT-GC) after methylation using diazomethane. The GC was equipped with a cold on-column injection and a metal column with a non-polar stationary phase Cp-SimDist Ultimetal (Chrompack WCOT, 5 m x 0.53 mm x 0.17 µm) and the components detected with a Flame Ionisation Detector (FID) based on retention time. The carrier gas was He with a constant flow of 20 mL/min. The temperature program used was: initial temperature of 60 °C, hold for 1 min; temperature increase of 30 °C/min until 150 °C; hold 0 min; temperature increase of 12 °C/min until 380 °C; hold 10 min. The detector was set at 400 °C. The injection volume was 1 µL for a concentration of 1 mg/mL.

The hydrogenated monomer fractions were analysed by GC after methylation with diazomethane. The GC was equipped with a split injection and a fused silica capillary column with a polar stationary phase FFAP-CB (Chrompack WCOT, 25 m x 0.32 mm x 0.30 µm), and the components detected with FID based on retention time. The carrier gas was He with a constant flow of 2.1 mL/min and a split flow of 75 mL/min. The temperature program used was: initial temperature of 120 °C, hold for 0 min; temperature increase of 8 °C/min until 250 °C; hold 20 min. The detector was set at 270 °C. The injection volume was 1 µl for a concentration of 40 mg/mL.

For ICP-MS analysis, the crude mixtures were first digested using a closed vessel microwave system (CEM). 8.0 mL 70% HNO_3 and 2.0 mL 37% HCl were added to 0.5 g sample. The mixture was submitted to the following temperature program: 10 min ramp to 120 °C; hold 5 min; 5 min ramp to 180 °C; hold 30 min. The resulting material was diluted to 50.0 mL with ultrapure water (18 MΩ.cm at 25 °C). Elemental analyses were carried out using an ICP-MS (Agilent 7500ce with Shield Torch System) equipped with an Agilent Octopole Reaction System (ORS) with the option for adding reaction gases, Agilent Quartz torch and Shield Plate and Glass Expansion 'Micromist' nebulizer. The first sample of each series was determined by standard addition. The next samples were analysed by external calibration, with an

internal standard. Al was measured at m/z 27; helium was used as collision gas and Ge (m/z 72) as internal standard.

TGA analyses of the (spent) catalysts were performed on a Mettler Toledo TGA/SDTA851 using a platinum pan (no lid). The measurements were carried under air (flow of 100 mL/min) at a heating rate of 10 °C/min from RT to 1000 °C. The first derivative was used to define the step limits of the "coke" losses.

Nitrogen physisorption on the (spent) catalyst materials was performed with an automated gas sorption system Micromeritics TriStar 3000. Before the measurements, the samples were outgassed for 12 h at 250 °C (fresh catalyst only) or at 150 °C. Surface areas were calculated using the BET model. The external surface area (S_E), micropore surface area (S_μ), and micropore volume (V_μ) were determined by applying the t-plot method.

FT-IR spectra of the (spent) catalyst materials were obtained by first pressing the material into a self-supporting wafer of 14-17 mg with a diameter of about 13 mm. The wafer was placed in a FT-IR cell connected to an oven. Adsorbed water was removed by heating it at 120 °C under vacuum (1.6 mbar) for 24 h. A Perkin-Elmer System 2000 was used to record the FT-IR spectra in transmission mode from 4000 to 400 cm^{-1} (resolution of 4 cm^{-1} and 25 scans), with the spectrum of the empty cell as background (ratio).

A Varian Cary 500 Scan spectrophotometer was used to record UV-Vis spectra of the (spent) catalyst materials in diffuse reflectance mode, in the range 200-800 nm (scan speed 600 nm/min and 1 cycle).

FT-IR spectra of the "coke" residues isolated after HF treatment were recorded on a FT-IR spectrometer (Digilab FTS 7000 series) equipped with a DTGS detector. The spectra of the film on KBr (128 scans) were recorded at RT between 4000 and 400 cm^{-1}, with a spectral resolution of 4 cm^{-1}.

Extracts obtained after HF dissolution were dissolved in $CDCl_3$ and ^1H, ^{13}C and DEPT NMR spectroscopic measurements were conducted at 25 °C on a Varian Oxford AS400 MHz spectrometer. Chemical shifts (δ) are given in ppm referenced to the residual solvent signal.

For GC-MS analysis, the "coke" residues were re-dissolved in 1,1,2-trichloro-trifluoroethane (TTE) and the components separated by HT-GC. The GC was equipped with a cold on-column injection and a capillary column with a non-polar stationary phase ZB-1HT (Zebron Inferno, 30 m x 0.32 mm x 0.1 µm). The carrier gas was He with a constant flow rate of 2.5 mL/min. The temperature program used was: initial temperature of 50 °C, hold for 1 min; temperature increase of 15 °C/min until 400 °C; hold 20 min. The injection volume was 0.5 µL. The components were detected with a quadrupole MS detector (Agilent MSD 5975 B Inert) in electron ionization mode (70 eV). The interface temperature was set at 350 °C, the source temperature at 230 °C and the quadrupole temperature at 150 °C. The scan range was 29-1050 amu with 1.48 scans/s.

2.3. Results

2.3.1. Catalyst Testing

The skeletal isomerisation of OA was carried out following the procedure of Ngo and co-workers [12], using a weight loading of 5% H-Ferrierite (H-FER) and an addition of 1.0-1.5% of water (on OA). **Table 2.2** gives an overview of the 16 experiments (Exp.).

Conversion and selectivity (wt%) for the 6 h runs are summarised in **Table 2.3**, while the detailed compositions (wt%) of the crude mixtures are shown in **Table 2.4**. A control reaction was carried out in the absence of TPP (Exp. 4), to assess its influence. TPP addition (Exp. 9) resulted in a significant increase of the selectivity towards BUFA (from 70 to 88%), while conversion remained similar (95 and 92%). The total amount of lactones formed is only slightly lower in the reaction with TPP (9 wt%) compared to the one without (11 wt%). Therefore, the gain in BUFA yields can be almost fully attributed to the drop in oligomer yield. HT-GC analyses of distillation residues indicate that the higher molecular weight, oligomer fraction contains both estolides (product **8**, **Table 2.1**) and dimers (product **7**, **Table 2.1**), with an estolide:dimer weight ratio of 2.3 when using TPP, and 0.14 in its absence. As expected, the bulky base efficiently neutralises external acid sites, which are known to promote dimer acid formation [23]. The only bimolecular reaction that occurs is (poly)estolide formation, commencing at much lower temperature. A possible explanation is that the equilibrium between the TPP and the catalyst surface is not fully established at this early stage.

Linoleic acid (reactant **3**, **Table 2.1**) is found in most commercially important vegetable oils, and its influence on the mechanisms of deactivation therefore needs to be assessed. OA, which already contains 3.2 wt% of linoleic acid (**3**), was spiked with additional linoleic acid, resulting in a marked decrease in both activity and selectivity. Comparison of experiments 9, 11 and 12, shows that increasing the concentration of linoleic acid in the feed leads to a concomitant loss in yield of BUFA. This result suggests that the presence of polyunsaturations in the feed is significantly accelerating catalyst deactivation.

The effect of the carboxylic acid functionality was assessed by using the methyl ester of OA, methyl oleate (MO), as feedstock in two reactions (i.e., experiments 13 with methanol only, and 14 with a methanol/water mixture). These reactions showed a considerable drop in conversion (57 and 72 wt%, respectively). Interestingly, in both experiments, the yield of the monomer fraction was very high (98 and 96 wt%, respectively); a possible explanation is the absence of an acid - base reaction between TPP and MO (unlike OA), leaving an excess of TPP available to block the external acid sites. Selectivity towards skeletal isomerisation was worsened if a methanol/water mixture was used; the gain in conversion resulted only

in extra lactones (product **6**, **Table 2.1**). The water therefore appears to have several functions; in addition to increasing the number of Brønsted sites as mentioned in the introduction, it also seems to promote the formation of esterification products, mostly lactones and to a minor extent estolides (product **8**, **Table 2.1**).

Table 2.3: Overview of conversion and selectivity determined after 6 h reaction at 260 °C for the skeletal isomerisation over H-FER with different feeds.

Exp.	Feed type	H-FER loading (wt%)	Additive	Promoter	Conversion (wt%)	Monomer yield (wt%)	BUFA selectivity (wt%)
4	OA	5	H_2O	-	95	83	70
9	OA	5	H_2O	TPP	92	95	88
11	OA+3%C18:2(**3**)	5	H_2O	TPP	88	94	87
12	OA+9%C18:2(**3**)	5	H_2O	TPP	79	92	79
13	MO	5	CH_3OH	TPP	57	98	79
14	MO	5	CH_3OH/H_2O [a]	TPP	72	96	63
15	OA	1.5	H_2O	-	85	88	75
16 [b]	OA	1.5	H_2O	-	56	90	60

a: Weight ratio CH_3OH/H_2O = 3.5.
b: Spent catalyst from Exp. 15 after filtration and acetone washing.

Table 2.4: Detailed composition (wt%) of crude product determined after 6 h reaction at 260 °C for the skeletal isomerisation over H-FER with different feeds.

Exp.	Stearic acid [a] (**2**)	Hydrogenated BUFA (**4**)	Lactones (**6**)	Oligomeric components (**7** + **8**)
4	5.7	61.7	11.3	17.1
9	8.7	74.7	8.8	5.1
11	12.8	70.4	7.6	5.6
12	20.9	57.3	10.0	7.8
13	41.5	41.7	13.4	2.0
14	27.1	42.0	25.6	3.6
15	15.1	59.2	10.2	11.6
16 [b]	41.8	31.2	13.5	10.2

a: From 3 sources : 1) present in the feed, 2) formed by H-transfer reactions during isomerisation, and 3) post-reaction, by hydrogenation of unreacted OA.
b: Spent catalyst from Exp. 15 after filtration and acetone washing.

Conversion and selectivity were further studied as a function of time (2 min - 12 h). **Figure 2.1** shows the crude product composition (with and without TPP) and conversion (with TPP). The reaction without promoter reached a maximum conversion of 94 wt% after 2 h, with the yield of branched products also at a maximum after 2 h of 63 wt%. At longer reaction times, the oligomer content of the mixture increased at the expense of the BUFA. The reactions with TPP were much slower, but resulted in a significant increase in BUFA yield, reaching a maximum of 75 wt% after 6 h. Importantly, in the presence of TPP, the oligomer content was found to remain constant (at around 5 wt%) once reaction temperature was reached (Exp. 6), suggesting that most oligomers are formed during the heating stage. The TPP is probably first protonated by the abundant OA, and its adsorption onto the

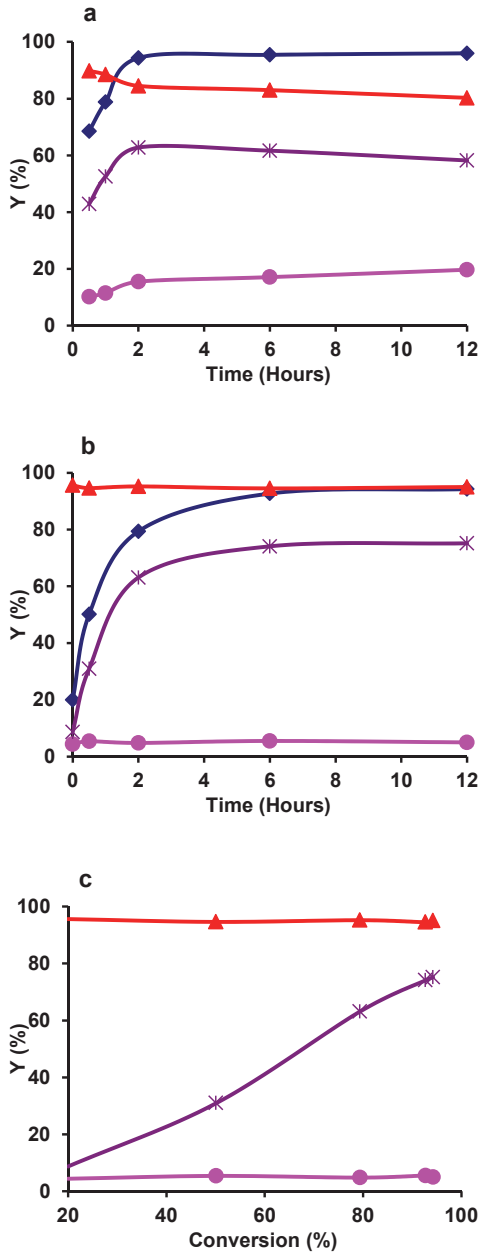

Figure 2.1: Overview of the catalytic performances of H-FER in the skeletal isomerisation of OA at 260 °C; comparison of crude production composition versus: **(a)** reaction time in absence of TPP; **(b)** reaction time in presence of TPP; **(c)** conversion in presence of TPP.
♦: OA conversion; ▲:Monomeric fraction; ×: Hydrogenated BUFA; and ●: Oligomeric fraction.

external acid sites therefore competes with this acid - base equilibrium. Up to three times less oligomer was formed with TPP.

In order to further assess the effect of catalyst deactivation on activity and selectivity, a re-use experiment (16) was carried out with spent catalyst collected from experiment 15 and subsequently washed with acetone. Conversion was found to drop by 34% (**Table 2.3**). While the ratio between the oligomer and monomer fractions remained unchanged, the selectivity towards BUFA also decreased, but to a lesser extent (20%, **Table 2.3**). These results demonstrate the severe deactivation of the catalyst after a single run.

2.3.2. Catalyst Structural Integrity

The XRD pattern recorded for the spent catalyst showed that the crystallinity was preserved under the reaction conditions. Aluminium content was determined by ICP-MS in the crude products, in the absence/presence of promoter and as a function of reaction time and feed (**Table 2.5**). Addition of TPP did not result in any significant differences in aluminium leaching after 6 h reaction (Exp. 9 versus Exp. 4). With OA, the aluminium content in the total product increased to 14 mg/kg after 12 h reaction (Exp. 5), while with MO it remained very low (below 1 mg/kg after 6 h, Exp. 13). The carboxylic acid group is, as expected, responsible for some Al leaching. The maximum Al loss from the spent catalyst samples (estimated assuming 1.79 mmol/g Al [13]) is 0.6 mol%; this seems too small to account for the severe deactivation observed.

Table 2.5: Estimation of maximum aluminium loss for the spent catalysts after 6 h reaction at 260 °C for the skeletal isomerisation of OA and MO with H-FER (5 wt% on feed).

Exp.	Feed type	Additive	Promoter	Reaction time (h)	Measured Al in product (mg/kg)	Estimated[a] Al loss from catalyst (% mol/mol)
3	OA	H_2O	-	2	0.2	0.01
4	OA	H_2O	-	6	6	0.25
5	OA	H_2O	-	12	14	0.58
9	OA	H_2O	TPP	6	4	0.17
13	MO	CH_3OH	TPP	6	0.2	0.01

a: Assuming 1.79 mmol/g Al [13].

The conservation of the catalyst structure was confirmed by nitrogen physisorption measurements (**Table 2.6**). All parameters recorded for a typical spent catalyst after calcination (calcined spent catalyst from Exp. 9) are equivalent to those obtained for the freshly activated catalyst.

Table 2.6: N_2 physisorption data of fresh and spent H-FER before/after skeletal isomerisation of OA at 260 °C (5 wt% of H-FER on feed).

Exp.	H-FER status	Promoter	Reaction time (h)	Out-gassing temp.[a] (°C)	BET area (m^2/g)	S_E, External area (m^2/g)	V_μ, Micropore volume (cm^3/g)
-	Fresh	-	-	150	255	36	0.108
-	Fresh	-	-	250	254	33	0.108
4	Spent	-	6	150	28	25	0.001
6	Spent	TPP	0	150	31	20	0.005
9	Spent	TPP	6	150	26	22	0.002
9	Spent/calcined[b]	TPP	6	250	259	33	0.112
10	Spent	TPP	12	150	26	24	0.001

a: Outgassing temperature used prior to N_2 physisorption measurements.
b: Spent catalyst calcined at 500 °C for 12 h.

2.3.3. "Coke" Formation

Thermogravimetric analyses (TGA) under air showed build up or organic deposits on the spent catalysts, and the heating profiles provided some first insight into the "coke-like" nature of these deposits. All spent catalysts showed three successive phases of mass loss (**Table 2.7** and **Figure 2.2**, exemplified for Exp. 9); the first from RT to 250 °C which is mostly due to water loss and possibly traces of acetone, the second one from 250 to 370 °C and the third one, the "soft coke" region, from 370 to 685 °C. Mass loss above 685 °C was not detected, which suggests that highly condensed polyaromatic residues are not formed in substantial amounts during the reaction [22]. Note that TPP is burning just below 300 °C under the applied TGA conditions, so it will only influence the second and not the third step, if present. The thermograms recorded for the experiments carried out without and with TPP (4 and 9 respectively) show very little difference in region 2, suggesting that most of the TPP is washed out during the acetone rinsing step of our protocol.

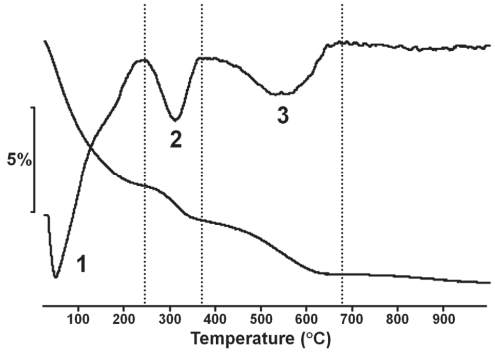

Figure 2.2: Typical thermogram recorded for a spent catalyst sample after 6 h reaction with H-FER and TPP (Exp. 9); the 1st derivative used to define the step limits of the mass losses (1, 2, 3) is also shown.

Table 2.7: Spent catalyst mass loss (%) recorded by TGA determined after 6 h reaction at 260 °C for the skeletal isomerisation of different feeds over H-FER (5 wt% on feed).

Exp.	Feed type	Promoter	Mass loss Region 2 (250-370 °C) (wt%)	Mass loss Region 3 (370-685 °C) (wt%)
4	OA	-	1.5	2.3
9	OA	TPP	1.4	2.6
11	OA+3%C18:2(**3**)	TPP	1.2	2.9
12	OA+9%C18:2(**3**)	TPP	1.3	3.0

Overall, the amount of “coke” deposited after 6 h reaction with OA and TPP corresponds to 4.0% of the initial spent catalyst weight. In the absence of promoter, somewhat less “coke” is formed after 6 h (~ 3.8 wt%). By comparison, in butene isomerisation complete blockage of the pores of protonated ferrierite (Si/Al = 13.8) was found to corresponded to 8 wt% of “coke” [22].

Addition of 9 wt% of extra linoleic acid to the feed (Exp. 12 versus Exp. 9) resulted in a 15% increase in mass loss in the second region (from 2.6 to 3.0%). This coincides with the loss of both activity and selectivity mentioned earlier and linoleic acid therefore seems to play some role in the catalyst deactivation.

N_2 physisorption data (**Table 2.6**) were recorded for a series of spent catalysts collected after 2 min to 12 h of reaction at reaction temperature (Exp. 6 to 10) in the presence of TPP. The outgassing temperature prior to the physisorption measurements was decreased from 250 to 150 °C to minimize any loss of chemisorbed components. Surprisingly, all samples showed a BET surface area of 26-31 m^2/g, corresponding to only about 10% of the initial value and hardly larger than the external area (20-25 m^2/g); the micropore volume also almost completely disappeared (below 0.005 cm^3/g). These results suggest a very quick deactivation of the catalyst by severe blockage of the pores, already after 2 min of reaction time. The presence of TPP did not influence the speed and extent of pore blockage, as no significant differences in the physisorption data were found between experiments 4 and 9. This finding is confirmed by the TGA data; mass losses measured between 380-685 °C for the same series of spent catalysts collected as a function of reaction time, show that the “coke” content remained roughly constant from the moment the mixture in the autoclave reached the reaction temperature (data not shown). This suggests that most of the “soft coke” had already been formed at this point.

2.3.4. “Coke” Composition

A combination of IR and UV-VIS spectroscopy was employed to determine the chemical nature of the “coke” components, after which the major ones were identified by NMR and GC-MS following extraction from the zeolite.

2.3.4.1. FT-IR Spectroscopy of the Spent Catalyst Material

Figure 2.3 shows the FT-IR spectra of the spent catalyst recovered from experiment 9 before and after subtraction of the relevant H-FER spectrum. The difference spectrum shows a series of negative peaks, suggesting that some "coke" components have adsorbed onto silanol (3747 cm^{-1}) and bridging Brønsted acidic OH groups (3609 cm^{-1} for the 10-MR channels and 3601 cm^{-1} for the intersections between 10- and 8-MR channels [14]); the intensity decrease should not be interpreted further however, as the sample pre-treatment conditions do not allow for the complete removal of adsorbed water. Its presence at residual level is confirmed by the band at 1640-1630 cm^{-1} (H-O-H bending vibration). Unsurprisingly, a number of absorption bands can be seen corresponding to the vibrations characteristic for the functional groups from feed and products. The presence of long chain aliphatic carbon chains is confirmed by two sets of sharp vibrations: the first ones in the stretching range have very strong intensity (ν_{asym} CH_3 at 2960 cm^{-1}, CH_2 at 2940-2936 cm^{-1} and ν_{sym} CH_2 at 2866-2865 cm^{-1}), while those in the bending range have medium intensity ($\delta_{scissors}$ CH_2 or CH_3 at 1470-1468 cm^{-1}, CH_2 next to CO (COOH or COOR) at 1415-1407 cm^{-1}, δ_{sym} CH_3 at 1384-1380 cm^{-1}). The C=O stretching region shows the presence of carbonyls originating from 3 types of carbonyl-containing functional groups: γ-lactones with a shoulder at 1772-1770 cm^{-1}, esters and/or estolides at 1752-1748 cm^{-1} [28] and fatty acids and/or dimer fatty acids at 1711-1708 cm^{-1}. The latter is characteristic of carboxylic acids involved in hydrogen bonding, either between two fatty acids or with the catalyst.

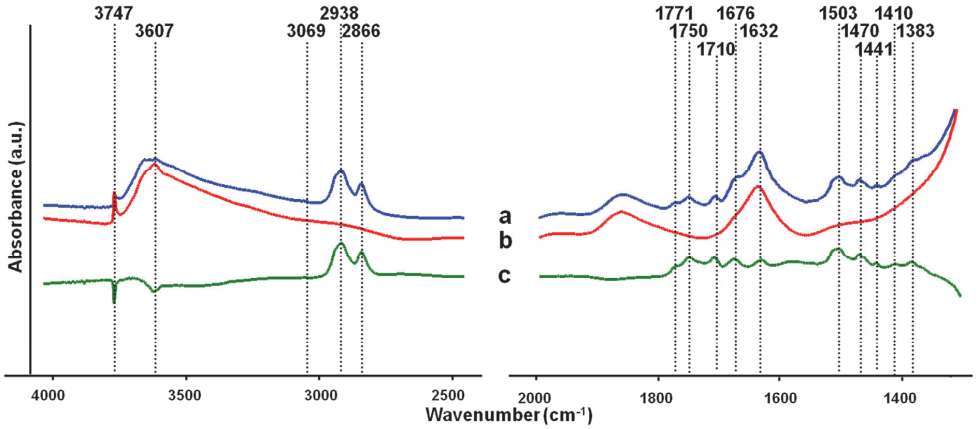

Figure 2.3: FT-IR spectra recorded for: **(a)** the spent H-FER collected after 6 h alkyl isomerisation of oleic acid in presence of TPP (Exp. 9); **(b)** the fresh catalyst and **(c)** their difference.

New bands appeared as a result of the carbonaceous deposits. Vibrations that can be attributed to various double bonds were identified (**Figure 2.4a**), of which only

one small but sharp band at 1441 cm^{-1} can be attributed solely to traces of the TPP promoter, by comparison of experiments 3 and 8 (both 2 h at reaction temperature). The strong band at 1513-1500 cm^{-1} is assigned to highly conjugated double bonds. This could point at the presence of aromatics, although only one additional small, broad band can be found at 1583-1558 cm^{-1}. Alternatively, conjugated double bonds could be part of neutral and/or cationic long hydrocarbon chains [29-31]. In **Figure 2.4b**, FT-IR difference spectra of spent catalyst samples recovered during the reaction in absence of TPP (Exp. 1 to 5) show that the intensity of the C=C vibration at 1513-1510 cm^{-1} decreased in the first two hours; the band also became broader in the course of the reaction with the appearance of a second peak above 1510 cm^{-1}, especially between 6 and 12 h. This could be explained by an increase of the aromatic "coke" and a simultaneous decrease of the conjugated double bonds in long hydrocarbon chains (neutral and/or cationic). Meunier et al. came to a similar interpretation of their FT-IR data recorded during butene isomerisation with H-FER [31].

The final feature of interest is a strong and sharp band at 1683–1673 cm^{-1}, which is found in all experiments except from those starting with MO (Exp. 13 and 14, **Figure 2.4c**). It originates from a C=O stretching vibration shifted to lower wavenumbers due to either very strong hydrogen bonding interactions and/or conjugation; this feature is tentatively assigned to a conjugated cyclic ketone thought to be a precursor to the alkylbenzenes that are detected in the "coke" extracts (see below). Other assignments can be ruled out; C=C stretching of tri- or tetra-substituted olefins, or from a trans-configuration of the double bond, would be expected above 1665 cm^{-1} based on studies of the alkylation of isobutane with n-butene over a H-FAU zeolite [29]. However, the band is absent when starting with MO, indicating involvement of the carboxylic acid head group. The frequency is also too high to allow an assignment to CO_2^- asym stretching, which would be expected at 1650-1550 cm^{-1}.

Without TPP, the first few hours of the reaction showed a significant increase of the band at 1683–1673 cm^{-1} to a maximum after about 6 h, followed by a decrease to a constant level after 6 h (**Figure 2.4b**). In the presence of the promoter, this maximum is already reached after only 0.5 h (data not shown); it seems that the TPP is therefore favoring the formation of the species responsible for this specific band.

Surprisingly, addition of extra linoleic acid in the feed (Exp. 11 and 12) did not result in much spectral variation in the infrared (data not shown), while both conversion and selectivity dropped significantly (**Tables 2.3 and 2.4**). Clearly, techniques other than FT-IR spectroscopy are needed to provide insights into specific deactivation mechanisms.

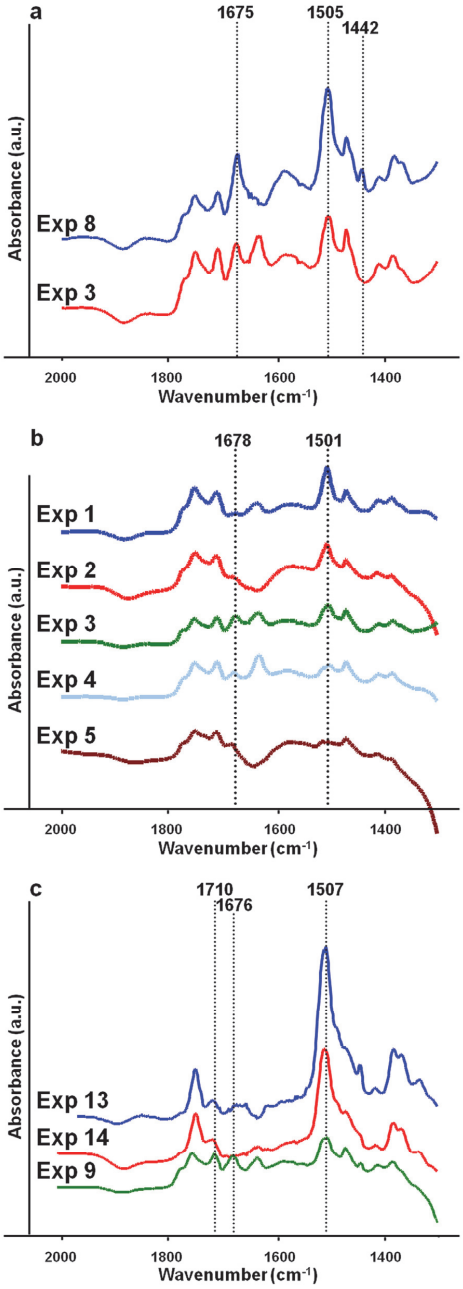

Figure 2.4: Overlay of part of the difference FT-IR spectra recorded for spent H-FER catalysts collected after: **(a)** 2 h alkyl isomerisation of oleic acid (OA) in absence of TPP (Exp. 3) and in its presence (Exp. 8); **(b)** alkyl isomerisation of OA in absence of TPP, for: 0.5 h, 1h, 2h, 6h and 12h (Exp. 1, 2, 3, 4 and 5, respectively; **(c)** 6 h alkyl isomerisation in presence of TPP of: OA/water (Exp. 9), methyl oleate (MO), and methanol/water (Exp. 14) and MO and methanol (Exp. 13).

2.3.4.2. UV-Vis Spectroscopy of the Spent Catalyst Material

Complementary information about unsaturated components and carbocations in the "coke" was provided by UV-Vis spectroscopy. H-FER, TPP, acetone, lactones and linoleic acid [33] do not absorb in the 280–800 nm range and any observed bands are therefore considered to originate from "coke" species. The spectra recorded for the spent catalysts show at least five absorption bands (**Figures 2.5a** to **2.5c**). Those at 290 nm, 355-360 nm and 440-445 nm are attributed to respectively monoenyl, dienyl and trienyl carbocations, formed through consecutive hydrogen transfer reactions [30, 32]. The structures observed at 410-415 nm and 485-490 nm can be assigned to aromatic species (methyl-substituted benzenium cations for the former) [30, 32]. The spent catalyst recovered after 2 h runs with OA, in absence and in presence of promoter (**Figure 2.5a**, Exp. 3 and 8, respectively), gave a very similar profile, with all absorption bands above 280 nm being somewhat more intense when the promoter was used. This suggests that the "coke" species that are detected in the UV-Vis spectra are mostly formed inside the catalyst structure through monomolecular processes.

The trends observed in the UV-Vis spectra of the spent catalyst samples as a function of reaction time, correlate with those seen in the FT-IR spectra. The intensities of all absorption bands attributed to enylic carbocations decreased, while those associated with aromatic species increased (**Figure 2.5b**, exemplified for Exp. 6, 7 and 9). Addition of linoleic acid (**3**) (Exp. 11 and 12 respectively) causes a significant increase in intensity of all absorption bands attributed to aromatic species, especially the one at 485-490 nm (**Figure 2.5c**). This provides further evidence for the importance of the enylic carbocations as a precursor to "coke" formation and subsequent deactivation, the additional double bonds speeding up these processes.

2.3.4.3. FT-IR, MS and NMR of the "Coke" Extract

Deposited and occluded organics were isolated by hydrofluoric acid destruction of selected spent catalysts, followed by extraction with dichloromethane, and analysed by FT-IR and NMR spectroscopy and mass spectrometry. The FT-IR spectra of all three "coke" extracts are in many ways very similar to those recorded for the spent H-FER catalysts (**Figure 2.6**, exemplified for Exp. 9). The bands characteristic of long aliphatic carbon chains can be found both in the stretching range (just below 3000 cm^{-1}) and in the bending range (at 1458-1463 cm^{-1}, 1411-1412 cm^{-1} and 1377 cm^{-1}). The carbonyl stretching range confirms the presence of a small amount of esters and/or estolides (shoulder at about 1750 cm^{-1}), along with the expected fatty acids (at 1708-1711 cm^{-1}).

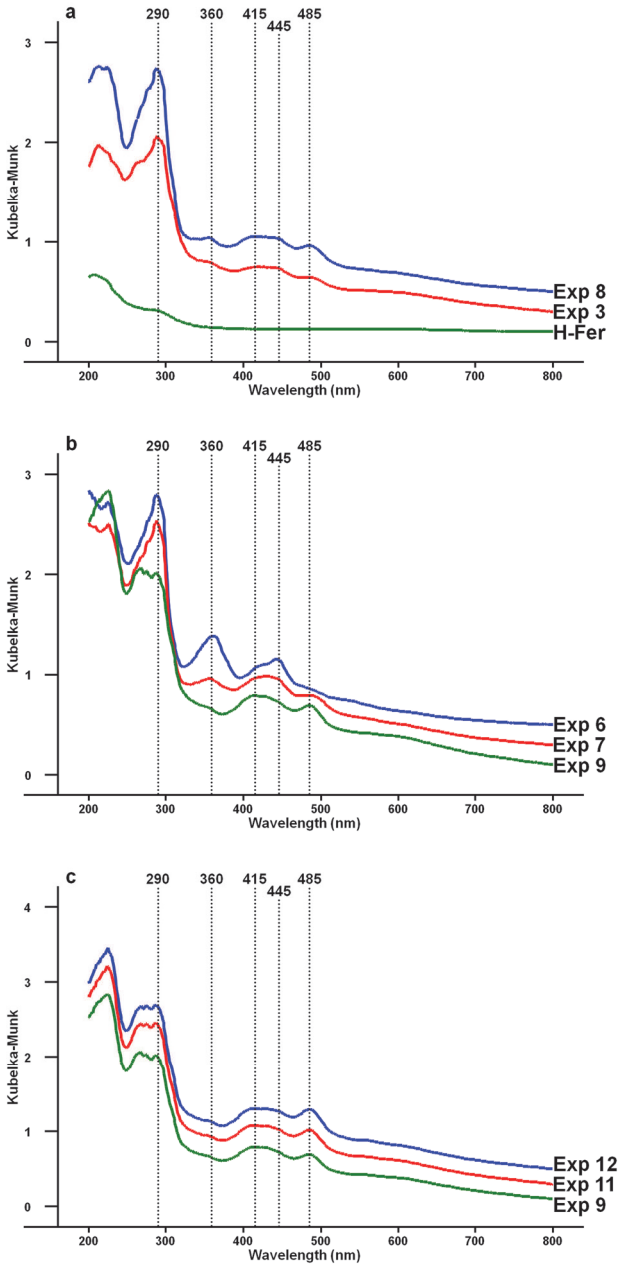

Figure 2.5: Overlay of UV-Vis spectra recorded for the spent H-FER catalysts collected after: **(a)** 2 h alkyl isomerisation of oleic acid (OA) in absence of TPP (Exp. 3) and in its presence (Exp. 8); UV-Vis spectrum of H-FER is also given; **(b)** alkyl isomerisation of OA in presence of TPP, for: 2 min, 0.5 h and 6 h (Exp. 6, 7 and 9, respectively); **(c)** 6 h alkyl isomerisation in presence of TPP for: OA, OA + 3 wt% linoleic acid (**3**) and OA + 9 wt% linoleic acid (**3**) (Exp. 9, 11, and 12, respectively); the spectra have been individually recorded and treated.

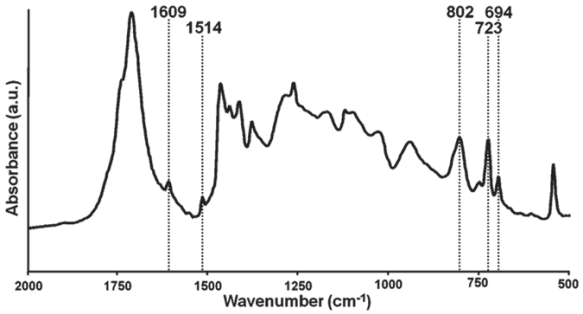

Figure 2.6: Part of the FT-IR spectrum recorded for the "coke" extract from the spent H-FER catalyst collected after 6 h skeletal isomerisation (Exp. 9, OA, 5 wt% H-FER and TPP).

However, the "coke" extracts spectra also differ from the spectra of the spent catalysts by a number of features. γ-lactones (**6**) are probably opened by the hydrofluoric acid, as they were detected. In the absence of the characteristic catalyst bands, traces of TPP-related species can be clearly found (series of bands at 1485, 1439, 1109, 1063, 750, 693 and 532 cm^{-1}). Other aromatics species, at low concentration, are confirmed by a series of bands (1610-1510 cm^{-1}), which increase in intensity in the order: experiment 4 < experiment 9 < experiment 12. The fingerprint region suggests at least the presence of ortho- (~720 cm^{-1}), para- (800-815 cm^{-1}) and monosubstituted aromatics (700-695 cm^{-1} and ~720 cm^{-1}). Another key difference with the FT-IR spectra of the spent catalysts is the absence of the two absorption bands at 1675 and 1500 cm^{-1}, which are assigned to a conjugated cyclic ketone and (poly)enylic species respectively. This proposal is consistent with their observed disappearance following HF destruction of the catalyst.

MS analysis of the "coke" extracts after high temperature chromatography (HT-GC) shows traces of TPP and a relatively large peak assigned to its oxide, possibly formed during the acid treatment. More importantly, the chromatograms of all three residues are characterised by three major peaks of which two (of similar magnitude) correspond to linear saturated carboxylic acids; palmitic (hexadecanoic) acid and stearic acid (**2**). Both components are present in the feed, but additional stearic acid is formed from OA via hydride transfer during the reaction. Being linear, both diffuse quicker into the catalyst and would be preferentially retained due to their poor solubility in acetone. The third and largest peak is a C18-compound clearly identified from its ionization fingerprint as dodecyl benzene, which must derive from the OA. Only a very small amount of condensed aromatics (e.g. substituted naphthalene) was found. Finally, HT-GC does not show any higher molecular weight components, but small amounts of C36 dimer acids (**7**) and estolides of OA (**8**) are detected by gel permeation chromatography. These species form mostly at the very

beginning of the reaction, and could contribute to early-stage blockage of the ferrierite channels.

The HT-GC-MS analyses thus strongly support the interpretation of both the FT-IR and UV-Vis data of the spent catalysts. The proposed “coke” composition is also confirmed by the NMR data recorded for the three extracts (**Figure 2.7**), in particular with regards to the presence of three types of aromatic compounds. The presence of dodecyl benzene explains the NMR peaks recorded between 7.11-7.26 ppm. The integration ratio between this latter range and the peak at 2.2–2.45 ppm (methylene alpha to the carboxylic group) is increasing in the order: 0.30 (Exp. 4), 0.42 (Exp. 9) and 0.54 (Exp. 12). NMR peaks for condensed aromatics are expected above 7.20 ppm. The promoter is not detected as TPP (chemical shift expected at 7.34 ppm), however, a number of peaks above 7.20 ppm suggest the presence of related species. Experiments without TPP show hardly any aromatic protons above 7.3 ppm. However, starting with a feed enriched in linoleic fatty acid led to an increase in the relative aromatic content, while intensity of the peaks associated with the TPP-related species remained constant. Based on the above data, there are at least two processes responsible for the formation of carbonaceous species: one leading to dodecyl benzene from the OA, and a second process that yields more condensed aromatics; the latter process is enhanced by the presence of additional double bonds on the fatty acid alkyl chains.

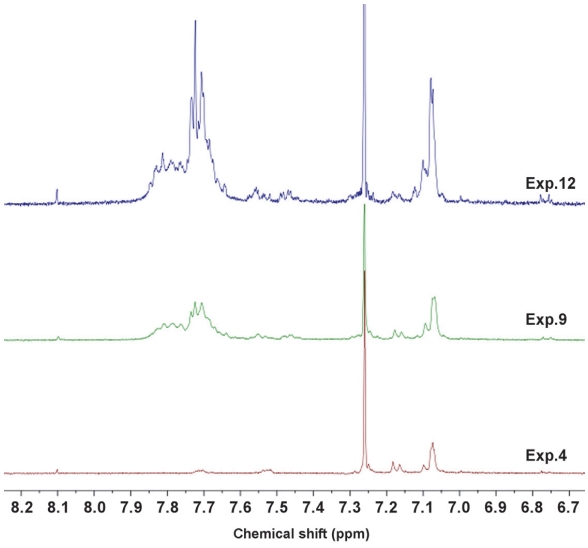

Figure 2.7: NMR spectra of “coke” extract from the spent H-FER catalysts collected after 6 h skeletal isomerisation with 5 wt% H-FER and: OA without TPP (Exp. 4), OA and TPP (Exp. 9) and OA/9% linoleic acid (**3**) and TPP (Exp. 12).

2.4. Discussion

The combination of both catalytic data and a number of analytical techniques has allowed the deactivation mechanism for the protonated zeolite ferrierite (H-FER) catalyst material during OA isomerisation to be determined. The physisorption measurements of the spent catalyst show the de facto disappearance of any micropore volume and the ten-fold reduction of BET surface area, already at the onset of the reaction and independently of the addition of TPP. Based on TGA data, the “coke” content hardly increases thereafter, suggesting that the small amount of “coke” formed is enough to lead to the observed severe pore blockage. Despite this, very high initial conversions and selectivities towards BUFA are observed, clearly indicating that the internal pore volume is hardly used. Furthermore, as TPP can only adsorb onto the external sites, catalysis therefore must mostly take place within the pore mouths. In the absence of TPP, side reactions such as oligomerisation, catalysed by the external acidic sites, have a significant effect on the product composition. Catalysis involving the entrance of the pores has been previously proposed for the hydroisomerisation of long chain n-alkanes in presence of Pt/zeolite bi-functional catalyst [34, 35]. However, these examples involve gas-phase reactions under different conditions, with feed and products that are much more volatile and lack polar functional groups; a direct comparison is therefore not possible.

UV–Vis spectroscopy suggests that unsaturated carbocations play a key role in the deactivation of the catalyst. They are formed via hydride transfer (**Scheme 2.1**) and are detected from the start of the reaction. Their concentration is highest at the onset of the reaction (when both OA concentration and acid site density are highest) and appears to decrease during the first two hours to a steady value. The (poly)enylic carbocations formed are very stable and remain almost irreversibly adsorbed at the active sites, competing with the carbocation precursor to alkyl isomerisation. They are detected by FT-IR in the spent catalyst, but (as expected) not in the extracts obtained after zeolite dissolution in HF. The (poly)enylic carbocations have been proposed to have a poisoning effect on zeolites used in liquid-phase reactions [32, 36]. Further evidence is provided by the re-use experiments: acetone washing of the spent catalyst leads to a drop of 34% in conversion, which is not the expected result if pore blockage is the sole mechanism of deactivation, because this has been shown to occur very early in the reaction without loss of activity (see above). However, an additional wash with HCl almost completely recovers the initial activity [12], indicating the presence of polar/charged organic species, which can only be displaced with highly acidic protons.

Additionally, carbocations with multiple double bonds are known to undergo cyclisation reactions [29-30], which could explain the formation of low levels of (condensed) aromatics, as revealed by FT-IR of spent H-FER catalysts and confirmed by FT-IR, MS and NMR measurements of the extract after destruction by

HF. This hypothesis is strongly supported by two independent observations: firstly, the presence of TPP increases the concentration of polyenylic carbocations and condensed aromatics, and reduces the rate of alkyl chain isomerisation. This is likely to be due to the reaction of TPP at the external surface, favouring monomolecular processes within the structure, including the formation of the polyenylic carbocations. Secondly, the concentration of both (poly)enylic carbocations and aromatics increases with the concentration of linoleic acid (**3**) in the feedstock, accompanied by a significant decrease in activity. This is due to the energetically favourable hydride extraction from conjugated double bonds, formed by positional isomerisation under the acidic conditions employed. However, based on the TGA data of the spent catalyst and NMR analyses of the extract after destruction by HF, the amount of (condensed) aromatics remains very limited and it is difficult to explain the observed severe catalyst blockage solely through this process.

MS and NMR characterisation of the extracts after destruction by HF also indicate the presence of a significant concentration of a long-chain monosubstituted alkylbenzene, i.e., dodecyl benzene. This type of aromatic must derive ultimately from OA, and Scheme 2.1 proposes a mechanism for its formation via a cyclic conjugated ketone intermediate; this mechanism is supported experimentally by the detection in FT-IR of a conjugated ketone (band at ~1675 cm^{-1}) within the spent catalyst material, which is absent when using MO as feedstock. Further evidence comes from the observation that TPP accelerates the formation of both the conjugated ketone and the long chain alkylbenzene, confirming the ketone as a likely intermediate species for this aromatic. The ketone would contribute to poisoning of the active sites, while the dodecyl benzene would participate in pore blockage.

2.5. Conclusions

The skeletal isomerisation of OA in the presence and absence of TPP has been investigated with the protonated zeolite ferrierite (H-FER) as catalyst material. Details of the pore mouth catalysis and related deactivation processes have been investigated by a combination of analytical techniques, including UV-Vis and FT-IR spectroscopy. The results confirm that this catalyst system shows superior activity and selectivity, compared to the numerous zeolite types previously investigated. Nevertheless, there is scope for improvement in its robustness to deactivation, and in designing a more efficient distribution of the reactive sites. While the ferrierite framework was found to be unaffected by the catalytic reaction, and little aluminium was leached, severe pore blockage was detected as soon as the mixture reached reaction temperature. Estolides, which are already formed during the initial heating phase, probably contribute to the first stages of blockage of the zeolite channels.

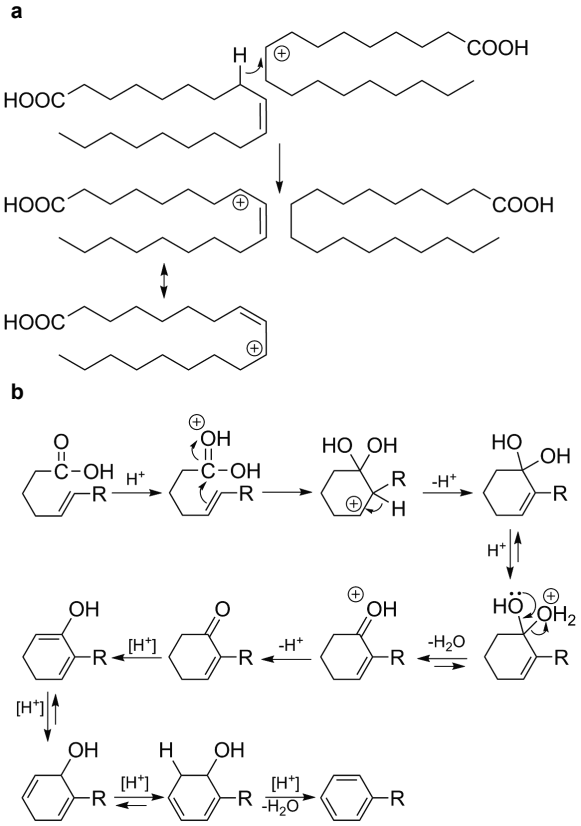

Scheme 2.1: Proposed mechanisms for the deactivation of zeolite H-FER during the skeletal isomerisation of oleic acid; **(a)** poisoning of active sites by monoenylic carbocations generated through H-transfer reactions; **(b)** formation of (long carbon chain) alkyl benzene molecules from unsaturated fatty acids after positional isomerisation of the double bond.

Coking reaches a constant level within the first minutes at reaction temperature, and this level increases with the concentration of polyunsaturated acids in the feed. Dodecylbenzene and other long chain alkylbenzenes were identified as the major “coke” constituents. They are believed to be formed from OA via a cyclic conjugated ketone.

Pore mouth catalysis is confirmed by the use of TPP, which selectively blocks non-specific surface reactions. Addition to the reactant mixture increases the selectivity to BUFA, by binding reaction sites at the zeolite external surface where oligomerisation can occur. Since the pores are already blocked at the onset of the reaction, only the pore mouth is available for the isomerisation reaction. Polyenylic carbocations, formed through hydrogen transfer reactions between reactant species are responsible for poisoning acid sites in the pore mouth and slowing down the skeletal isomerisation process. These polyenylic species eventually undergo

cyclisation, and are precursors to a very small amount of condensed aromatics. Consistent with this phenomena, higher levels of polyunsaturated acids in the feedstock enhance the above effects. Evidence for pore mouth catalysis is further substantiated in the next Chapter.

The elucidation of the mechanisms responsible for ferrierite deactivation during skeletal isomerisation of OA provides valuable insights for the industrial development of this new and promising route to BUFA.

Acknowledgements

Marius Westgaard Erichsen, Prof. dr. Unni Olsbye (University of Oslo) and Dr. Inés Lezcano González (Utrecht University) are gratefully acknowledged for their help with the HF treatment method. Dr. Tamara Eggenhuisen (Utrecht University) is thanked for helping with the physisorption measurements. Fouad Soulimani (Utrecht University) is acknowledged for his contribution to the FT-IR experiments and, together with Dr. Pieter de Peinder (VibSpec), for the fruitful discussions of the FT-IR data interpretation. Joseph Stewart (Utrecht University) and Stephan Langelaar (Croda) are thanked for carrying out the “coke” analyses by NMR and GC-MS (respectively), providing the data interpretation and contributing to the related discussions. Tanja van Bergen-Brenkman (Croda) generously shared her knowledge and experience in OA alkyl isomerisation, and carried out a number of syntheses. Negar Rashidi, Henkjan Abbes, Marvin Burger and Wim Otten (Croda) are thanked for their assistance with a number of syntheses and analyses.

References

[1] Y. Nakano, T.A. Foglia, H. Kohashi, T. Perlstein, S. Serota, J. Am. Oil Chem. Soc., 62 (1985) 888.
[2] R.M. Koster, M. Bogert, B. de Leeuw, E.K. Poels, A. Bliek, J. Mol. Catal. A: Chemical, 134 (1998) 159.
[3] S.C. Cermak, T.A. Isbell, J. Am. Oil Chem. Soc., 77 (2000) 243.
[4] M.J.A.M. Den Otter, Fet. Seife. Anstrichm., 72 (1970) 875.
[5] T.A. Isbell; R. Kleiman; B.A. Plattner, J. Am. Oil Chem. Soc., 71 (1994) 169.
[6] T. Tomifuji, H. Abe, Y. Matsumura, Y. Sakuma, US Patent 5677473 (1997), to Kao Corporation.
[7] W.R. Hodgson, W.T. Koetsier, C.M. Lok, G. Roberts, European Patent 0774451 (1996), to Unichema Chemie B.V.
[8] W.R. Hodgson, C.M. Lok, G. Roberts, W.T. Koetsier, US Patent 5856539 (1999), to Unichema Chemie B.V.
[9] Z.C. Zhang, M. Dery, S. Zhang, D. Steichen, J. Surf. Deterg., 7 (2004) 211.
[10] S. Zhang, Z.C. Zhang, Catal. Lett., 115 (2007) 3.

[11] H.L. Ngo, A. Nunez, W. Lin, T.A. Foglia, Eur. J. Lipid Sci. Technol., 108 (2007) 214.
[12] H.L. Ngo, E. Hoh, T.A. Foglia, Eur. J. Lipid Sci. Technol., 114 (2012) 213.
[13] G.D. Pirngruber, K. Seshan, J.A. Lercher, Micropor. Mesopor. Mater., 38 (2000) 221.
[14] V.L. Zholobenko, D.B. Lukyanov, J. Dwyer, J. Phys. Chem. B, 102 (1998) 2715.
[15] L. Domokos, L. Lefferts, K. Seshan, J.A. Lercher, J. Mol. Catal. A: Chemical, 162 (2000) 147.
[16] M. Trombetta, G, Busca, J. Catal., 187 (1999) 521.
[17] S. Van Donk, J.H. Bitter, K.P. de Jong, Appl. Catal. A: General, 212 (2001) 97.
[18] M. Guisnet, L. Costa, F.R. Ribeiro, J. Mol. Catal. A: Chemical, 305 (2009) 69.
[19] L. Ha; J. Mao, J. Zhou, Z.C. Zhang, S. Zhang, Appl. Catal. A: General, 356 (2009) 52.
[20] P. Granvallet, K.P. de Jong, A.G.T.G. Kortbeek, B. Kraushaar-Czarnetzki, H.H. Mooiweer, European Patent 0501577 (1992), to Shell.
[21] R.A. Comelli, Z.R. Finelli, N.S. Figoli, C.A. Querini, Stud. Surf. Sci. Catal., 111 (1997) 139.
[22] P. Andy, N.S. Gnep, M. Guisnet, E. Benazzi, C. Travers, J. Catal., 173 (1998) 322.
[23] B. Wichterlova, N. Zilkova, E .Uvarova, J. Cejka, P. Sarv, C. Paganini, J.A. Lercher, Appl. Catal. A: General, 182 (1999) 297.
[24] S. Van Donk, E. Bus, A. Broersma, J.H. Bitter, K.P. de Jong, Appl. Catal. A: General, 237 (2002) 149.
[25] S. Van Donk, E. Bus, A. Broersma, J.H. Bitter, K.P. de Jong, J. Catal., 212 (2002) 86.
[26] B. de Ménorval, P. Ayrault, N.S. Gnep, M. Guisnet, J. Catal., 230 (2005) 38.
[27] R. Rachwalik, Z. Olejniczak, B. Sulikowski, Catal. Today, 101 (2005) 147.
[28] S.M. Erhan, R. Kleiman, T.P. Abbott, J. Am. Oil Chem. Soc., 73 (1996) 563.
[29] J. Pater, F. Cardona, N.S. Gnep, G. Szabo, M. Guisnet, Ind. Eng. Chem. Res., 38 (1999) 3822.
[30] C. Paze, B. Sazak, A. Zecchina, J. Dwyer, J. Phys. Chem. B, 103 (1999) 9978.
[31] F.C. Meunier, L. Domokos, K. Seshan, J.A. Lercher, J. Catal., 211 (2002) 366.
[32] R. Klingmann, R. Josl, Y. Traa, R. Glaser, J. Weitkamp, Appl. Catal. A: General, 281 (2005) 215.
[33] B.A. Brice, M.L. Swain, S.F. Herb, J.P.L. Nichols, R.W. Riemenschneider, J. Am. Oil Chem. Soc., 29 (1952) 279.
[34] M.C. Claude, J.A. Martens J. Catal., 190 (2000) 39.
[35] W. Huybrechts, G. Vanbutsele, K.J. Houthoofd, F. Bertinchamps, C.S.L. Narasimhan, E.M. Gaigneaux, J.W. Thybaut, G.B. Marin, J.F.M. Denayer, G.V. Baron, P.A. Jacobs, J.A. Martens, Catal. Lett., 100 (2005) 235.
[36] A.N. Parvulescu, D. Mores, E. Stavitski, C.M. Teodorescu, P.C.A. Bruijnincx, R.J.M. Klein Gebbink, B.M. Weckhuysen, J. Am. Chem. Soc., 132 (2010) 10429.

Chapter 3

Large Ferrierite Crystals as Models for Catalyst Deactivation during Skeletal Isomerisation of Oleic Acid: Evidence for Pore Mouth Catalysis

Abstract

Large zeolite crystals have been used to study the deactivation of ferrierite catalyst, at the single particle level, for the alkyl isomerisation of oleic acid and elaidic acid with a combination of visible micro-spectroscopy and fluorescence microscopy (in both polarised wide-field and confocal mode). The large crystals did show the desired activity, but with only traces of the isomerisation product and low conversions being observed compared to commercial ferrierite powders. This limited activity is in line with their much lower external non-basal surface area, supporting the hypothesis that pore mouth catalysis dominates the isomerisation reaction. Further evidence for the latter comes from visible micro-spectroscopy, which shows that the accumulation of aromatic species associated with deactivation is limited to the crystal edges. Fluorescence microscopy data strongly suggest the presence of polyenylic carbocations, and images taken under polarised light reveal that these carbonaceous deposits are aligned only in the larger 10-MR channels of ferrierite at all crystal edges. The reaction is thus found to be further limited to these specific pore mouths only.

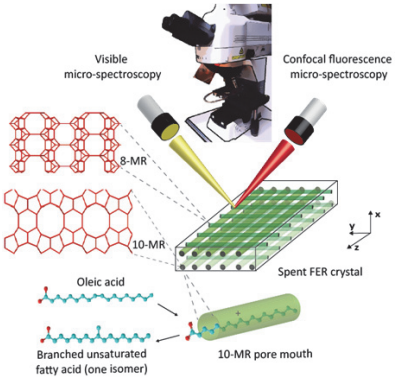

This Chapter is based on the manuscript: S.C.C. Wiedemann, Z. Ristanović, G.T. Whiting, V.R.R. Marthala, J. Kärger, J. Weitkamp, B. Wels, P.C.A. Bruijnincx and B.M. Weckhuysen, accepted for publication in Chem. Eur. J.

3.1 Introduction

The shape selectivity is considered as one of the defining properties of zeolite-based materials and originates from their well-defined internal microstructure [1], e.g. where the formation of potential bulky transition state or intermediate species is inhibited by the size of the channels (or their intersection) and cages around the active sites.

Nonetheless, the external surface may in some cases also play an important role in the selectivity of zeolite-catalysed reactions towards a particular isomer or product [2]; indeed, in the past decades a number of mechanisms have been proposed to explain non-statistical product distributions based on specific features of the outer surface of the zeolite material [3]. For example, the methyl-branching pattern observed in the hydroisomerisation of long chain n-alkanes (> C7) with one-dimensional medium-pore zeolites (e.g. of framework topologies MTT [4] and TON [5]) has been attributed to pore mouth and key-lock catalysis [6-10]. The former assumes entry of the molecule to optimise the Van der Waals interactions with the channel atoms; subsequently, branching occurs preferentially at acid sites located within the pore mouth in order to ease desorption, and the molecule shows an unimodal distribution of the methyl-branching, close to the chain end. In the key-lock configuration, both the length and polarity of the carbon chain allow it to enter by its extremities in two adjacent pores, resulting in a bimodal distribution of methyl-branching. However, the relative importance of the different models for catalysis applied to this reaction has, since their initial introduction, been subject of debate [11-12]. Enthalpic and entropic considerations, for instance, suggest that they apply only in the case of an inaccessible internal structure, or in zeolites with small-membered ring channels [13].

Pore mouth catalysis has also been postulated as an explanation for the increase in selectivity shown by protonated ferrierite (H-FER) at longer time-on-stream (TOS) in the butene to isobutene alkyl isomerisation [14-17]. Here, the concept of pore mouth catalysis is limited to the location of reaction at the extremities of the pores, since steric factors in the approach to the channel are less important with such small molecules. The improvement in isobutene selectivity, resulting from the decrease in cracking reactions, correlates with build-up of hydrocarbon deposits in the pore system [14-15]. In fact, only a small fraction (10%) of the catalyst volume is accessible to nitrogen, and hence reactants, when isobutene yield is maximum [14]. Scanning transmission electron microscopy (STEM), combined with electron energy loss spectroscopy (EELS), showed a two-stage filling process, starting at the pore inlets of the smaller channels, and then gradually progressing to the larger ones [15]. A study of diffusion in the butene to isobutene reaction by operando IR spectroscopy revealed, in the aged catalyst, the filling of the H-FER volume by slowly diffusing carbonaceous species, which is consistent with the model where the reaction is limited to the outer part of the catalyst [16]. The specific pore (mouth)

ellipticity has been held responsible for the remarkable performance at high TOS; furthermore, decreasing the crystallite volume by a factor of 8000 (and thus increasing significantly the pore mouth area per unit volume), led to a large increase in its isomerisation activity. Both pieces of evidence support the pore mouth catalysis hypothesis for this particular reaction [17].

In Chapter 2, the pore mouth catalysis model has also been proposed for the liquid-phase skeletal isomerisation of oleic acid (OA, mainly *cis*-9-octadecenoic acid) in the presence of H-FER at 260 °C (**Figure 3.1**). Despite very early pore blockage, high OA conversion and selectivity to branched-chain unsaturated fatty acids (BUFA) have been reported; the high conversion may be explained by catalysis on the external surface, however the high selectivity suggests a constrained active site with shape-selective features, such as pockets or pore mouths, to be involved. The latter proposal is further substantiated by the observation that the selectivity to BUFA over oligomerisation is enhanced by the introduction of a bulky Lewis base, such as triphenylphosphine (TPP) [18]; it is believed that such a promoter compound binds with any active sites at the external surface, eliminating residual non-shape-selective reactions there.

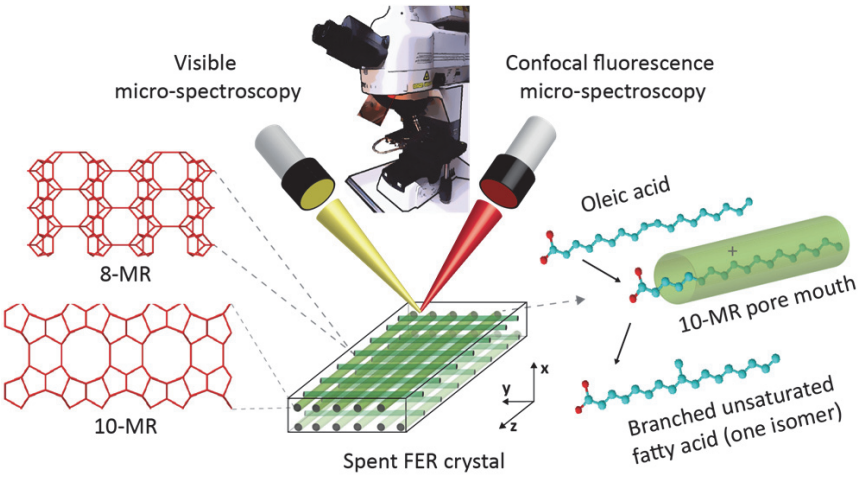

Figure 3.1: Skeletal isomerisation of OA in the presence of protonated zeolite ferrierite (H-FER); the left side of the figure illustrates the concept of pore mouth catalysis, postulated to control the selectivity of this catalytic reaction, while the right shows a schematic representation of the spent H-FER crystal analysis successively by visible and confocal micro-spectroscopy.

In Chapter 2, pore blockage was correlated to the amount of carbonaceous deposits formed in the spent catalyst powder. Long chain alkyl benzenes were identified as the major coke-like constituent. In addition, catalyst deactivation has been found to worsen by the poisoning of the pore mouth acid sites due to the formation, via hydrogen transfer reactions, of enylic carbocations. To further substantiate and confirm this model at the molecular level, the precise distribution of

carbonaceous deposits in individual zeolite crystals should be investigated, which is the aim of the current study.

To add to the complexity of this chain-branching reaction, geometric and positional isomerisation of the OA double bond also occurs under the applied reaction conditions. *Cis/trans* isomerisation has an activation energy of about 125 kJ/mol, and is known to occur during physical refining of vegetable oils above 250 °C [19]. Strong (Lewis or Brønsted) acids also catalyse geometric isomerisation at much lower reaction temperatures [20]. The crude products analysed in Chapter 2, showed indeed a significant amount of the trans-isomer elaidic acid (EA, *trans*-9-octadecenoic acid) before reaching reaction temperature, and as a result are solid at low conversion. Detection of γ-lactones in the reaction mixture shows that the zeolite material also catalyses positional isomerisation of the double bond, as this is a necessary preliminary step to the formation of lactones. These side reactions are therefore to be included in an investigation of the catalyst at the molecular level. In particular, the configuration of the double bond seems to be a key parameter in the mechanism of isomerisation, as it determines the interaction with the acid sites of the pore mouth.

Various micro-spectroscopy methods [21], including scanning transmission X-ray microscopy [22], coherent anti-Stokes Raman micro-spectroscopy [23], confocal fluorescence microscopy [24-25], UV-Vis-NIR micro-spectroscopy [26] and IR micro-spectroscopy [27-29], have been used extensively in recent years to study the spatiotemporal formation of hydrocarbons in the crystals of various zeolites and zeotypes, including ones with MFI, CHA, FER and BEA topologies [30-35]. This multi-technique approach has also been successfully applied to the study of spatiotemporal heterogeneities in e.g. individual fluid catalytic cracking catalyst particles of different age [36], or catalyst powder before/after steaming [37-39]. UV-Vis and IR micro-spectroscopies are limited in resolution, but have proven to be valuable tools for the chemical identification of hydrocarbon deposits; confocal fluorescence microscopy on the other hand enables their 3-D visualisation with a resolution down to ~ 500 nm. In addition, measurements based on absorption of polarised visible light [40], or the study of the polarisation of emitted fluorescent light [41], can be used to reveal the location *and specific orientation* in the zeolite framework of the chromophore under investigation, and link their formation and presence to specific channel types. This powerful use of polarised light in combination with micro-spectroscopy has also been applied to “coke” molecules, carbocations and their precursors which, due to their elongated structures, have a clearly oriented dipole moment vector [31-32]. It should be noted that large zeolite crystals are typically used as catalyst materials for investigations with the techniques listed above, as dictated by their spatial resolution.

Taken together, the techniques listed above have generated some detailed insights into catalyst deactivation. Carbon deposition was, for example, found to be

highly dependent on the framework type. For example, a UV-Vis micro-spectroscopy and confocal fluorescence microscopy study of the methanol-to-olefin (MTO) reaction over protonated ZSM-5 (MFI), revealed a coking profile that gradually moved from the edge of the crystal to the centre [30], with small aromatic compounds being detected through the entire crystal body and extended aromatic species blocking the straight pores near the surface [33]. In contrast, with SAPO-34 (CHA), the aromatic species responsible for deactivation remain localised at the crystal edges [30]. For protonated ZSM-5, an increase in the coking process with the acid site density was furthermore observed (as reflected by the Si/Al ratio) [31]. When switching to the CHA framework, deactivation was again found to be strongly influenced by the acid site density for the MTO reaction, while in the ethanol-to-olefin (ETO) deactivation process acid strength rather than density was found to be key [33].

Micro-spectroscopic characterisation has also provided insights into the deactivation of zeolite-catalysed liquid phase reactions [35, 40]. Mapping of carbonaceous species by confocal fluorescence microscopy, for example, highlighted the importance of the interactions between reactants and H-Beta zeolite (BEA) at the external crystal surface. The key role of these interactions in catalyst deactivation was hereby revealed in the etherification of alcohols with long linear alkenes [35].

It was anticipated that the micro-spectroscopic, multitechnique approach can be equally useful to the investigation into deactivation during the OA alkyl chain isomerisation reaction; the main “coke” components (i.e., long chain alkylbenzenes and enylic carbocations) can in principle be detected by the above-mentioned characterisation techniques. The synthesis of the large H-FER crystals required for such studies has been reported in the literature [42-43] and these model catalysts have been used in a number of fundamental diffusion studies [44-46].

In this Chapter, we build on our recent results on ferrierite deactivation obtained with bulk characterisation techniques and study the deactivation of H-FER during the skeletal isomerisation of OA using large zeolite crystals as model catalysts, in order to seek additional evidence supporting the concept of pore mouth catalysis, as illustrated in **Figure 3.1**. Scanning electron microscopy (SEM) confirmed the integrity of the large crystals after catalysis, while visible micro-spectroscopy allowed a comparison of the bulk with local electronic spectra in order to determine the nature of the carbonaceous deposits formed on the large zeolite crystals. Finally, a combination of wide-field and confocal fluorescence microscopy has enabled us, together with polarisation-dependent laser light excitation, to determine the 3-D location of the carbonaceous deposits on a number of ferrierite crystals. The different carbonaceous species were found to be located at all edges of the 10-MR channels of the large H-FER crystals, and hence at the pore mouths of these channels, providing additional experimental evidence for pore mouth catalysis in H-FER materials during the liquid-phase skeletal isomerisation of OA.

3.2. Experimental

3.2.1. Chemicals and Catalyst Materials

OA (tradename Priolene™ 6936; composition: 92.2% C18:1, 3.2% C18:2, 0.2% C18:3 and 3.7% saturated fatty acids (mainly octadecanoic acid)) was obtained from Croda. Elaidic acid (EA, > 98%) was purchased from ABCR. The EA was found to have a high content of Na^+ and K^+ (total 100 mg/kg), which was reduced by distillation to 5 mg/kg (ICP-MS). The OA contained less than 1 mg/kg Na^+ and K^+.

The different ferrierite samples used are listed in **Table 3.1**. The reference K^+-ferrierite (REF1) was activated by conversion to its protonated form, further denoted as H-FER, using an ion-exchange procedure with hydrochloric acid (HCl, 1 M) at room temperature (RT) [47], before air drying the material for three days at RT. The reference NH_4^+-ferrierite (REF2) was calcined for 5 h at 500 °C. The model, large crystal catalyst (MOD, B3 in [46]) had been treated after synthesis with sodium hydroxide (NaOH, 0.1 M) to remove any EFAl and therefore it had to be re-activated by multiple wet ion exchange (4 times NH_4NO_3, 0.5 M) and 5 h calcination at 500 °C (heating at 4 °C/min). NH_4NO_3 (> 99%) was purchased from Merck.

Table 3.1: Overview of the ferrierite samples tested in this work, including their sample name, some physicochemical properties and activation method.

Symbol	Name	Origin	Crystal size (µm)	Supplied form	Nominal Si/Al	Activation method
REF1[b]	HSZ720KOA	Tosoh	0.3–0.5	K^+	8.5[a]	Wet exchange
REF2	CP914	Zeolyst	~ 1	NH_4^+	27[a]	Calcination
MOD	B3 in [46]	[46]	> 150	Na^+	23	Wet exchange/ calcination

a: Commercial values.
b: Same batch of REF1 as used in Chapter 2.

3.2.2. Catalytic Testing

Testing of the model catalyst MOD required the use of a small-volume reactor, and some adaptation of the reaction conditions, compared to the standards described for the commercial powder catalyst REF1 in Chapter 2. All reactions were carried out with 1.0 or 2.0 wt% H-FER loading on OA in a 10 mL swagelock reactor, starting with the following amounts: 4.5 g OA or EA and 49.0 µL demineralised water. After heating to 260 °C, resulting in a calculated pressure of 7.15 bar, reaction temperature was typically held for 96.5 h, while tumbling (6 rpm), before the reactors were cooled to 50 °C and their content directly filtered using a syringe filter (PTFE, 0.20 µm).

Because of the large differences in molecular weight of the components in the crude reaction mixture, its composition was determined in two steps. First, the oligomer concentration in the crude reaction mixture was determined by high

temperature GC (HT-GC). Secondly, the monomeric fraction was separated from the oligomers by distillation at a temperature of 260 °C under a pressure of < 1 mbar. Subsequently, to reduce chemical complexity and facilitate analyses, a small amount of the collected monomeric fraction was diluted in ethyl acetate (40 mg/mL), hydrogenated at RT for 45 min using 40 mg Adam's catalyst (reduced in situ, hydrogen flow of 50 mL/min) and subjected to GC analyses.

OA (with an initial mass fraction $x_{C18:1,0}$), linoleic acid ($x_{C18:2,0}$) and linolenic acid ($x_{C18:3,0}$), are considered as the reactive components of OA; positional and *cis*/*trans* isomers are implicitly included in the simplified nomenclature. Their mass conversion (y_t) was determined by quantification of the mass fraction of stearic acid ($x_{C18,t}$) in the hydrogenated monomer fraction as a function of time t. The onset of the reaction (t = 0) is designated as the time when the reaction mixture reaches the temperature setpoint of 260 °C. A correction is made for the distillation yield of the monomeric species ($y_{M,t}$) as determined by HT-GC, and for the initial mass fraction of unreactive species, i.e. the amount of stearic acid ($x_{C18,0}$) present in OA. The mass conversion of all unsaturated components, subsequently referred to simply as "conversion", is then given by:

$$y_t = 1 - \frac{\left[\left(x_{C18,t} + x_{C18:1,t}\right) \times y_{M,t} - x_{C18,0}\right]}{\left[x_{C18:1,0} + x_{C18:2,0} + x_{C18:3,0}\right]} \quad \text{(E 3.1)}$$

Note that due to the similar molecular weights of these molecules, mole and mass conversions can be considered almost equivalent.

The selectivity towards BUFA ($s_{B,t}$) is derived from the mass fraction of all hydrogenated BUFA ($x_{B,t}$) in the hydrogenated monomer fraction. Again, a correction was made for the distillation yield of the monomeric species ($y_{M,t}$):

$$s_{B,t} = \frac{\left[x_{B,t} \times y_{M,t}\right]}{\left[\left(x_{C18:1,0} + x_{C18:2,0} + x_{C18:3,0}\right) \times y_t\right]} \quad \text{(E 3.2)}$$

The composition of the crude reaction mixtures was determined using High-Temperature GC (HT-GC) after methylation using diazomethane. The GC was equipped with a cold on-column injection and a metal column with a non-polar stationary phase Cp-SimDist Ultimetal (Chrompack WCOT, 5 m x 0.53 mm x 0.17 µm) and the components detected with a Flame Ionisation Detector (FID) based on retention time. The carrier gas was He with a constant flow of 20 mL/min. The temperature program used was: initial temperature of 60 °C, hold for 1 min; temperature increase of 30 °C/min until 150 °C; hold 0 min; temperature increase of 12 °C/min until 380 °C; hold 10 min. The detector was set at 400 °C. The injection volume was 1 µL for a concentration of 1 mg/mL.

The hydrogenated monomer fractions were analysed by GC after methylation with diazomethane. The GC was equipped with a split injection and a fused silica

capillary column with a polar stationary phase FFAP-CB (Chrompack WCOT, 25 m x 0.32 mm x 0.30 µm), and the components detected with FID based on retention time. The carrier gas was He with a constant flow of 2.1 mL/min and a split flow of 75 mL/min. The temperature program used was: initial temperature of 120 °C, hold for 0 min; temperature increase of 8 °C/min until 250 °C; hold 20 min. The detector was set at 270 °C. The injection volume was 1 µL for a concentration of 40 mg/mL.

For GC-MS identification, the crude mixtures were dissolved in heptane and the components separated by HT-GC. The GC was equipped with a cold on-column injection and a capillary column with a non-polar stationary phase ZB-1HT (Zebron Inferno, 30 m x 0.32 mm x 0.1 µm). The carrier gas was He with a constant flow rate of 2.5 mL/min. The temperature program used was: initial temperature of 50 °C, hold for 1 min; temperature increase of 15 °C/min until 400 °C; hold 20 min. The injection volume was 0.5 µL. The components were detected with a quadrupole MS detector (Agilent MSD 5975 B Inert) in electron ionization mode (70 eV). The interface temperature was set at 350 °C, the source temperature at 230 °C and the quadrupole temperature at 150 °C. The scan range was 29–1050 amu with 1.48 scans/s. The samples have been analysed directly and after hydrogenation and methylation with diazomethane.

For the *cis/trans* determination, the monomeric fractions were analysed by GC after methylation with diazomethane. The GC was equipped with a split injection and a fused silica capillary column with a highly polar stationary phase CP Sil 88 (Agilent 25 m x 0.32 mm x 0.20 µm) and the components detected by FID based on retention time. The carrier gas was He with a constant flow of 1.41 mL/min and a split flow of 141 mL/min. The temperature program used was: initial temperature of 160 °C, hold for 10 min. The detector was set at 275 °C. The injection volume was 1 µL for a concentration of 10 mg/mL.

3.2.3. Catalyst Characterisation

The scanning electron microscopy (SEM) images were recorded using a FEI XL30SFEG microscope, after sputtering with Pt/10%Pd.

The set-up used for the UV-Vis micro-spectroscopy is based on an Olympus BX41 upright microscope working in reflectance mode, equipped with a 50× 0.5 NA high working-distance microscope objective lens. A 75 W tungsten lamp was used for illumination. Reflected light was directed to a CCD video camera (ColorView IIIu, Soft Imaging System GmbH) via a 50/50 double viewport tube, and to a UV-Vis spectrometer (AvaSpec-2048TEC, Avantes BV) via a 200 µm core fibre.

The fluorescence microscopy measurements were carried out using an upright Nikon Eclipse 90i confocal fluorescence microscope, equipped with a 50× 0.55 NA dry objective lens. Both wide-field illumination and confocal scanning modes were used for imaging. For wide-field fluorescence experiments, excitation light was

provided by a Xe arc lamp. Fluorescence light was collected in reflectance mode with an EMCCD camera (QuantEM: 512SC). Two filter cubes were used to control the excitation and emission ranges: (1) BV-2A filter cube with an excitation pass band 400-440 nm, a 455 nm dichroic mirror and a long pass emission filter at 470 nm; (2) G-2A filter cube with an excitation pass band 510-560 nm, 575 nm dichroic mirror and a long pass emission filter at 590 nm. A rotatable polariser was used to selectively polarise the excitation light in order to yield the maximum and minimum of fluorescence emission. Confocal fluorescence images were recorded using excitation from two laser light sources (488 nm and 561 nm) connected to a Nikon-Eclipse A1R scanning head equipped with corresponding dichroic mirrors to reject the excitation light. The emission light was detected in the range of (400-750 nm) by using a spectral detection unit equipped with a diffraction grating and a 32 photomultiplier tube array.

3.3. Results and Discussion

The model ferrierite catalyst used in this study, further denoted as MOD, consists of large crystals with typical dimensions of 170 x 70 x 5 μm^3 and has a low Brønsted acidity (Si/Al = 23, **Table 3.1**). The large size of the zeolite crystallites, required for the Vis and (polarised) confocal fluorescence microscopy measurements for reasons of spatial resolution, means that only a relatively small external surface is available. Because the alkyl isomerisation is believed to happen within the channel pore mouths (Chapter 2), this low surface area and acidity is expected to severely limit the activity of the model catalyst, precluding a direct comparison with catalyst performance results previously reported for larger scale reactions run with conventional zeolite powders. Therefore, two additional protonated ferrierite reference samples of smaller zeolite crystal size, have been included in the smaller-scale catalytic testing for comparison; these are annotated as REF1 (Si/Al = 10) with a crystal size below 1 µm and REF2 (Si/Al = 27) with a crystal size around 1 µm.

3.3.1. Model Catalyst Morphology

SEM has been used to evaluate the morphology of the MOD crystals after activation, and after post-reaction cleaning (**Figure 3.2**). The SEM images confirm that morphology is conserved after the various physical treatments involved in the catalytic activation and testing (respectively shaking, slow swirling and filtration). Two types of zeolite crystals can be discerned; i.e., thin platelets and exfoliated platelets. Only a small amount of twinning can be seen (e.g. bottom-right corner of **Figure 3.2a**). A number of broken pieces, as well as some crystal amalgams, are clearly visible, complicating further micro-spectroscopic analysis. We therefore focused on

isolated intact crystals; their sizes vary within 3-5 μm (thickness, X), 20-90 μm (width, Y) and 150-200 μm (length, Z). It is important to note that the 10-MR channels (4.2 x 5.4 Å) run along the length of the MOD crystals, crossing perpendicularly with the 8-MR channels (3.4 x 4.7 Å) which run along the width of the crystal [48], as shown in the schematic representation of a flat crystal (**Figure 3.2c**). In the case of pore mouth catalysis, the non-basal plane external surface is the relevant parameter in estimating the number of accessible channels for reaction.

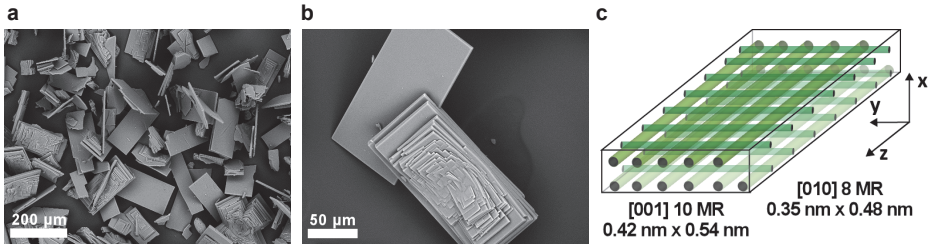

Figure 3.2: SEM images of typical MOD crystals **(a)** after activation; **(b)** after activation & alkyl isomerisation of OA (260 °C, 96.5 h, Experiment 7) and post-reaction cleaning; **(c)** depicts the microchannel orientation [48].

3.3.2. Catalytic Testing

The set of the three catalyst materials under study, i.e. MOD, REF1 and REF2, has been tested for the alkyl isomerisation of OA, at two loading levels (1.0 and 2.0 wt% on fatty acid reactant). Reactions starting from EA, before and after distillation, have also been carried out with both REF2 and MOD. Together with the blank, the design includes 12 parallel experiments of 96.5 h each at 260 °C. The experiments (Exp.), consisting of a combination of gentle tumbling for very long reaction times (8–16 times longer than in Chapter 2) were designed in a way such that the conversion with the MOD catalyst was enhanced, while preserving as much as possible its integrity. The main results of the catalytic testing are summarised in **Table 3.2**.

Despite the very long reaction times, only REF1 showed (almost) complete OA conversion at 1.0 wt% loading (96 wt%, Exp. 1). The lower OA conversion recorded for REF2 (83 wt%, Exp. 3) clearly reflects its lower total acidity (Si/Al). As expected, increasing the catalyst loading to 2.0 wt% resulted in higher conversion (97 wt% for REF1 and 96 wt% REF2, respectively; Exp. 2 and 4 in **Table 3.2**), but at the cost of selectivity to BUFA (e.g. from 68 to 65 wt% for REF2). Most of the decrease in BUFA selectivity can be explained by the increase in oligomers, while the amount of lactones formed remain approximately constant. The conversion levels obtained here for REF1 and REF2 are much higher than those reported later in Chapter 4 for standard, large-scale reactions, and at 1.5% loading. When comparing the yields from the two sets of experiments at 260 °C and at quasi-quantitative conversion, in

the present experiments the oligomers are formed at approximately twice the normal yield, at the expense of BUFA formation.

Geometric isomerisation of OA is an (acid-catalysed) equilibrium reaction with lower activation energy than the alkyl chain isomerisation, with the *cis/trans* ratio tending to ~0.5 under the given reaction temperature. As the branching reaction takes place at the pore mouth, the geometric configuration of the fatty acid is expected to have an influence on the overall reaction rate. In order to verify this influence, and potentially enhance both conversion and BUFA selectivity, pure EA was also used as substrate (Exp. 5 and 6). The commercial EA was unfortunately found to contain significant levels of Na^+ and K^+ ions, which are known to limit conversion [49], by blocking the channels, deactivating the active sites and/or lowering the acidity [50]. The detrimental effect of these cations was confirmed by a dramatic fall in conversion from 83 to 25 wt% (Exp. 5). When the EA was purified by distillation, activity and selectivity were significantly higher than in the reaction starting from OA under comparable conditions (Exp. 6 versus Exp. 3), and oligomers and lactones yields were also lower.

The conversion of OA with MOD at 1.0 wt% loading (Exp. 7) is equivalent to the control (Exp. 10), and much lower, under the same conditions, than that of REF2 of similar acidity. With EA and a 2.0 wt% catalyst loading (Exp. 9), the conversion increases by only 2 wt%, in contrast to the large increase seen with EA for the smaller ferrierite crystals. The low OA conversion measured with MOD can be attributed to the much lower (non-basal) external surface area, and thus pore mouth concentration. The very low activity of MOD is therefore consistent with the pore mouth catalysis hypothesis.

Importantly, though, the composition of the crude mixtures obtained from the MOD catalyst with OA or distilled EA (Exp. 7 and 9, respectively) clearly differs from those characterising the blanks (Exp. 10 and 12). For both OA and EA, the MOD is catalysing the *cis/trans* isomerisation towards its equilibrium value, starting from above (EA) and below (OA). Positional isomerisation also takes place over the MOD crystals, as γ-lactones are also detected (**Table 3.2** and chromatograms shown in **Figure 3.3b** for Exp. 9 with distilled EA). When starting with non-distilled EA (Exp. 8), the few acid sites available for reactions were, as expected, deactivated by the presence of Na^+, K^+. Furthermore, in the run with distilled EA and a 2.0 wt% catalyst loading (Exp. 9), BUFA traces could be identified by GC-MS. Detection of these traces required distillation, hydrogenation and methylation of the sample, to ensure adequate chromatographic resolution between branched product and linear feed (**Figure 3.3b**). The fact that they are formed, albeit in small amounts, and are not detected at all in the blank runs, shows that MOD crystals are able to catalyse the desired reaction.

Table 3.2: Crude product analysis, for the skeletal isomerisation of OA or EA over various H-FER (1.0 and 2.0 wt% loading) samples after 96.5 h at 260 °C.

Exp.	Cat.	Cat. loading (wt%)	Feed type	Oligomer yields (wt%)	BUFA yields (wt%)	Lactone yields (wt%)	Conversion (wt%)	Selectivity to BUFA (wt%)	EA/ (EA+OA) (wt%)
1	REF1	1.0	OA	20	56	9.3	96	61	68
2	REF1	2.0	OA	25	53	9.2	97	57	72
3	REF2	1.0	OA	14	54	8.1	83	68	66
4	REF2	2.0	OA	20	60	7.0	96	65	63
5	REF2	1.0	EA[a]	10	7.7	6.0	25	34	56
6	REF2	1.0	EA	11	65	5.6	89	77	59
7	MOD	1.0	OA	10	ND[b]	Traces	12	0	41
8	MOD	1.0	EA[a]	10	ND	ND	15	0	81
9	MOD	2.0	EA	11	Traces	Traces	14	≠ 0	77
10	Blank	/	OA	9	ND	ND	12	0	26
11	Blank	/	EA[a]	11	ND	ND	14	0	82
12	Blank	/	EA	10	ND	ND	12	0	87

a: Non-distilled EA contains ~ 100 ppm Na^+, K^+.
b: Not detected.

The higher rate of skeletal isomerisation with EA compared to OA suggests that the *trans* form is favoured for entry into the channels, and this is also intuitively expected as it has a smaller molecular cross-section; such shape-selective sorption has been recently demonstrated in the selective hydrogenation of methyl esters of EA over OA [51]. Under our reaction conditions, even weakly acidic sites on the external catalyst surface are thought to be able to catalyse the initial isomerisation of OA to EA. However, it is not believed to be a *prerequisite* for further reaction, as **Table 2.3** in Chapter 2 shows that reaction occurs with OA, even when the external acid sites are blocked with triphenylphosphine (TPP). Nevertheless, the reaction *rate* in the presence of TPP is significantly lower, confirming that the OA has a more hindered entry into the pore mouth. In this paper, the slow stirring conditions reduce the rate of transfer of reactants from the bulk liquid to the active sites, to the point where it is probably overall rate-limiting. The formation of EA from OA requires an additional adsorption/desorption step on an external acid site, so the slow stirring amplifies the differences seen between OA and EA. By starting with EA, under these slow stirring conditions, this additional *cis/trans* isomerisation step (mainly on the external sites) is not required, and consequently the rate of entry into the pore mouths is higher-furthermore, the final concentration of bulky by-products from

external surface reactions, such as estolides and dimerised acids, is lower resulting in a higher BUFA yield.

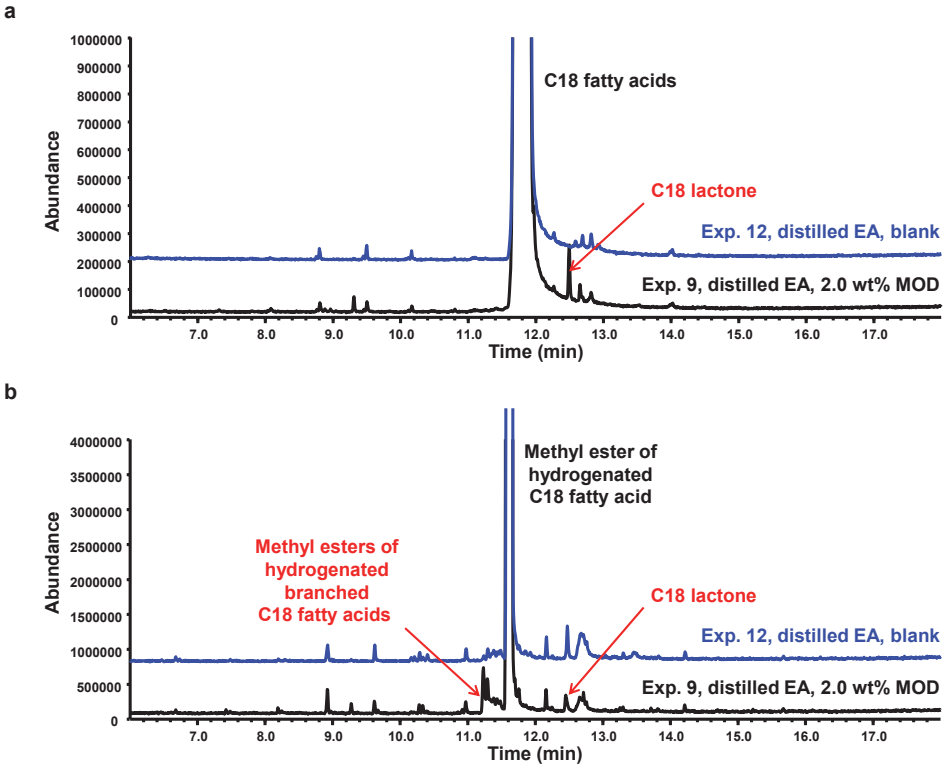

Figure 3.3: GC-MS Total Ion Chromatogram of distilled product from the alkyl isomerisation (96.5 h at 260 °C) of distilled EA: Exp. 12 in the absence of catalyst and Exp. 9 in the presence of the MOD H-FER (2.0 wt% loading); **(a)** the samples have first been analysed without derivatisation; **(b)** the same samples have been reanalysed after hydrogenation and methylation, in order to ensure resolution between methylated product and feed.

The slow stirring and very long reaction time were necessary in order to preserve the morphology of the evidently more fragile, large crystals. Despite the intrinsic experimental limitations imposed by the use of large zeolite crystals, the expected reaction intermediates, by-products and products have been observed. Geometrical isomerisation of the double bond increases significantly in the presence of the large H-FER crystal, with equilibrium being reached under the applied reaction conditions; positional isomerisation of the double bond is also confirmed by the detection of γ-lactones, absent in the corresponding control run (blank). Finally, the presence of BUFA at trace level after reaction with the large H-FER crystals is consistent with the pore mouth catalysis hypothesis; activity is significantly diminished by the much lower non-basal surface (and therefore number of pore

mouths) presented by the large ferrierite crystals (MOD) compared to the commercial reference catalysts, including REF2 of similar acidity as defined by its Si/Al ratio. In order to further confirm this working hypothesis, the spent zeolite catalyst materials have been studied using a combination of three micro-spectroscopy methods, as outlined below.

3.3.3. Spent Catalyst Characterisation

3.3.3.1. Micro-spectroscopy of Powder Reference FER Catalyst

Deactivation of the reference powdered catalysts has already been studied in detail in Chapter 2. The UV-Vis bulk diffuse reflectance (DR) spectroscopy of spent powdered catalyst (REF1) from alkyl isomerisation of OA (260 °C and 5.0 wt% loading) showed at least two types of carbonaceous deposits to be present: enylic carbocations (absorbing at 290 nm, 355-360 nm, 440-445 nm and 500-650 nm) and aromatic species (at 410-420 nm and 480-490 nm). The intensities of all absorption bands attributed to the enylic species decreased with reaction time, while those associated with the aromatic species increased with reaction time.

In this work, the same spent powder samples have been analysed by Vis micro-spectroscopy (in DR mode). The Vis spectra shown in **Figure 3.4a** are characterised by the same absorption bands above 400 nm with similar intensity trends, so that their assignment can be directly transposed. Next, these spent powder samples have been investigated by wide-field fluorescence, in order to confirm the fluorescent properties of the carbonaceous deposits, and (when possible) to optimise the excitation light to target certain specific species. **Figure 3.4b** and **3.4c** show the changes in fluorescence as a function of excitation light and reaction time (0.5 and 6 h) for the catalyst particles (crystal agglomerates). The images obtained with two different excitation ranges are shown in **Figure 3.4a**. Based on the Vis absorption data, light between 400-440 nm excites aromatic species (those with absorption at 415 nm, but also those with absorption at 480-490 nm) and trienylic carbocations (with absorption at 445 nm). The fluorescence level hardly varies between 0.5 and 6 h. Since the aromatic species are formed at an early stage of the reaction, while the enylic carbocation concentration decreases with OA conversion (Chapter 2 - **Figure 2.5**), the aromatic species must dominate the fluorescence signal. When switching to excitation light between 510-560 nm, the fluorescence originates from more conjugated systems which, based on the Vis micro-spectroscopy work, are tentatively attributed to tetraenylic carbocations absorbing at about 540 nm. While the formation of such cations requires successive hydrogen transfer reactions and their concentration must therefore be low, detection of these carbocations is aided by the high fluorescence sensitivity to such species. The fluorescence level is significant at the beginning of the reaction, and then decreases

after 6 h. This decreasing intensity also confirms that the fluorescence level is not significantly affected by any aromatic species formed, at least during the first 6 h of the reaction. This is perhaps surprising, because the characteristic absorption band (480-490 nm) of these aromatics is intense and relatively close to the excitation range; however, if they had contributed significantly to the fluorescence, its intensity would be expected to remain constant with reaction time, contrary to what is actually observed.

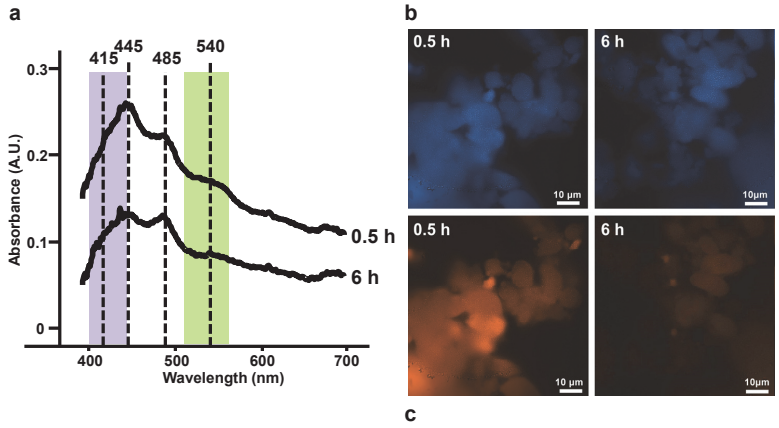

Figure 3.4: (a) Vis micro-spectroscopy spectra of two spent powder ferrierite samples (REF1) collected after performing alkyl isomerisation of OA (260 °C, 5.0 wt% loading, 0.5 and 6 h, Chapter 2 - Exp. 1 and 4 respectively); the bands (shoulders) at 445 and 540 nm are assigned to enylic carbocations, while those at 415 and 485 nm are attributed to aromatic species; the two light excitation ranges (400-440 nm and 510-560 nm) used in the wide-field fluorescence experiments are highlighted in the Vis micro-spectroscopy spectra; **(b, c)** wide-field fluorescence micro-spectroscopy images recorded for the same two spent powder ferrierite samples (REF1); the (b) images are obtained after light excitation at 400-440 nm (emission above 470 nm), while the (c) images are recorded after excitation at 510-560 nm (emission above 590 nm); the scale bars represent 10 µm.

Figure 3.5a displays a 3-D image obtained from confocal fluorescence microscopy after laser excitation at 488 nm for a spent powder ferrierite sample collected at an early stage of the reaction (REF1 at 5.0 wt% loading, 0.5 h reaction with OA at 260 °C, Chapter 2 - Exp. 1); fluorescence emissions in the range 495-545 nm and 550-600 nm are separately colour-coded. For two typical particles shown in **Figure 3.5b**, the fluorescence spectra are overlaid in **Figure 3.5c**. The latter data confirm the fluorescence to originate from different species: The fluorescence (with a maximum below 515 nm) is assigned to the aromatic species absorbing at 480-490 nm; the large shoulder between 550 and 580 nm of the fluorescence curve indicates the presence of a small number of highly conjugated and charged species, tentatively attributed to polyenylic carbocations (e.g. tetraenylic). Measured differences in fluorescence between these two particles suggest that they are differently or to

different extents deactivated, and indicate significant structural inhomogeneity of the crystal agglomerates.

Building up a spatial distribution from intensity and density of fluorescent points, the 3-D image (**3.5a**) clearly shows some disparities at this early stage of the reaction. As discussed above, aromatic species are mainly responsible for the fluorescence in the range 495-545 nm and are already present on a large number of particles; polyenylic carbocations (detected by their fluorescence in the range 550-600 nm) seem concentrated on certain agglomerates, independently of the agglomerate size. From Chapter 2, the aromatics are believed to block the channels and the polyenylic species to poison the acid sites. Therefore, the observed disparities in fluorescence suggest large differences in acidity between particles (with respect to accessibility and/or strength), for the powder ferrierite.

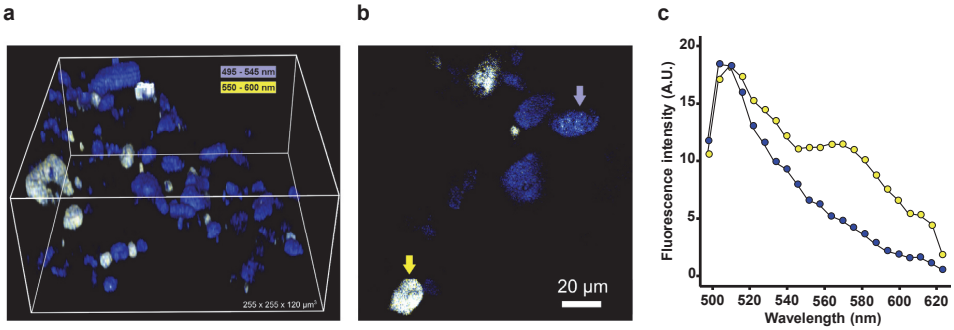

Figure 3.5: Confocal fluorescence micro-spectroscopy images of spent powder ferrierite (REF1) collected after alkyl isomerisation of OA (260 °C, 0.5 h, 5.0 wt% loading, Chapter 2 – Exp. 1): **(a)** 3-D fluorescence image of the catalyst particles after laser light excitation at 488 nm; the image is colour-coded in blue for the 495-545 nm emission and in yellow for the 550-600 nm emission; the dimensions of the volume under study are 255 x 255 x 120 μm^3; **(b)** 2-D fluorescence image; two typical particles are marked with the blue and yellow arrows; **(c)** the fluorescence spectra recorded for these particles are overlaid, using the same colour coding.

Taken together, the data mentioned above show that aromatic and polyenylic cationic species have distinct fluorescent properties, which allow the use of fluorescence microscopy to precisely locate the carbonaceous deposits formed on the zeolite during alkyl isomerisation. For the spent reference catalyst, the excitation light could be tuned to detect specific species. However, the resolution between the absorption bands is too poor to ensure selectivity with the spent model catalyst, which contains a lower level of carbonaceous deposits.

3.3.3.2. Micro-spectroscopy of Large FER Crystals

The spent powdered samples discussed above served as reference for the DR Vis micro-spectroscopy analysis of the spent large ferrierite crystals (MOD) collected

from experiments 7-9. The thin platelets are grey with darker edges (**Figure 3.6a**) and the exfoliated ones are darkened mainly at the edges (**Figure 3.6b**); in some cases, brown patches can also be seen close to the middle. A number of crystals from each type were studied, focusing on spectral differences between edges (both along Y and Z) and the rest of the basal surface YZ. Each Vis spectrum collects information from a cross-section of about 5 μm^2. As expected, the spectra recorded from most fresh crystals do not show any absorption (data not shown). A few of them show a brown patch, however, which is characterised by a band at about 415 nm; this could be the result of traces of compounds formed from thermal decomposition of organics used during the synthesis of the crystals (e.g. the pyridine solvent [45]).

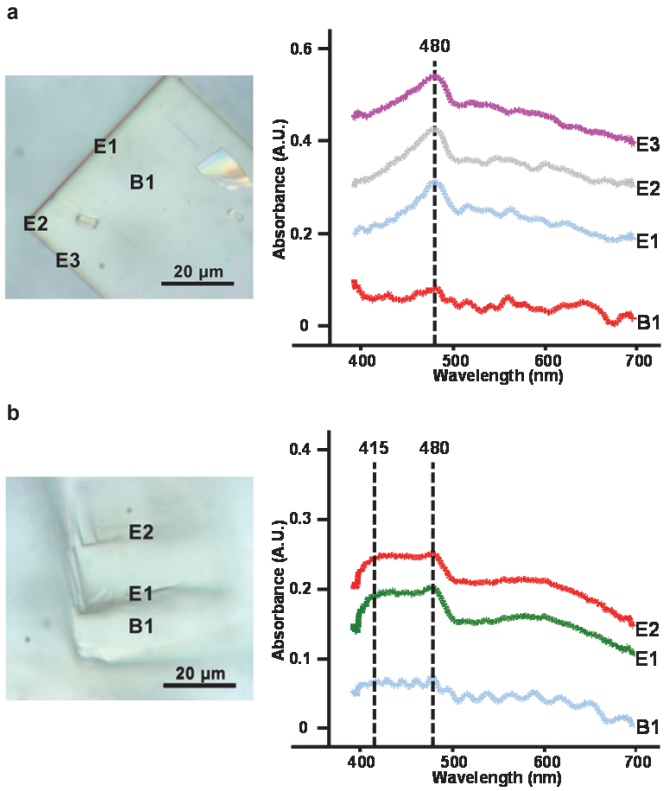

Figure 3.6: Vis micro-spectroscopy image and spectra recorded for: **(a)** a flat H-FER spent crystal (MOD) collected from experiment 7 (OA reactant with 1.0 wt% MOD loading, 260 °C, 96.5 h); **(b)** for an exfoliated H-FER spent crystal (MOD) collected from experiment 9 (distilled EA reactant with 2.0 wt% MOD loading, 260 °C, 96.5 h); each image shows the position of the sampling points, where the Vis spectra have been recorded (i.e., edges vs basal planes of the large H-FER spent crystals); the bands at 415 and 485 nm are attributed to aromatic species.

Absorption spectra recorded at the edges of a spent flat platelet from experiment 7 (OA, 1.0 wt% MOD, **Figures 3.6a**) are characterised by a distinct band

at 480-485 nm associated with aromatic species. Its intensity is somewhat stronger along the width edge (Y, E1) and at the corner E2 than along the length edges (Z, E3). Bands related to the enylic carbocations (440-445 nm) cannot be clearly seen. Importantly, Vis spectra recorded at spots on the basal surface far removed from the edges do not show any light absorption (B1). A spent exfoliated MOD crystal collected from experiment 9 (distilled EA, 2.0 wt% MOD, **Figure 3.6b**) shows similar features, with all edge spectra characterised by the 480-485 nm band (E1-E2) and those recorded in the step between two edges without any absorption (e.g. B1). In addition, a broad absorption band between 415 and 480 nm can be seen in the spectra recorded at the edges. This suggests the presence of trienylic carbocations and/or aromatic species absorbing at 415 nm.

The two spent crystals described above provide representative examples, with similar observations having been made for a number of other samples measured, including different crystal types and OA/EA feedstocks. The Vis method thus allows a first mapping of the carbonaceous deposits at all edges of the spent large crystals (MOD). Width and length edges are characterised by similar Vis spectra and therefore host the same species. By comparison with the Vis analysis of the reference ferrierite powder (REF1), the carbonaceous components must include alkyl aromatics. The detection of aromatic species in sections of the channels running within both width (Y) edges and length (Z) edges is surprising, since it suggests that *similar* carbonaceous species are produced in the 10-MR channel openings (Y edges) and the 8-MR channel openings (Z edges), despite their significant size difference; this unexpected result is later explained from the fluorescence microscopy after excitation with polarised light. Determination of any monoenylic and dienylic carbocations that are formed (absorbing below 400 nm) is not possible with Vis microscopy, and the detection of tri- and other polyenylic species is hindered by their very low level. Based on trends recorded with the reference bulk catalyst, the very long reaction time (96.5 h) would be expected to further decrease their concentration, and therefore our ability to detect them.

In addition to Vis micro-spectroscopy, polarised confocal fluorescence micro-spectroscopy has been applied in order to gain further spatial resolution, and to attempt to discriminate between the role of the 10-MR and 8-MR channels. The excitation light wavelength was first checked using flat spent crystals from experiment 9 (distilled EA, 2.0 wt% MOD), as this run did show traces of the BUFA product. To understand whether the catalyst activity plays any role in the “coking” process, images were also recorded for flat spent crystals from experiment 8 (non-distilled EA, 1.0 wt% MOD), in which conversion was much lower. The influence of double bond configuration (EA instead of OA), and crystal type (exfoliated vs. flat), are illustrated with data obtained for a spent exfoliated crystal collected from experiment 7 (OA, 1.0 wt% MOD).

Figures 3.7a and **3.7b** show the confocal fluorescence micro-spectroscopy 2-D images recorded for a flat spent crystal (MOD) from experiment 9 (distilled EA, 2.0 wt% MOD), for laser excitation at 488 nm and 561 nm (a and b, respectively).

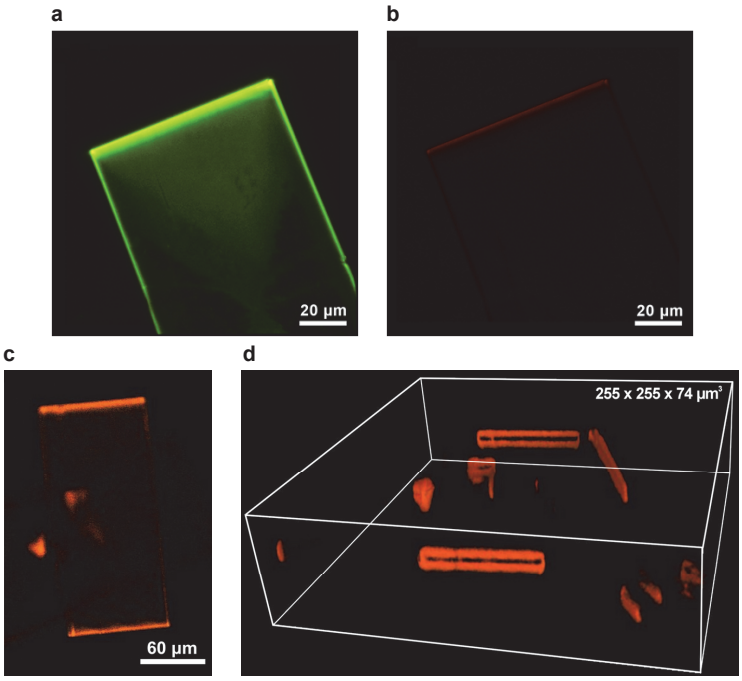

Figure 3.7: (a, b) 2-D confocal fluorescence micro-spectroscopy images recorded for a flat H-FER spent crystal (MOD) collected from experiment 9 (distilled EA reactant with 2.0 wt% MOD loading, 260 °C, 96.5 h) following laser light excitation at 488 nm (a) and 561 nm (b); similar laser power and collection time have been used to allow direct comparison; **(c, d)** confocal fluorescence micro-spectroscopy images in 2-D (c) and 3-D (d) recorded for a flat H-FER spent crystal (MOD) collected from experiment 8 (non-distilled EA reactant with 1.0 wt% MOD loading, 260 °C, 96.5 h) following laser light excitation at 561 nm; laser power has been increased to enable visualisation of the fluorescent carbonaceous species; the dimensions of the volume under study are 255 x 255 x 74 μm^3.

The micro-spectroscopy Vis spectra recorded for the spent powder catalyst (REF1, **Figure 3.4**) and the spent crystals (MOD, **Figure 3.6**) are used to help with the assignment of the carbonaceous species responsible for the observed fluorescence with the flat spent crystal (MOD) from experiment 9. Results obtained with the spent large crystals are similar to those observed with the spent reference powders: excitation with light of 488 nm (**Figure 3.7a**) seems optimum, as the aromatic species absorb at 480-485 nm, again giving the image with the highest fluorescence intensity. Polyenylic carbocations are excited by 561 nm laser (**Figure 3.7b**), although their measured intensity is weak due to their very low concentration. The high sensitivity of the fluorescence method for such species, and its approach from the low energy end

of the spectrum, helps to detect them while minimising interference from the aromatics that absorb at lower wavelengths.

In both cases (**Figures 3.7a and 3.7b**), the fluorescent species are clearly restricted to the edges, independently of the excitation laser and therefore their nature. Interestingly, the fluorescent edges of the width (which house the pore mouths of the 10-MR channels) seem more intense than those of the length (which house the pore mouths of the 8-MR channels). Similar observations can be made when switching feedstock to OA (data not shown). The images delivered by this method for the flat crystal are consistent with the mapping recorded from the Vis absorption microscopy, i.e. they show that similar aromatic species are present on *both* the width and length edges of the crystals, albeit with differing intensities.

Additionally, **Figure 3.7** shows the 2-D (c) and 3-D (d) fluorescence microscopy images of a flat spent crystal (MOD) from experiment 8 (non-distilled EA, 1.0 wt% MOD) after excitation at 561 nm. The results show that already at lower conversion (compared to experiment 9), the deposits (and therefore the reaction) are already restricted to the very edges of the width cross section. The 3-D image pinpoints the precise location as the width edge *corners*, the central area of the width cross-section being free from deposits. This is a surprising finding, as “coke” may be expected to cover the complete (10-MR) edge area in a uniform layer. The inhomogeneous deposition observed seems too distinct and regular to be explained solely by the easier approach of the bulky reactant molecules to these exposed edges, and/or the more favourable location for growth of the larger carbonaceous species. The distinct hollowing of the width of the crystals, as evidenced by closer inspection of the SEM images, is postulated to be the result of preferential desilication (by the NaOH post-treatment/cleaning) and that this inhomogeneity of the width structure is the reason for the distinct localisation of the fluorescence.

The distribution of the carbonaceous deposits at the very edges of the crystal has been studied in more detail. **Figure 3.8** shows wide-field fluorescence micro-spectroscopy 2-D images following excitation at 510-560 nm recorded for the flat spent crystal (MOD) from experiment 8 (non-distilled EA, 1.0 wt% MOD), the same crystal imaged in **Figures 3.7c and d**. Based on the Vis adsorption and fluorescence results presented earlier for the spent powder catalyst (REF1), the fluorescence is tentatively attributed to the polyenylic carbocations. When polarisation is parallel to the crystal length (**Figure 3.8b**), light is clearly emitted from most edges, with a thicker and more homogeneous fluorescent band at the width edges. For this platelet crystal, the thickness of the fluorescent width edges is estimated at about 5 µm, while the thickness of the length edges is estimated at about 3 µm (**Figure 3.8c**). Again, emission is especially strong at the corners, and is also visible at a crack in the crystal. However, when rotating the crystal by 90° (**Figure 3.8a**), the edges can no longer be seen, while a small crystal (piece) with a perpendicular orientation appears via the fluorescence of its edges (as indicated by the arrow in **Figure 3.8a**). This

result confirms the transition dipole moment orientation of the fluorescent species along the crystal length, and therefore along the 10-MR channels. Fluorescence along the two length edges cannot be explained by "coking" of the 8-MR channel openings; these are perpendicular to the polarisation and their diameter seems too small to allow a perpendicular orientation of the fluorescent molecules there, knowing that these species are already constrained in the larger 10-MR channels. The two fluorescence bands are also too thick (well above 500 nm) to be attributed to a monolayer of molecules at the pore mouths. Therefore, the fluorescence must originate from accessible 10-MR channels running along the length edges.

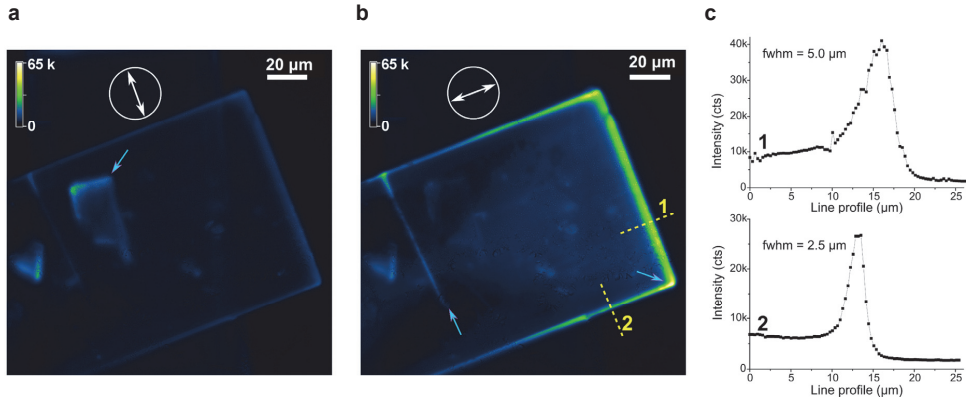

Figure 3.8: Polarised 2-D wide-field fluorescence micro-spectroscopy images recorded for a flat spent H-FER crystal (MOD) collected from experiment 8 (non-distilled EA reactant with 1.0 wt% MOD loading, 260 °C, 96.5 h) following light excitation at 510-560 nm (emission above 590 nm); the excitation light has been polarised, as indicated by the double arrows, along the 8-MR channels (image **a**) and along the 10-MR channels (image **b**); graph **c** shows the estimation of the fluorescence thickness of the width edge and the length edge, curves 1 and 2 respectively.

Similar conclusions can be drawn for the exfoliated spent model crystals (MOD). **Figure 3.9** shows a 2-D image obtained by polarised confocal fluorescence micro-spectroscopy after excitation at 488 nm (aromatic species) for a specific exfoliated crystal from experiment 9 (distilled EA, 2.0 wt% MOD). Its crossed structure allows direct visualisation of the light polarisation effect. **Figure 3.9a** clearly shows the light emitted by all edges from the bottom sub-structure with the length parallel to the polarisation, while the edges from the perpendicular top sub-structure are not visible. When rotating the crystal by 90° (**Figure 3.9b**), the edges of the top sub-structure become visible via their fluorescence, while those of the bottom one disappear. This again clearly confirms the orientation of the aromatic species along the length and the 10-MR channels.

The presence of carbonaceous species exclusively in the 10-MR channels is supported by the experimental evidence reported in Chapter 4, where the relationship between ferrierite acidity and performance was studied for five

commercial catalysts; initial pore conversion was found to correlate with Brønsted acidity in the 10-MR channels, as determined by adsorption/desorption of pyridine and FT-IR. With the 10-MR extremities occupied and blocked by the “coke” species, the observed fluorescence distribution is clearly consistent with the alkyl isomerisation reaction being restricted to the pore entrance, and therefore further supporting the pore mouth catalysis hypothesis. Additional evidence comes from Chapter 2, in which pore blockage has been found to occur at the very beginning of the reaction (as soon as the reaction temperature is reached).

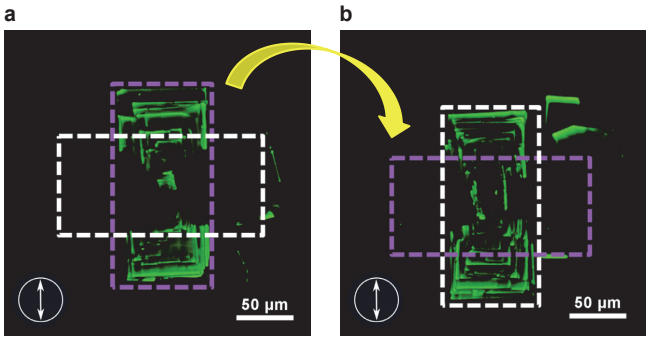

Figure 3.9: Polarised 2-D wide-field fluorescence micro-spectroscopy images recorded for a crossed exfoliated spent H-FER crystal (MOD) collected from experiment 9 (distilled EA reactant with 2.0 wt% MOD loading, 260 °C, 96.5 h) following laser light excitation at 488 nm; in image **(a)**, only the bottom part of the crystal, where the 10-MR channels are aligned along the (laser) polarised light, is visible via the fluorescence of the carbonaceous species; after rotation by 90°of the sample support, image **(b)** shows exclusively the top part of the crystal.

The restriction of carbonaceous species to the very edges of the crystal is different from earlier findings reported for H-ZSM-5 in the conversion of alcohols to olefins, where a gradual “coking” from the edges to the centre has been observed [30]. With SAPO-34 on the other hand, the narrow windows characteristic of the CHA framework block the formation of carbonaceous deposits at the edges of the crystal, resulting in rapid deactivation of the catalyst [30]; this mode of “coke” formation and deactivation is somewhat closer to that seen in H-FER. Although the pore mouth size of the studied ferrierite catalysts is optimal for the alkyl isomerisation reaction, their crystal morphology is far from ideal, as only the pore mouths of the 10-MR channels at the width cross-section are actively employed in the catalysis. Reduction of the crystal size has the expected effect of increasing the activity of the catalyst, simply by increasing the pore mouth concentration per unit volume/mass - in the study above, we estimate a factor of ~ 40 times when comparing the model crystals to the reference commercial ferrierites. Further optimisation of the morphology could, for instance, be focused on the synthesis of thin, platelet-like crystals in which the 10-MR channels run perpendicular to the basal plane. Relatedly, Roberts et al. investigated the alkyl isomerisation of unsaturated fatty acids using zeolite types

omega (MAZ), mordenite (MOR) and L (LTL); they similarly confirmed the importance of the crystal morphology to reactivity and selectivity, and proposed a minimum crystallite diameter to depth ratio of 10 [53-54].

3.4. Conclusions

The liquid-phase skeletal isomerisation of OA and EA has been carried out over large ferrierite model crystals (MOD). A combination of Vis and polarised confocal fluorescence microscopy has been applied to the spent catalyst materials in order to gain insights - at the single particle level - into the deactivation mechanisms, and to provide support to the earlier proposed concept of pore mouth catalysis.

SEM has confirmed the integrity of the MOD catalyst after activation and reaction under the selected conditions. Two types of large H-FER crystals are identified, namely thin and exfoliated zeolite platelets. Despite their very low non-basal surface area and pore mouth density, careful selection of the reaction conditions (i.e., slow stirring and long reaction time) enabled the catalysis of geometrical, positional and (to a minor extent) alkyl isomerisation.

Comparison of the catalytic results obtained for the MOD catalyst and the commercial powdered zeolite ferrierite material references REF1 and REF2, shows that the large crystals are indeed valid models for the study of catalyst deactivation during the skeletal alkyl isomerisation of OA. The results also point at importance of crystal size (and thus number of pore mouths per unit mass) for catalyst activity and BUFA yields and provide evidence for pore mouth catalysis.

The spent zeolite catalyst materials have subsequently been studied by a combination of microscopy and micro-spectroscopy techniques. Using Vis micro-spectroscopy, aromatic species could be identified in the model catalysts. The presence of traces of more conjugated species, such as polyenylic carbocations, is suggested by fluorescence microscopy. Both species are shown to be formed, independently of double bond configuration (OA or EA) and crystal type.

With respect to the spatial mapping, Vis microscopy shows the same aromatic species at most edges of the spent large crystals (MOD), once again independently of crystal type and feedstock. The spatial resolution of the (confocal) fluorescence micro-spectroscopy confirms that all carbonaceous deposits are located at most edges in both thin and exfoliated zeolite platelets, as well as at a number of fissures in flat crystals. In addition, polarisation of the excitation light has revealed their presence *exclusively* in the 10-MR channels: close to the opening of the 10-MR channels, these deposits result in complete blockage, while the absence of “coke” species deeper into the 10-MR channels confirms that access has been prevented. Deposits found at the length edges suggest that some coking of the 10-MR channels also runs along these edges; we hypothesise that this is due to imperfections in the

external 10-MR channel wall, created either during manufacture or due to attrition in the reaction.

In conclusion, the investigation of spent large ferrierite crystals after skeletal isomerisation of OA and EA provided further experimental evidence for the existence of pore mouth catalysis in H-FER materials. Our study confirms that only a very limited number of acid sites are accessible to the reactant, despite the ideal pore size and acidity of ferrierite for this reaction. Therefore, activity could be further enhanced by better catalyst design, opening up the potential for an effective and economically viable catalytic route to selective alkyl branching of natural lipid materials.

Acknowledgements

Dr. Reddy Marthala and Prof. dr. Jens Weitkamp (University of Stuttgart), Prof. dr. Jörg Kärger (University of Leipzig) are gratefully acknowledged for providing the large ferrierite crystals. Zoran Ristanović and Dr. Gareth Whiting, (Utrecht University) are acknowledged for performing the fluorescence microscopy measurements, for providing their insights and expertise in the related discussions, and for their contribution to Figure 3.1. Marjan Versluijs-Helder (Utrecht University) is thanked for performing the SEM analyses, and Marjolein Velthoen and Suzanne Verkleij (Utrecht University) are acknowledged for helping with the Vis micro-spectroscopy. Tanja van Bergen-Brenkman, Negar Rashidi, Marvin Burger and Stephan Langelaar (Croda) are thanked for performing a number of syntheses and analyses used in this study.

References

[1] F.R. Ribeiro, F. Alvarez, C. Henriques, F. Lemos, J.M. Lopes, M.F. Ribeiro, J. Mol. Catal. A: Chemical, 96 (1995) 245.
[2] J.P. Gilson and E.G. Derouane, J. Catal., 88 (1984) 538.
[3] T.F. Degnan, J. Catal., 216 (2003) 32.
[4] S. Ernst, R. Kumar, J. Weitkamp, Catal. Today, 3 (1988) 1.
[5] S. Ernst, J. Weitkamp, J.A. Martens, P.A. Jacobs, Appl. Catal., 48 (1989) 137.
[6] M.C. Claude, J.A. Martens, J. Catal., 190 (2000) 39.
[7] J.A. Munoz Arroyo, G.G. Martens, G.F. Froment, G.B. Marin, P.A. Jacobs, J.A. Martens, Appl. Catal. A: General, 192 (2000) 9.
[8] J.A. Martens, G. Vanbutsele, P.A. Jacobs, J.F.M. Denayer, R. Ocackoglu, G. Baron, J.A.M. Arroyo, J.W. Thybaut, G.B. Marin, Catal. Today, 65 (2001) 111.
[9] M.C. Claude, G. Vanbutsele, J.A. Martens, J. Catal., 203 (2001) 213.
[10] W. Huybrechts, G. Vanbutsele, K.J. Houthoofd, F.Bertinchamps, C.S.L. Narasimhan, E.M. Gaigneaux, J.W. Thybaut, G.B. Marin, J.F.M. Denayer, G.V. Baron, P.A. Jacobs, J.A. Martens, Catal. Lett., 100 (2005), 235.
[11] T.L.M. Maesen, M. Schenk, T.J.H. Vlugt, J.P. de Jonge, B. Smit, J. Catal., 188 (1999)

403.
[12] G. Sastre, A. Chica, A. Corma, J. Catal., 195 (2000) 227.
[13] T.L.M. Maesen, R. Krishna, J.M. van Baten, B. Smit, S. Calero, J. M. Castillo Sanchez, J. Catal., 256 (2008) 95.
[14] P. Andy, N. S. Gnep, M. Guisnet, E. Benazzi, C. Traversy, J. Catal., 173 (1998) 322.
[15] S. van Donk, J.H. Bitter, K.P. de Jong, Appl. Catal., A: General, 212 (2001) 97.
[16] F.C. Meunier, L. Domokos, K. Seshan, J.A. Lercher, J. Catal., 211 (2002) 366.
[17] S-H. Lee, C-H. Shin, S.B. Hong, J. Catal., 223 (2004) 200.
[18] H.L. Ngo, R.O. Dunn, E. Hoh, Eur., J. Lipid Sci. Technol., 114 (2012) 213.
[19] C. Scrimgeour, in *Bailey's Industrial Oil and Fat Products* (eds. F. Shahidi), John Wiley & Sons Inc., New York (2005) pp 1-43.
[20] T.A. Isbell, R. Kleiman, B.A. Plattner, J. Am. Oil Chem. Soc., 71 (1994) 2, 169.
[21] B.M. Weckhuysen, Angew. Chem. Int. Ed., 48 (2009) 4910.
[22] A.M. Beale, S.D.M. Jacques, B. M. Weckhuysen, Chem. Soc. Rev., 39 (2010) 4656.
[23] M.H.F. Kox, K.F. Domke, J.P.R. Day, G. Rago, E. Stavitski, M. Bonn, B.M. Weckhuysen, Angew. Chem. Int. Ed., 48 (2009) 8990.
[24] G. De Cremer, B.F. Sels, D.E. De Vos, J. Hofkens, M.B.J. Roeffaers Chem. Soc. Rev., 39 (2010) 4703.
[25] K.P.F. Janssen, G. De Cremer, R.K. Neely, A.V. Kubarev, J. van Loon, J.A. Martens, D.E. De Vos, M.B.J. Roeffaers, J. Hofkens, Chem. Soc. Rev., 43 (2014) 990.
[26] R.A. Schoonheydt, Chem. Soc. Rev., 39 (2010) 5051.
[27] E. Stavitski, B.M. Weckhuysen, Chem. Soc. Rev., 39 (2010) 4615.
[28] C. Chmelik, J. Kärger, Chem. Soc. Rev., 39 (2010) 4864.
[29] J. Kärger, T. Binder, C. Chmelik, F. Hibbe, H. Krautscheid, R. Krisna, J. Weitkamp, Nature Mater., 13 (2014) 333.
[30] D. Mores, E. Stavitski, M.H.F. Kox, J. Kornatowski, U. Olsbye, B.M. Weckhuysen, Chem. Eur. J., 14 (2008), 11320.
[31] D. Mores, J. Kornatowski, U. Olsbye, B.M. Weckhuysen, Chem. Eur. J., 17 (2011) 2874.
[32] J.P. Hofmann, D. Mores, L.R. Aramburo, S. Teketel, M. Rohn, J. Janek, U. Olsbye, B.M. Weckhuysen, Chem. Eur. J., 19 (2013) 8533.
[33] Q. Qian, J. Ruiz-Martinez, M. Mokhtar, A.M. Asiri, S.A. Al-Thabaiti, S.N. Basahel, B.M. Weckhuysen, Catal. Today, 226 (2014) 14.
[34] Q. Qian, J. Ruiz-Martinez, M. Mokhtar, A.M. Asiri, S.A. Al-Thabaiti, S.N. Basahel, B.M. Weckhuysen, ChemCatChem., 6 (2014) 772.
[35] A.N. Parvulescu, D. Mores, E. Stavitski, C.M. Teodorescu, P.C., P.C.A. Bruijnincx, J.M.K. Gebbink, B.M. Weckhuysen, J. Am. Chem. Soc., 132 (2010) 10429.
[36] I.L.C. Buurmans, B.M. Weckhuysen, Nat. Chem., 4 (2012) 873.
[37] L.R Aramburo, E. de Smit, B. Arstad, M.M. van Schooneveld, L. Sommer, A. Juhin, T. Yokosawa, H.W. Zandbergen, U. Olsbye, F.M.F. de Groot, B.M. Weckhuysen, Angew. Chem. Int. Ed., 51 (2012) 3616.
[38] L.R Aramburo, J. Ruiz-Martinez, L. Sommer, B. Arstad, R. Buitrago-Sierra, A. Sepúlveda-Escribano, H.W. Zandbergen, U. Olsbye, F.M.F. de Groot, B.M. Weckhuysen, ChemCatChem., 5 (2013) 1386.
[39] L.R Aramburo, S. Teketel, S. Svelle, S.R. Bare, B. Arstad, H.W. Zandbergen, U. Olsbye, F.M.F. de Groot, B.M. Weckhuysen, J. Catal., 307 (2013) 185.
[40] M.H.F. Kox, E. Stavitski, B.M. Weckhuysen, Angew. Chem. Int. Ed., 46 (2007) 3652.
[41] C. Sprung, B.M. Weckhuysen, J. Am. Chem. Soc., 137 (2015) 1916.
[42] A. Kuperman, S. Nadimi, S. Oliver, G.A. Ozin, J.M. Garcés, M.M. Olken, Nature, 365

(1993) 239.
[43] R.E. Morris, S.J. Weigel, Chem. Soc. Rev., 26 (1997) 309.
[44] J. Kärger, P. Kortunov, S. Vasenkov, L. Heinke, D. B. Shah, R. A. Rakoczy, Y. Traa, J. Weitkamp, Angew. Chem. Int. Ed., 45 (2006) 7846.
[45] V.R.R. Marthala, M. Hunger, F. Kettner, H. Krautscheid, C. Chmelik, J. Kärger, J. Weitkamp, Chem. Mater., 23 (2011) 2521.
[46] F. Hibbe, V.R.R. Marthala, C. Chmelik, J. Weitkamp, J. Kärger, J. Chem. Phys., 135 (2011) 184201.
[47] R. Rachwalik, Z. Olejniczak, B. Sulikowski, Catal. Today, 101 (2005) 147.
[48] P.A. Vaughan, Acta Crystallogr., 21 (1966) 983.
[49] H.L. Ngo, A. Nunez, W. Lin, T.A. Foglia, Eur. J. Lipid Sci. Technol., 108 (2007) 214.
[50] J. Datka, M. Kawalek, K. Góra-Marek, Appl. Catal., A: General, 243 (2003) 293.
[51] A. Philippaerts, S. Paulussen, S. Turner, O. Lebedev, G. Van Tendeloo, H. Poelman, M. Bulut, F. De Clippel, P. Smeets, B. Sels, P. Jacobs, J. Catal., 270 (2010) 172.
[52] W.R. Hodgson, C.M. Lok, G. Roberts, W.T. Koetsier, European patent 0774451 (1997), to Unichema Chemie B.V.
[53] W.R. Hodgson, W.T. Koetsier, C.M. Lok, G. Roberts, US patent 5856539 (1999), to Unichema Chemie B.V.

Chapter 4

Skeletal Isomerisation of Oleic Acid over Ferrierite: Influence of Acid Site Number, Accessibility and Strength on Activity and Selectivity

Abstract

Protonated ferrierite (H-FER) shows superior activity and selectivity in the liquid-phase isomerisation of linear unsaturated fatty acids to (mono-)branched-chain unsaturated fatty acids, (Mo)BUFA. This high selectivity is remarkable, as most of the interior surface of the zeolite is blocked already at the onset of reaction, limiting reaction to the pore mouth. A detailed study of the relationship between ferrierite acidity and performance is reported for five commercial catalyst materials; significant differences were found, independently of their bulk Si/Al ratios. Initial pore conversion correlates with Brønsted acidity in the 10-MR channels, as determined by adsorption/desorption of pyridine and FT-IR spectroscopy. A low density of external acid sites reduces oligomerisation of fatty acids, while a high ratio of Brønsted to Lewis sites explains the observed high BUFA yield. The combination of FT-IR with CO adsorption, and temperature-programmed desorption of NH_3, confirms that the presence of strong *but few* Brønsted acid sites in the 10-MR channels increases selectivity to MoBUFA.

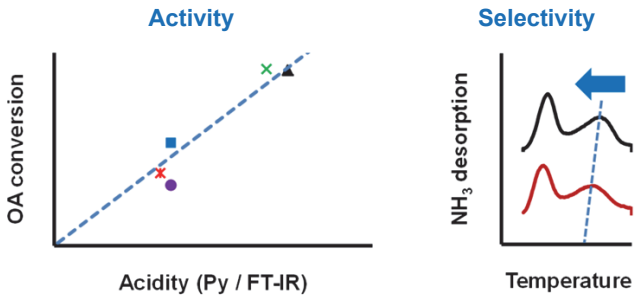

This Chapter is based on the manuscript: S.C.C. Wiedemann, A. Muñoz-Murillo, R. Oord, T. van Bergen-Brenkman, B. Wels, P.C.A. Bruijnincx, B.M. Weckhuysen, J. Catal., 329 (2015) 195 (DOI:10.1016/j.jcat.2015.05.013).

4.1. Introduction

In the gas phase isomerisation of butene to isobutene, the major challenge in achieving a high selectivity to isobutene is addressing the competition with butene oligomerisation, as both reactions share the same carbocation transition state. The remarkable selectivity and stability of the medium-pore zeolite ferrierite for this reaction, has been extensively studied [1-3]. Although the exact mechanism of isomerisation is still a matter of discussion, the excellent performance of this zeolite is commonly agreed to be a direct consequence of its unique topology, as described in Chapter 1 (section 1.11). In addition to pore size, the void volume available at the channel intersections must also play a role. When compared to MFS and STI (two other two-dimensional 10- and 8-MR channel zeolites with similar micropore volumes), 3-methylpentane adsorption capacity and rate measurements have shown that ferrierite is characterised by the most restrictive micropore structure [5]; this constrains the transition state, enhancing selectivity to isomerisation above oligomerisation [6]. At longer time-on-stream (TOS), the selectivity to isobutene was found to increase significantly; this was believed to be due to blocking of the channels, leaving only the acid sites near the 10-MR pore mouth available for the isomerisation reaction [7-8]. Parameters such as the specific ellipticity of the pore mouth, and the crystallite size (which is inversely proportional to the *number* of pore mouths), have been found to correlate with selectivity [8], supporting the above hypothesis. However, despite such evidence, pore mouth catalysis has remained a subject of debate for butene isomerisation.

In addition to the specific location of acid sites as a function of pore topology and morphology, the precise nature of the acidic sites in ferrierite also plays an important role in selective skeletal isomerisation. High isobutene yields thus require Brønsted acid sites with intermediate acidity [9], while the simultaneous presence of Lewis sites and/or highly acidic Brønsted sites instead promote oligomerisation and cracking reactions [10]. Notably, the protonated form of Ferrierite (H-FER) is characterised by a low ratio of Lewis to Brønsted acid sites compared to other 10-MR zeolites (Table 1 in [11]). Other important parameters are the location and distribution of the active sites inside, and on the surface of, the catalyst crystallite. Five different Brønsted acidic sites could be distinguished in H-FER, based on their FT-IR fingerprint; hydroxyl groups in 10-MR channels (20% of Si(OH)Al), in large pockets of the 8-MR channels (50% of Si(OH)Al), in the 8-MR channels, and finally in the 6-MR and 5-MR-windowed cavities [12]. Their distribution has since been found to vary with the template (when the synthesis is performed in the absence of sodium cations), and can therefore be controlled by optimising the synthetic procedure [13]. FT-IR studies using bulky probe molecules furthermore showed that the external surface of protonated ferrierite has terminal silanols (some with significant Brønsted acidity), as well as Lewis acid sites, but no bridging hydroxyl groups [14]. However,

such information on the location and density of acid sites in ferrierites does not yet allow one to correlate structure with catalytic activity, since accessibility of the Brønsted acidic sites in relation to the size, shape and polarity of the reactant molecules also plays a key role.

The key role that acidity plays in isomerisation reactions is illustrated by the literature, where the relation between acidity and performance has been studied for some commercial ferrierite grades. A number of parameters describing the acidity of these samples are listed in **Table 4.1**. These ferrierites show different selectivities in the gas-phase transformation of butene to isobutene; selectivity to isobutene has been reported to increase with Si/Al ratio [15] and with an optimum amount of extra-framework aluminium (EFAl) [16]. However, the selectivity of ferrierite samples with very similar Si/Al ratio has been found to differ significantly in the liquid-phase isomerisation of monoterpene hydrocarbons [17]. A combination of techniques (MAS NMR and FT-IR) confirmed that the Si/Al ratio alone is indeed not sufficient to predict the catalytic performance, and acidity needs to be described in more specific terms, that is, the precise type, strength, location and accessibility of the sites.

Recently, H-FER has also been found to show superior activity and selectivity in the liquid-phase isomerisation of linear unsaturated fatty acids to branched-chain species (Branched-chain Unsaturated Fatty Acids or BUFA) [18]. Quantitative oleic acid (OA) conversion and BUFA yields above 70 wt% have been reported, representing a step change compared to the numerous zeolite types previously investigated. As in butene isomerisation, the unique topology of ferrierite is believed to be responsible for the transition-state selectivity observed. Further improvements in BUFA production were made by the use of the bulky Lewis base triphenylphosphine (TPP), which has been shown to enhance selectivity by binding to the external acid sites and suppressing residual oligomerisation at the zeolite surface [19]. The selectivity that ferrierite displays in this reaction is remarkable, given that the reaction is limited to the pore mouth from a very early stage due to severe deactivation, as reported in Chapter 2.

Table 4.1: Literature data reported for the acidity of commercial ferrierites after protonation.

Sample # in this study	Commercial name	Si/Al ratio[a]	Brønsted acidity by MAS NMR (mmol/g) [17]	Brønsted acidity by FTIR (mmol/g) [17]	Acid strength Δν CO (cm^{-1}) [17]	CEC[b] (mmol/g) [16]	EFAl (mmol/g) [16]
2	HSZ720KOA	8.9	1.389	1.172	286	ND	ND
4	CP914C	10.0	0.904	0.840	295	0.92	0.64
5	CP914	27.5	ND	ND	ND	0.40	0.15

a: Determined by chemical wet analysis.
b: CEC = Cation-exchange Capacity from NH_3 during calcination.

In addition to its selectivity to isomerisation over oligomerisation, the ferrierite topology promotes a very specific branching pattern. The BUFA obtained by H-FER-catalysed alkyl isomerisation are a mixture of at least 30 alkyl isomers, predominantly methyl-branched ones [19]. Mono-branched fatty acids (MoBUFA) dominate the reaction mixture with the methyl group being found preferentially at positions 8 to 14 [19]. Ethyl-branching and propyl-branching are not reported, which is in contrast to fatty acid isomerisation reactions performed with larger pore zeolites [20]. Multiple-branched fatty acid isomers are detected, albeit in limited amounts in ferrierite-catalysed reactions, and are believed to be formed by successive rearrangements [20]; this multiple-branching occurs preferentially at specific positions along the carbon chain, that is 11,14 and 14,15 [19], excluding any quaternary carbon formation [19,20]. The MoBUFA are of particular commercial interest; single methyl-branched fatty acids have been shown to maintain good biodegradability [21], and the position of the methyl group close to the centre of the molecule ensures maximum impact on low temperature properties [22], highly desirable in for example lubricant applications [23]. Furthermore, oleochemicals derived from hydrogenated BUFA are reported to bring performance benefits in many consumer and industrial applications [20, 24-26], and the special properties of the MoBUFA are similarly expected to be carried over in their derivatives. Therefore, it is important to optimise (Mo)BUFA yield and to understand how to control the formation of multiple-branched products.

In this Chapter, we present our findings regarding the liquid-phase skeletal isomerisation of OA in the presence of various ferrierite catalysts. Five samples, four of which have very similar Si/Al ratios, were obtained from two manufacturers - in order to explore how subtle differences in morphology and acidity, including type, strength, location and accessibility of the acid sites, influence the results of catalytic testing. A number of complementary characterisation techniques have been combined to measure these key parameters, building on prior studies of established gas and liquid-phase reactions involving ferrierite. We focused on understanding the origin of the superior activity and selectivity towards (Mo)BUFA in the alkyl isomerisation of oleic acid.

4.2. Experimental

4.2.1. Chemicals and Catalyst Materials

Distilled OA with trade name Priolene™ 6936 (92.2% C18:1, 3.2% C18:2, 0.2 C18:3 and 3.7% saturated fatty acids, mainly octadecanoic) was obtained from Croda.

The ferrierite samples used are listed in **Table 4.2**. Sample 2, received in the sodium/potassium cation form, was activated by conversion to its protonated form, henceforth denoted as H-FER, using an ion-exchange procedure with hydrochloric acid (HCl, 1 M) at room temperature (RT) [27], before air drying for three days at RT. All samples received in the ammonia form were calcined for 5 h at 500 °C. For completeness, the XRD patterns of all catalysts were recorded after activation (data not shown); they were found to be consistent with the ferrierite structure and free of crystalline impurities. Based on the intensity of a number of characteristic diffraction lines, catalyst 1 shows somewhat lower crystallinity.

PtO_2 was purchased from Sigma Aldrich (Pt 80-85% and surface area ≥ 75 m^2/g).

Table 4.2: Overview of ferrierite samples tested.

Catalyst #	Name	Supplier	Supplied form	Nominal[a] Si/Al	Activation method
1	CP7145	Zeolyst	NH_4^+	8.5	Calcination
2[b]	HSZ720KOA	Tosoh	K^+	8.5	Wet exchange
3	HSZ722HOA	Tosoh	H^+	10	/
4[c]	CP914C	Zeolyst	NH_4^+	10	Calcination
5	CP914	Zeolyst	NH_4^+	27.5	Calcination

a: Commercial values.
b: Same batch as used in Chapter 2 and Chapter 3 (REF1).
c: Same batch as used in Chapter 3 (REF2).

4.2.2. Catalytic Testing

All catalytic testing was carried out with 1.5 wt% loading at two different scales:
A 1.8 L RC1 high-pressure reactor from Mettler Toledo was used to study both activity and selectivity starting with the following amounts: 1000 g OA, 15.0 g H-FER and 10.0 g demineralised water. After purging with nitrogen 3 times, the reactor was stirred with a mechanical stirrer at 400 rpm, pressurised to about 1 bar and heated to (a maximum of) 260 °C at a rate of 6 °C/min, resulting in a pressure of about 11 bar. Reaction temperature was typically held for 6 h (unless otherwise stated), before the mixture was cooled to 80 °C and filtered under nitrogen for a minimum of 4 h.

A 15 mL multi-autoclave SPR16generation2 from Amtech was used to compare the initial activities starting with the following amounts: 7.0 g OA, 105.0 mg H-FER and 73.0 µl demineralised water. Reactors were stirred with a magnetic stirrer at 500 rpm and purged with nitrogen 3 times, before heating them to (a maximum of)

260 °C; pressures between 6 and 7 bar were recorded. After a few minutes at reaction temperature (to achieve conversions of 10-20%), the reactors were cooled to 50 °C and their content was directly filtered using a syringe filter (PTFE, 0.45 µm). Because of the large differences in molecular weight of the components in the crude reaction mixture, its composition was determined in two steps. First, the oligomer concentration in the crude reaction mixture was determined by high temperature GC (HT-GC). Secondly, the monomeric fraction was separated from the oligomers by distillation at a temperature of 260 °C under a pressure of < 1 mbar. Subsequently, to reduce chemical complexity and facilitate analyses, a small amount of the collected monomeric fraction was diluted in ethyl acetate (40 mg/mL), hydrogenated at RT for 45 min using 40 mg Adam's catalyst (PtO_2 reduced in situ, hydrogen flow of 50 mL/min) and subjected to GC analyses.

OA (with an initial mass fraction $x_{C18:1,0}$), linoleic acid ($x_{C18:2,0}$) and linolenic acid ($x_{C18:3,0}$) are considered as the reactive components of OA. Their mass conversion (y_t) was determined by quantification of the mass fraction of stearic acid ($x_{C18,t}$) in the hydrogenated monomer fraction as a function of time t. The onset of the reaction (t = 0) is designated as the time when the reaction mixture reaches the temperature setpoint of 260 °C. A correction is made for the distillation yield of the monomeric species ($y_{M,t}$) as determined by HT-GC, and for the initial mass fraction of unreactive species, i.e. the amount of stearic acid ($x_{C18,0}$) present in OA. The mass conversion of all unsaturated components, subsequently referred to simply as "conversion", is then given by:

$$y_t = 1 - \frac{[(x_{C18,t} + x_{C18:1,t}) \times y_{M,t} - x_{C18,0}]}{[x_{C18:1,0} + x_{C18:2,0} + x_{C18:3,0}]} \quad \text{(E 4.1)}$$

Note that due to the similar molecular weights of these molecules, mole and mass conversions can be considered almost equivalent; positional and *cis*/*trans* isomers are implicitly included in the simplified nomenclature.

The selectivity towards BUFA ($s_{B,t}$) is derived from the mass fraction of all hydrogenated BUFA ($x_{B,t}$) in the hydrogenated monomer fraction. Again, a correction is made for the distillation yield of the monomeric species ($y_{M,t}$):

$$s_{B,t} = \frac{[x_{B,t} \times y_{M,t}]}{[(x_{C18:1,0} + x_{C18:2,0} + x_{C18:3,0}) \times y_t]} \quad \text{(E 4.2)}$$

The selectivity towards MoBUFA is calculated in a similar way from the mass fraction of all hydrogenated MoBUFA ($x_{MoB,t}$) in the hydrogenated monomer fraction.

4.2.3. Catalyst Characterisation

The SEM images were recorded using a FEI XL30SFEG microscope.

The particle size distributions for the crystal agglomerates were compared by static light scattering (Malvern Mastersizer 2000). All samples were analysed in duplicate as 7.5 mg/mL dispersions in water under sonication.

Nitrogen physisorption on the catalyst materials was performed with an automated gas sorption system, Micromeritics TriStar 3000. Before the measurements, the samples were outgassed for 12 h at 250 °C. The external surface area (S_E), micropore surface area (S_μ), and micropore volume (V_μ) were determined by applying the t-plot method. The relative standard deviations for these parameters have been calculated for sample 2 (as a typical example) after repeating the analyses 4 times, and were 7%, 24%, 3% respectively.

For Pyridine (Py) adsorption, IR spectra of the catalyst materials were obtained by first pressing the material into a self-supporting wafer of 12-16 mg with a 13 mm diameter. The wafer was placed in a dedicated FT-IR cell connected to an oven. Adsorbed water was removed by heating the sample to 550 °C at 4 °C/min under vacuum (10^{-2} mbar). A Perkin-Elmer System 2000 was used to record the FT-IR spectra in transmission mode from 4000 to 400 cm^{-1} (resolution of 4 cm^{-1} and 12 scans), with the spectrum of the empty cell as background (ratio). Py was adsorbed in situ at 50 °C on the dried wafer. The temperature of the cell was increased to 150 °C and kept at this temperature for 30 min to remove any physisorbed molecules, before recording the FT-IR spectra. All spectra have been normalised to the overtone range 1750-2100 cm^{-1}.

For CO adsorption, self-supporting wafers of 13-18 mg with a 13 mm diameter were prepared. The wafer was placed in a well-sealed FT-IR cell connected to an oven. Adsorbed water was removed by heating the sample to 400 °C at 4 °C/min under vacuum (10^{-6} mbar) and holding this temperature for one hour before cooling. The same Perkin-Elmer System 2000 was used to record the FT-IR spectra in transmission mode from 4000 to 1000 cm^{-1} (resolution of 4 cm^{-1} and 25 scans), with the spectrum of the empty cell as background (ratio). CO (10% in He, purity 99.9%) was adsorbed in situ at low temperature (-188 °C) on the dried wafers. Spectra were taken at several pressures (from 5 to 10^{-4} mbar), while adsorbing and desorbing CO. The spectra of the dried wafers recorded before adsorption at -188 °C were deconvoluted in the range 3730-3200 cm^{-1} using the Matlab-based BluePrintXAS software. The IR band areas were normalised by the wafer density.

The XPS measurements were carried out with a Thermo Scientific K-Alpha, equipped with a monochromatic small-spot X-ray source and a 180° double focusing hemispherical analyzer with a 128-channel detector. Spectra were obtained using an aluminium anode (Al Kα = 1486.6 eV) operating at 72 W and a spot size of 400 µm. Survey scans were measured at a constant pass energy of 200 eV and region scans

at 50 eV. The background pressure was 2 x 10^{-9} mbar and during measurement 3 x 10^{-7} mbar argon because of the dual beam charge compensation. Sputtering (for 30 s and 300 s) was done with an energy beam of 1000 eV at low current, for monitoring of the Si/Al ratio in depth. C 1s, O 1s, Si 2p and Al 2p bands were recorded.

A Varian Cary 500 Scan spectrophotometer was used to record the UV-Vis spectra of the catalyst materials in diffuse reflectance mode, in the range 200-800 nm (scan speed 600 nm/min and 1 cycle). Prior analysis, 1.0 g H-FER catalyst in 60 ml acetone was stirred with 5 wt% TPP on H-FER for 24 hours at RT. The excess of TPP was removed by washing the sample with acetone four times (i.e., until TPP could not be detected in the filtrate).

TPD was carried out using a Micromeritics Autochem II, equipped with a thermal conductivity detector (TCD). Prior to analyses, 0.100-0.110 mg of sample was dried by heating in a stream of He (50 cm^3/min) at a heating rate of 10 °C/min to 600 °C and subsequently cooled to 100 °C. Ammonia was added via pulses, and kept in a 25 cm^3/min He flow for 60 min, before increasing the temperature at 5 °C/min to 600 °C.

4.3. Results

This study is based on a series of five commercial ferrierites showing significant differences in activity and selectivity, of which four have very similar nominal Si/Al ratio (**Table 4.2**). The specified Si/Al ratio for samples 1 and 2 is 8.5, while the nominal bulk acidity of catalysts 3 and 4 is somewhat lower (Si/Al ratio = 10). Sample 5, with a much lower acidity (Si/Al ratio = 27.5), has been included for comparison. All catalysts are used in their protonated form, obtained by calcination of the ammonium form (1, 4 and 5) or after HCl wet exchange (2). Sample 3 was received in its protonated form. The Si/Al ratios of all catalysts were determined prior to activation.

4.3.1. Catalytic Testing

As shown in Chapter 2, protonated ferrierite undergoes a rapid and severe deactivation during the alkyl isomerisation reaction with OA as feedstock, resulting from two different mechanisms. The rapid loss of internal surface area is due to pore blockage, which occurs even before the reaction temperature is reached. Catalysis is therefore confined to the pore mouth from the start, and any study of the initial activity must probe this pore mouth region. Acid site deactivation, the second cause of deactivation, is not playing a major role at this early stage, and we can thus obtain a true picture of the catalyst potential by studying the *initial* activity.

Figure 4.1 shows large differences between the catalysts in OA conversion (i.e. to *all* products) for the first 30 min of the reaction at 260 °C with a 1.5 wt%

loading. Within the first 5 to 10 minutes at reaction temperature, the conversion-time plots are approximately linear, indicating that the catalysts still retain most of their initial pore mouth activity.

Catalyst 5 is characterised by the lowest activity, as was to be expected from its bulk acidity. On the other hand, the differences seen in activity for the other four samples are surprising, given their very similar Si/Al ratios; their activity can be ranked in the following order: 2 > 3 ~ 1 >> 4 >> 5. There is no correlation with the manufacture-specified Si/Al ratio, as both 3 and 4 are characterised by a Si/Al ratio of 10. Therefore, this bulk parameter is insufficient to account for the observed differences in rate and, as for the isomerisation of monoterpene hydrocarbons, more discriminating measurements of texture and acidity are required to properly explain and predict their activity as catalysts.

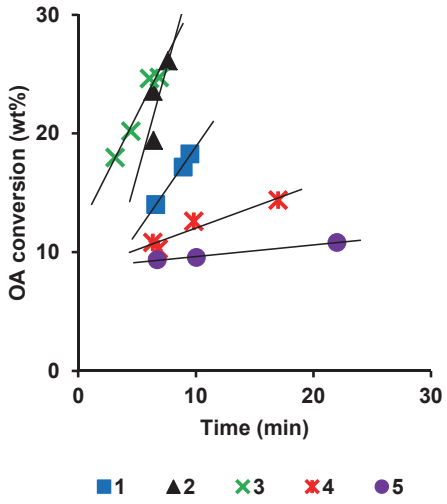

Figure 4.1: Initial activity of the ferrierite catalysts, expressed as OA conversion, during the alkyl isomerisation of OA at 260 °C in the presence of 1.5 wt% commercial H-FER catalysts: 1 and 2 (Si/Al = 8.5); 3 and 4 (Si/Al = 10); 5 (Si/Al = 27).

It can be seen in **Figure 4.1** that the conversion-time plots do not pass through the origin, when t = 0 is defined as the moment when the isomerisation reaction temperature is reached. The reason for this is that OA oligomerisation commences at somewhat lower temperatures than OA isomerisation. Indeed, it is known that estolides can be synthesised in high yield at 150 °C using a K-10 montmorillonite clay [28], and these estolides are also seen for most of the ferrierites tested here during the initial heating period. It is then assumed in comparing initial activity of the catalysts this way that the reactions taking place during the heating period are similar, which is largely confirmed by analysis of the reaction products. The differences in low-temperature activity that are indicated by the different intercept

values must be related to the number and strength of unconstrained (and thus non-selective) acid sites on the external surface of the catalyst.

The conversions achieved with the H-FER samples after more typical, elongated reaction times are illustrated by **Figure 4.2**. Catalysts 4 and 5 show the lowest conversion, as predicted from their low initial reaction rates. However, the ranking of the other catalysts changes to 3 > 1 ~ 2 >> 4 >> 5, indicating that 1 and 3 are somewhat more stable to deactivation than 2.

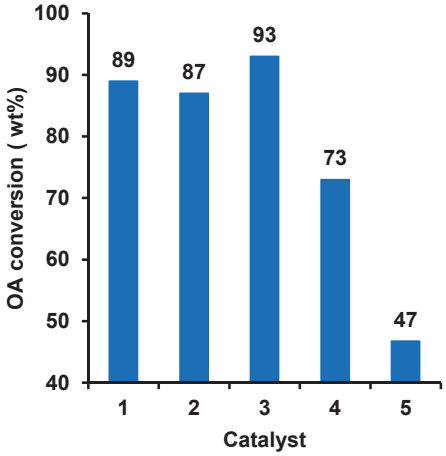

Figure 4.2: OA conversion after 6 h of isomerisation at 260 °C in presence of 1.5 wt% commercial H-FER catalysts: 1 and 2 (Si/Al = 8.5); 3 & 4 (Si/Al = 10); 5 (Si/Al = 27).

Additionally, the ferrierites show large differences in their selectivity. In order to allow a proper comparison, reaction times were selected such that 86-89% conversion was attained for each catalyst; beyond this conversion, oligomer yield increases significantly (**Figure 4.3a**). Catalyst 5 was not able to reach this conversion level, though, and the reaction was stopped arbitrarily after 16 h (i.e., at 69 wt% conversion). **Figure 4.3b** shows that each catalyst is characterised by a specific relation between BUFA and MoBUFA selectivity; for example, catalyst 4 produces almost exclusively MoBUFA while 2 more strongly promotes multiple branching.

Figure 4.4 compares the selectivity at two levels of conversion. At 88% conversion (4b), the catalysts can be ranked: 4 > 3 ~ 1 > 2. At lower conversion (69%, 4a), the selectivity of catalyst 5 is almost as good as 4; the differences between the others are somewhat smaller. Again, the acidity as determined by the Si/Al ratio cannot be linearly related to BUFA nor MoBUFA selectivity, although the experimental evidence points to an optimum which we estimate to be in the range of a Si/Al ratio of 10-15.

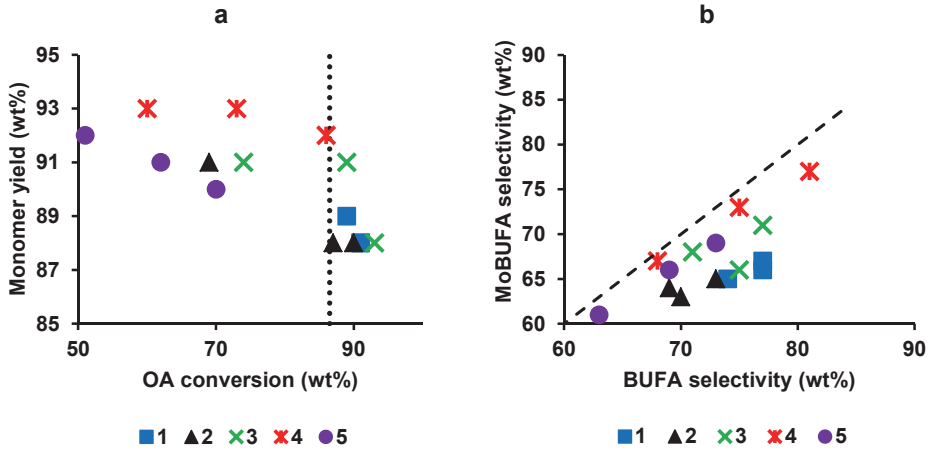

Figure 4.3: OA isomerisation at 260 °C in presence of a series of 1.5 wt% commercial H-FER catalysts: 1 and 2 (Si/Al = 8.5); 3 and 4 (Si/Al = 10); 5 (Si/Al = 27); **(a)** relation between monomer yield and OA conversion (wt%); note that the monomer yields in 3a include unreacted OA; see experimental section for the definition of yield; **(b)** relation between MoBUFA and BUFA selectivity (wt%) at different OA conversions.

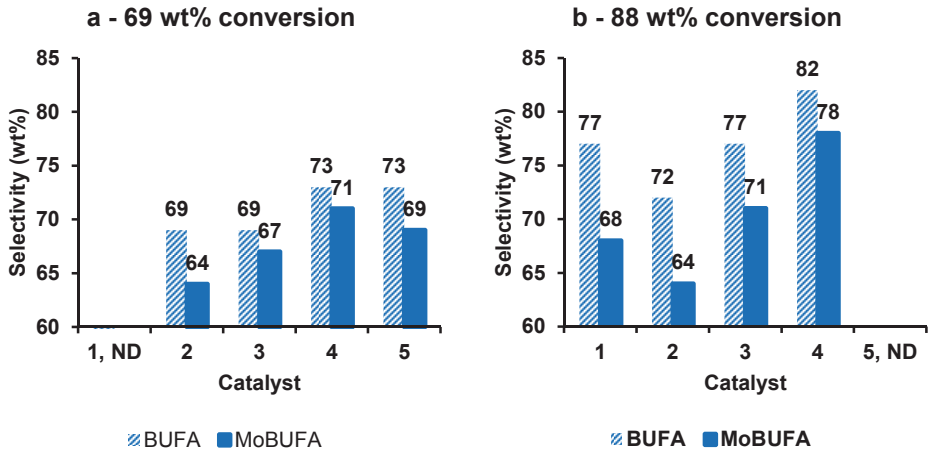

Figure 4.4: OA isomerisation at 260 °C in presence of 1.5 wt% commercial H-FER catalysts: 1 and 2 (Si/Al = 8.5); 3 and 4 (Si/Al = 10); 5 (Si/Al = 27); selectivities (wt%) to BUFA (diagonal fill) and MoBUFA (solid fill) at: **(a)** 69 wt% conversion (1 not included); **(b)** 88 w% conversion (5 not included as this conversion level cannot be reached with this catalyst).

4.3.2. Catalyst Characterisation

In order to explain the catalytic testing results and relate catalyst performance to structure, all catalysts were characterised in detail using a number of complementary techniques.

4.3.2.1. Morphology

Figure 4.5 shows the scanning electron microscopy images (SEM) of the commercial H-FER samples. All catalysts consist of plate-like crystals in the sub-micron range, with thicknesses ranging from 0.01 to 0.15 µm. While similar at first sight, the SEM images do show a number of important differences. The crystals of sample 4, for instance, differ from the other samples, with very irregular shapes and rounded edges. The same catalyst is studied in [17], where the authors suggested that a post-treatment, such as weak dealumination, had been applied; this explanation would be consistent with the observed morphology. The crystals of sample 5, in turn, are somewhat larger (0.5-2 µm). So in addition to the higher Si/Al ratio and resulting lower acidity, the low surface area per unit mass, and consequently fewer pore mouths, might thus also contribute to the very low conversion observed with this catalyst.

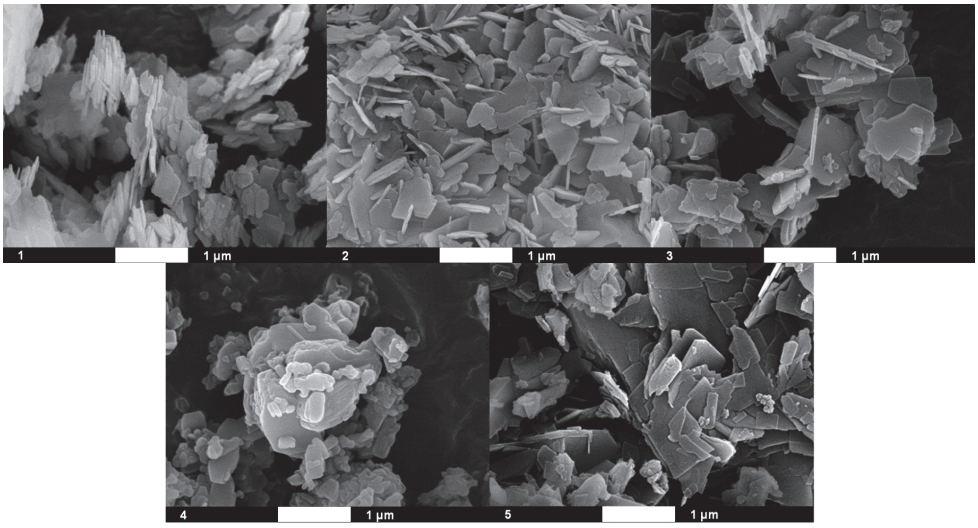

Figure 4.5: Scanning electron microscopy (SEM) images of the commercial H-FER catalysts 1 to 5; the scale bars represent 1 µm.

Static light scattering was used to determine the particle sizes of catalysts 1 to 4, particle being defined here as crystal agglomerates. The results are summarised in **Table 4.3**. Catalyst 2 consists of larger particles, with a diameter ranging from 3 to 36

µm and a median at 15 µm. Catalysts 1, 3 and 4 show very similar distributions, with a median diameter of 3 to 5 µm, but different activity. These differences in particle size thus cannot explain the catalytic data.

Table 4.3: Particle size distributions of the commercial H-FER catalysts; All particles (i.e. crystal agglomerates) are ranked based on their size and the diameter is reported for 10%, 50% (median) and 90% of the particle count.

Catalyst #	Diameter (µm) 10%	Diameter (µm) 50%	Diameter (µm) 90%
1	1.3	4	9
2	3.4	14	36
3	1.3	5	15
4	0.9	3	7
5	ND[a]	ND[a]	ND[a]

a: Not determined.

4.3.2.2. Textural Properties

Surface area and porosity of the H-FER series were determined by nitrogen physisorption measurements (**Table 4.4**). The external surface areas show a large variation, with the S_E of catalyst 1 (52 m^2/g) being ~50% larger than for 2 or 5 (both 32 m^2/g). As OA isomerisation is thought to occur mostly via pore mouth catalysis, this parameter should be taken into account when studying the differences in activity. In addition, there is a significant variation in total pore volume (~ 20%), while the micropore volume remains largely unchanged (< 2%). The maximum total pore volume is found for catalyst 1, which is in line with the other textural parameters. On the other hand, catalyst 4 is characterised by the smallest total pore volume, while its external area is above average. **Figure 4.6** shows that a type IV adsorption-desorption isotherm is obtained for catalyst 4, instead of the type I expected for microporous materials [29] and indeed seen for the others (only catalyst 2 is shown as example). Catalyst 4 must therefore include also a small amount of mesopores; their volume is too small, however, compared to the intercrystalline space to impact the total mesopore volume. The beneficial role that mesopores might play, has already been highlighted for the H-Beta-catalysed OA alkyl isomerisation, where high conversion was linked to a large amount of mesopores [30].

Table 4.4: Overview of textural properties of commercial H-FER catalysts based on N_2 physisorption.

Catalyst #	S_E, External area (m^2/g)	V_T, Total pore volume(cm^3/g)	V_μ, Micropore volume (cm^3/g)
1	52	0.235	0.126
2	32	0.212	0.124
3	36	0.206	0.124
4	40	0.193	0.124
5	32	0.229	0.126

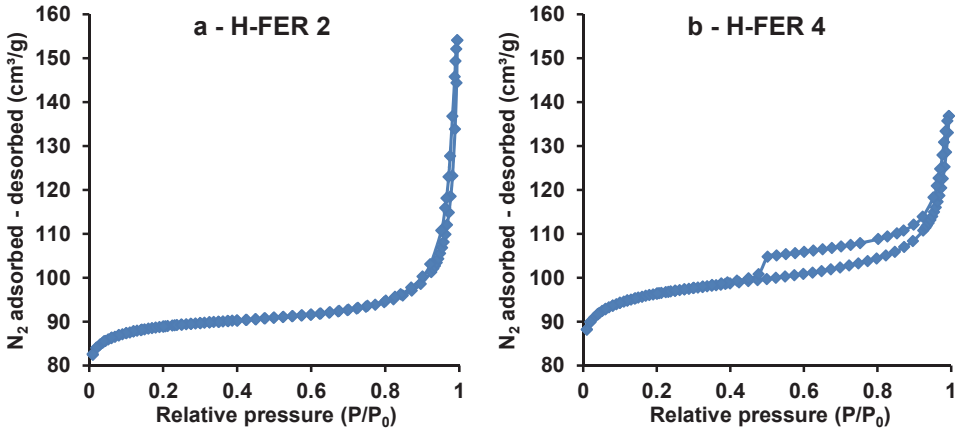

Figure 4.6: Comparison of nitrogen adsorption-desorption isotherms of two commercial catalysts: **(a)** H-FER 2; **(b)** H-FER 4.

4.3.2.3. Acidity Type and Accessibility

Catalyst 5, with a much higher Si/Al ratio, shows a very low activity but a high selectivity. However, the Si/Al ratios for the four remaining catalysts lie between 8.5 and 10, and this narrow range does not explain the large observed differences in activity and selectivity. Therefore, other acidity-determining parameters have been systematically investigated, in order to determine whether any link can be made with the observed performance of the catalysts.

FT-IR spectroscopy has been used to probe the Brønsted acid sites responsible for the alkyl isomerisation, and any Lewis acid sites if present. d_3-Acetonitrile is generally used as it is able to probe all acidic sites of the two-dimensional 10- and 8-MR channel structure [5]. We chose to use pyridine as probe instead (Py, kinetic diameter of 0.6 nm), in order to focus on the acid sites located in the 10-MR channels, and those accessible from these channels [5]. As a result of the pore mouth catalysis, only (part of) these channels are believed to take part in the isomerisation of the long-chain OA molecules. **Figure 4.7** gives the FT-IR spectra between 1600 and 1400 cm^{-1} with the key ring vibrations of the adsorbed Py. All five commercial catalysts show mostly Brønsted acidity; from the 4 major bands assigned to the protonated Py [31], the band at 1543 cm^{-1} was used to determine the relative Brønsted acidity, later shown to correlate with the activity. The very small band at 1454 cm^{-1} confirms that the Lewis acidity of the samples is insignificant compared to the Brønsted acidity, even after correction of the peak intensities for their extinction coefficients (respectively 2.22 and 1.67 cm/µmol [32]).

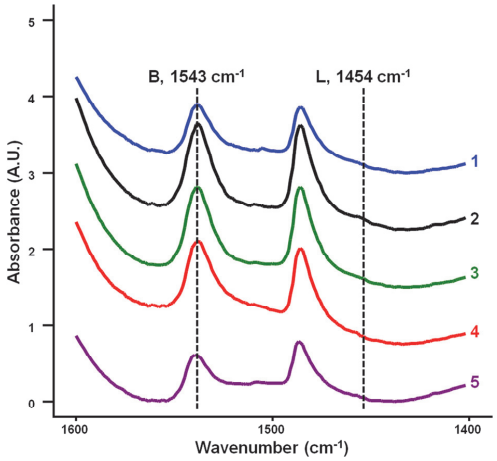

Figure 4.7: IR absorbance spectra of the commercial H-FER catalysts 1 to 5, after adsorption of Py at 50 °C and desorption at 150 °C.

4.3.2.4. External Crystallite Acidity

Two methods have been used to study the external crystallite acidity. Firstly, a combination of XPS and argon ion sputtering enabled us to check for any acidity gradients in the outer layer of the crystallites. **Figure 4.8** shows the resulting Si/Al ratios obtained for the commercial H-FER series directly, and after 30 s/300 s sputtering. Unsurprisingly, sample 5 shows the highest Si/Al ratio, although it is somewhat lower than the manufacturer-specified number; it is also the only catalyst with a higher Si/Al ratio after sputtering. On the other hand, the Si/Al of the outer layer as measured by XPS (1 < 2 ~ 4 < 3) does not exactly follow the manufacturer-specified Si/Al (1 ~ 2 < 3 ~ 4); the Si/Al ratio above 10 measured for catalyst 2 could be explained by some slight dealumination during the wet activation.

The Si/Al ratio of the outer layer for catalysts 2 and 4, as measured by XPS, is similar. However, this gives no indication of the accessibility of the acid sites to the OA. To assess any differences in accessibility, we used a bulky Lewis base (TPP) as a probe and quantified TPP chemisorption by diffuse reflectance UV-Vis spectroscopy. This way, it was possible to quantify the non-selective external acid sites in catalysts 2 and 4 (**Figure 4.9**). The use of TPP specifically is based on results from catalytic testing, in which it has been shown to enhance selectivity of H-FER catalysed alkyl isomerisation of OA by preventing unwanted oligomerisation reactions [19]. The spectra recorded for catalysts 2 and 4 after reaction with TPP show 3 distinctive bands: an intense one at 226 nm and two smaller ones at 267 and 274 nm, all originating from TPP cations. Interestingly, the intensity of the bands at 226, 267 and 274 nm for catalyst 2 is about two times larger than that for catalyst 4,

clearly showing that there are about twice as many non-selective sites on the external surface of sample 2.

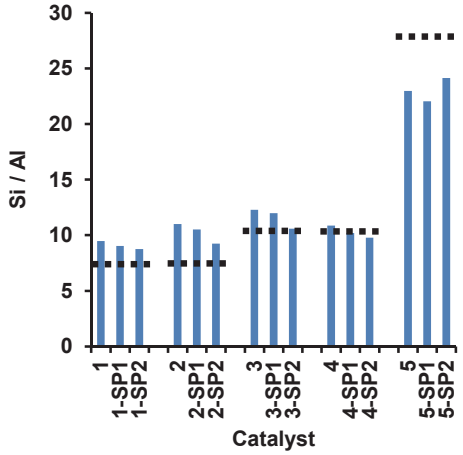

Figure 4.8: Si/Al of the commercial H-FER catalysts 1 to 5, determined by XPS of the original samples and after Ar sputtering (SP1 after 30 s and SP2 after 300 s); the nominal Si/Al is given as a horizontal dashed line for each catalyst.

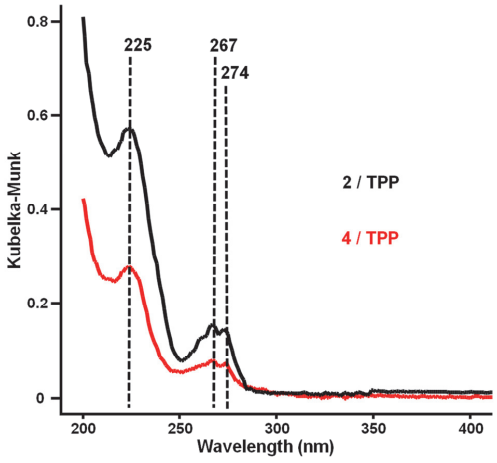

Figure 4.9: Overlay of diffuse reflectance UV-Vis spectra of two commercial H-FER catalysts 2 and 4, after reaction of their external acid sites with TPP; the spectra have been individually recorded and treated.

These results, together with the equivalence of the outer acidity profile of the two catalysts measured by XPS, show that a number of acid sites close to the external surface are not accessible to TPP for catalyst 4, for example, they must be located in the pore mouth of smaller channels or in small pockets close to the external surface.

4.3.2.5. Effective Acid Strength

The number and *effective* strength of *all* acid sites in the commercial H-FER samples were first determined by ammonia TPD. The manufacture-specified Si/Al ratio is, as expected, well correlated with the total acidity found with this technique (**Table 4.5**). All curves (**Figure 4.10**) show two peaks, one around 200 °C and one between 400 and 500 °C. The latter corresponds to the stronger acid sites that must be involved in alkyl isomerisation. Note that the temperature maxima for both peaks shift towards lower temperature down the series from 1 to 5 (**Table 4.5**). There is a weak negative correlation between the bulk Si/Al ratio (as indicated by the manufacturer) and the temperature maxima for the peak at 400-500 °C; this trend, which is based on the limited data set and variation observed within it, does not seem to be influenced by the platelet morphology. Indeed, the longest desorption time (as measured to the maximum of the second TPD peak) corresponds to catalyst 1 that comprises the smallest crystals, while the shortest desorption time is measured for catalyst 5 comprising the largest ones. For all catalysts, the 10-MR channels are running along the crystal length, so if there was redeposition or diffusion limitations of NH_3 in the 10-MR channels, the opposite result would be expected.

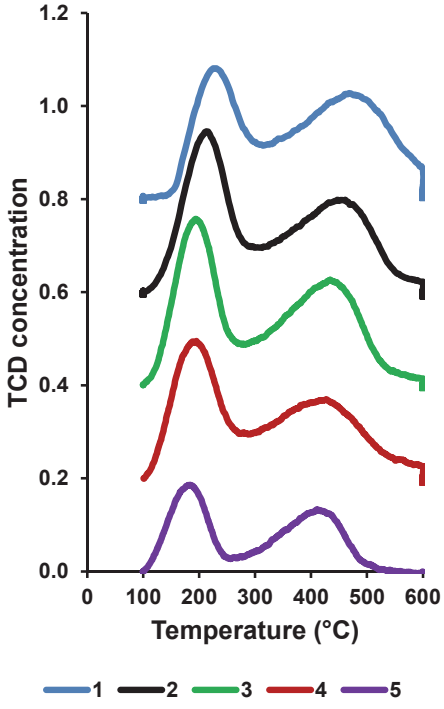

Figure 4.10: Ammonia TPD profiles for the commercial H-FER catalysts 1 to 5; the Y axis is proportional to the desorbed amount of NH_3; traces are offset for clarity.

Table 4.5: Overview of acidity parameters found for the commercial H-FER by XPS, NH_3-TPD and FT-IR analysis after CO adsorption/desorption.

Catalyst #	Nominal[a] Si/Al Ratio	Outer[b] Si/Al ratio	TPD acid sites concentration (mmol/g)	TPD 1st maximum temperature (°C)	TPD 2nd maximum temperature (°C)	Acid strength $\Delta\nu$ CO (cm^{-1})
1	8.5	9.5	1.61	231	471	293
2	8.5	11	1.66	213	461	292
3	10	12	1.52	194	441	292
4	10	11	1.35	195	414	298
5	27	23	0.82	184	411	295

a: Commercial values.
b: Measured by XPS.

4.3.2.6. Intrinsic Acid Strength

In addition, the *intrinsic* strength of the Brønsted acid sites has been probed by FT-IR analysis after CO adsorption/desorption. The spectra (in both the hydroxyl stretching and CO stretching regions) collected for all samples during the experiments are given in **Figures 4.11 to 4.16**. The CO-induced shifts are given in **Table 4.5**. Based on this technique, the acidity of the "exposed" acid sites (10-MR channels and cavities of the 8-MR channels [34]) is rather similar for all catalysts. The data point at very slightly lower proton affinities for samples 4 and 5; this is consistent with the evidence that catalyst 4 is dealuminated and the fact that catalyst 5 has a higher Si/Al ratio. The values found for samples 2 and 4 are also slightly higher than those of the literature (see **Table 4.1** in the introduction), but show a similar trend. Analysis of the CO stretching region revealed the presence of a small amount of K^+ ions in the 10-MR channels and 8-MR channels of sample 2 (**Figure 4.13b**), a small amount of K^+ ions in the 8-MR channels of sample 3 (**Figure 4.14b**), a residual amount of coordinatively unsaturated Al^{3+} ions in sample 1 (**Figure 4.12b**) and some EFAl in samples 1, 4 and 5 (**Figures 4.12b, 4.15b** and **4.16b**, respectively) [34-35].

Finally, deconvolution of the hydroxyl range at -188 °C before introduction of CO (**Figure 4.11**) gave the peak areas of the Brønsted acid sites in (i) the 10-MR channels, (ii) the large pockets of the 8-MR channels, (iii) the 8-MR channels, iv) the 6-MR, as well as the EFAl (**Table 4.6**). The distribution of these sites varies significantly between the 5 catalysts. Assuming that their extinction coefficients are similar, the 10-MR channels account for 12% of Si(OH)Al for catalysts 4 and 5, 15% for catalysts 1 and 2 and 22% for catalyst 3.

Table 4.6: Distribution in Brønsted acid sites and EFAl over the various channels and cavities for the five protonated ferrierite samples; the FTIR spectra of the dried wafers recorded at -188 °C were deconvoluted in the range 3730-3200 cm^{-1} using the Matlab based BluePrintXAS software; the distribution is based on hydroxyl peak areas %, the area being normalized by the wafer density.

Catalyst #	Nominal[a] Si/Al Ratio	Area of Si(OH)Al in 10-MR channels	Area of Si(OH)Al in 8 MR cavities	Area of Si(OH)Al in 8 MR channels	Area of Si(OH)Al in 8 MR channels	Area of EFAl
1	8.5	111	193	296	108	19
2	8.5	96	87	329	142	3
3	10	146	95	306	123	0
4	10	88	147	234	220	36
5	27	72	136	254	86	35

a: Commercial values.

4.4. Discussion

Taken together, the data obtained with various analytical techniques for the five commercial ferrierite catalysts provide further insight into the relationship between their structure, and their activity and selectivity in the liquid-phase isomerisation of linear unsaturated fatty acids. Despite four of the five having very similar Si/Al ratios, they show significant differences in OA conversion, as well as in (Mo)BUFA yields. With regard to their bulk properties, the Si/Al ratios are consistent with the acid site quantification based on ammonia TPD (**Table 4.5**): 1 ~ 2 > 3 > 4 >> 5. The acid site concentration found by TPD is also reasonably in line with the literature data on total Al content (1.65 mmol/g for catalyst 2 [33]; 1.56 mmol/g for catalyst 4 [16] and 0.55 mmol/g for catalyst 5 [16]). Therefore, with the exception of catalyst 5, a difference in Si/Al ratio of less than 20% has a significant effect for this application. In addition, the TPD results, together with the absence of EFAl (as evidenced by the FT-IR data after CO adsorption), confirm that catalyst 2 has not suffered any significant dealumination, despite the activation by ion exchange with HCl. This method was selected instead of the milder NH_4NO_3 exchange as it proved to be convenient and reproducible.

Additionally, these catalysts are characterised by similar morphologies and textural properties; only their external surface areas vary by ~50%. The latter is important though, and its variation can explain some of the differences observed in activity, as catalysis has been found in Chapter 2 to be constrained to the pore mouth due to very early pore blockage. Due to previously observed gradual poisoning of the active sites, comparison of the catalyst activities must be done at an early stage of the reaction. The linearity of the conversion-time plots at low conversion (**Figure 4.1**) is consistent with an active site model in which desorption of the branched species is the rate-limiting step (quasi zero order) [36]. At higher conversions, pore deactivation and competing reactions complicate the picture.

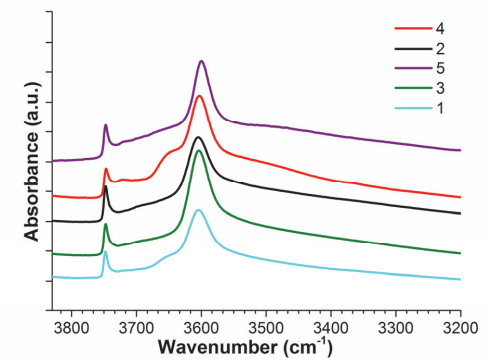

Figure 4.11: FTIR spectra of the five protonated ferrierite samples recorded at -188 °C after drying at 400 °C under vacuum (10^{-6} mbar), with the spectrum of the empty cell as background: sample 1 (blue), sample 2 (black), sample 3 (green), sample 4 (red), sample 5 (violet).

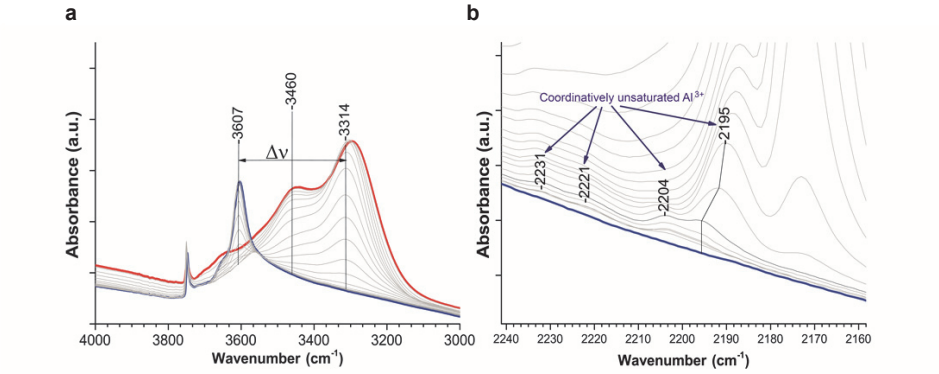

Figure 4.12: H-FER 1; FTIR spectra of the dried protonated ferrierite wafer recorded at -188 °C during CO adsorption: **(a)** in the hydroxyl stretching range; **(b)** in the carbonyl stretching range; the initial spectrum is marked in blue, while the red spectrum was recorded at maximum CO coverage.

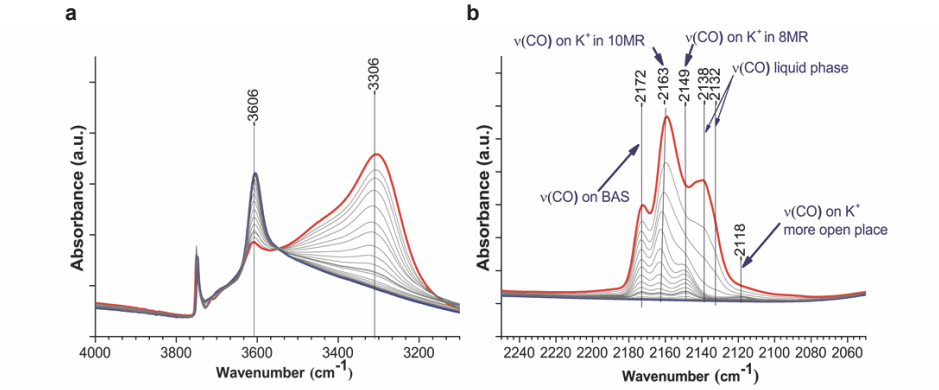

Figure 4.13: H-FER 2; FTIR spectra of the dried protonated ferrierite wafer recorded at -188 °C during CO adsorption: **(a)** in the hydroxyl stretching range; **(b)** in the carbonyl stretching range; the initial spectrum is marked in blue, while the red spectrum was recorded at maximum CO coverage.

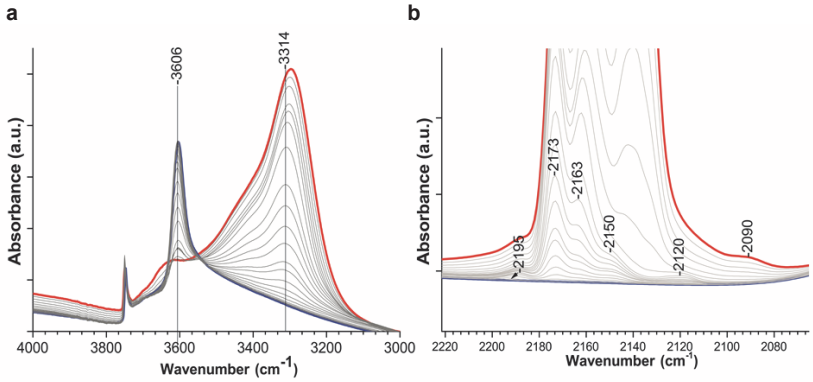

Figure 4.14: H-FER 3; FTIR spectra of the dried protonated ferrierite wafer recorded at -188 °C during CO adsorption: **(a)** in the hydroxyl stretching range; **(b)** in the carbonyl stretching range; the initial spectrum is marked in blue, while the red spectrum was recorded at maximum CO coverage.

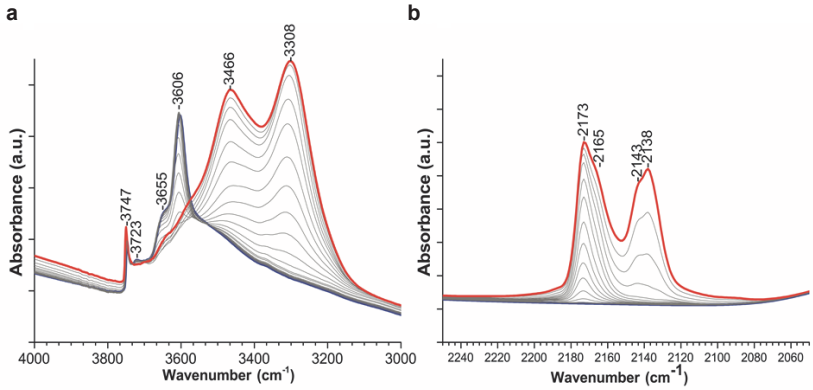

Figure 4.15: H-FER 4; FTIR spectra of the dried protonated ferrierite wafer recorded at -188 °C during CO adsorption: **(a)** in the hydroxyl stretching range; **(b)** in the carbonyl stretching range; the initial spectrum is marked in blue, while the red spectrum was recorded at maximum CO coverage.

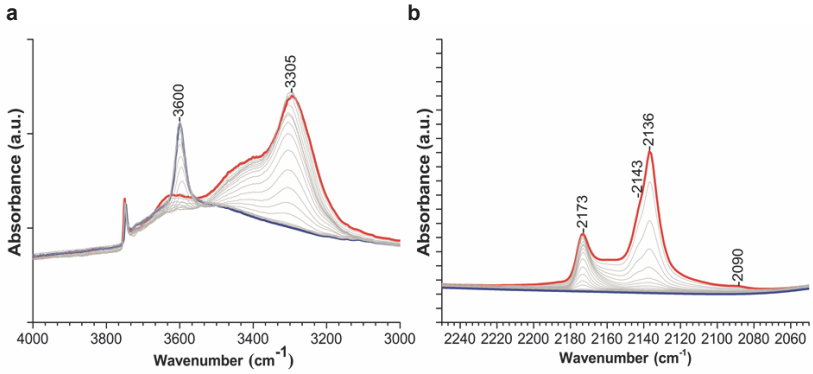

Figure 4.16: H-FER 5; FTIR spectra of the dried protonated ferrierite wafer recorded at -188 °C during CO adsorption: **(a)** in the hydroxyl stretching range; **(b)** in the carbonyl stretching range; the initial spectrum is marked in blue, while the red spectrum was recorded at maximum CO coverage.

Nonetheless, we observe that initial activity correlates well with the number of Brønsted acid sites present in the 10-MR channels, determined using Py as a 10-MR selective probe. This is illustrated in **Figure 4.17** (calculated at t = 8 min). This relationship assumes that the distribution of Brønsted acid sites in the 10-MR channels is homogeneous, that is, the probability that an active site is found close to the pore mouth (and thus accessible for reaction) is proportional to the total number of active sites in the 10-MR channels, as measured by Py desorption FT-IR. By comparison, in the gas phase isomerisation of butene to isobutene, a linear relationship was also found for isobutene yield (rather than butene conversion). In this case, the yield was found to be proportional to the total number of Brønsted acid sites, as determined by the acetonitrile probe (which in contrast to Py also probes Brønsted acid sites in the 8-MR channels) [33]; for the same reaction, the observed increase in selectivity with time-on-stream was also explained by pore mouth catalysis. Additionally, smaller crystal size (for a given Si/Al ratio) has been shown to increase isobutene selectivity for H-FER catalysts, confirming the importance of the 10-MR pore mouth density [8].

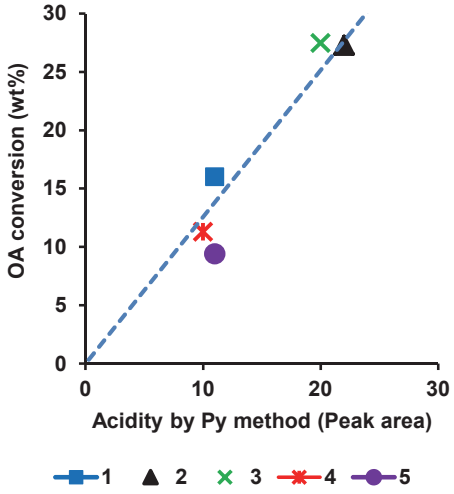

Figure 4.17: Relation between Brønsted acid site concentration (Total integrated area for the peak at 1543 cm^{-1}) as measured by Py-IR and the initial OA conversion (y_t) for the commercial H-FER catalysts at t = 8 min.

The relation seen between OA conversion and Brønsted acidity explains the differences between the five catalysts in terms of activity (i.e., they are the result of differences in overall Al distribution over the various possible T-sites), but it does not yet explain the differences observed in (Mo)BUFA selectivity. Indeed, the high Brønsted to Lewis acid site ratio of all catalysts (in line with findings from the literature [11]) explains the low level of oligomers and high BUFA yield found with all

five catalysts, as reported in the alkyl isomerisation of butene to isobutene [10]. It cannot however explain the significant variation in selectivity *within* the monomeric fraction; this suggests that there must be other parameters at play.

A first indication of what determines these selectivity differences to/within the monomer fractions is given by the XPS studies. These measurements show that a lower acidity of the outer crystallite surface seems beneficial to monomer selectivity, although the correlation is not perfect; catalyst 4 is significantly more selective than 2, despite their equivalent outer XPS acidity profile. Based on the TPP results, we can further refine the requirements for selective BUFA formation. Indeed, our UV-Vis results after TPP chemisorption show that sample 2 is characterised by twice as many non-selective sites on its external surface. Some of the sites seen by XPS must therefore be barely accessible to the OA reactant. XPS is therefore unable to fully discriminate the accessibility of sites. UV-Vis with TPP is therefore a necessary supplementary technique to XPS, when catalysts with similar external acidity are compared, in order to predict differences in selectivity to BUFA.

This finding can be further substantiated by characterisation data reported earlier for these catalysts by Rachwalik et al. [17]; these authors compared the acidity of catalysts 2 and 4 by FT-IR, and the resulting spectra were similar in the main features. However, the distribution of silanol groups is quite distinct; catalyst 4 has some silanol groups located inside zeolitic faults (3730 cm^{-1}) and fewer external silanol groups (3748 cm^{-1}). The authors concluded that this catalyst has been submitted to a post-synthesis treatment, which would have removed most of the external acidity. Our UV-Vis/TPP method shows an absence of non-selective sites for catalyst 4, supporting their hypothesis; our SEM pictures, and the presence of mesopores (detected by physisorption), provide further evidence. The highest selectivity to MoBUFA is found for catalysts 4 and 5. CO probing with IR shows that they are characterised by the strongest Brønsted acid sites, but based on the deconvolution of the OH-stretching range (see supporting information) their 10-MR channels contain the lowest concentration of these sites. On the other hand, catalyst 3 has somewhat weaker Brønsted acid sites, but approximately double the concentration in the 10-MR channels. We can conclude from these data that selectivity to MoBUFA is enhanced by having a low concentration of strong Brønsted acid sites in the 10-MR channels. Catalyst 1 cannot be compared in this way, as it appears to be incompletely crystallised (based on XRD and residual coordinatively unsaturated Al^{3+}). For catalyst 2, the traces of K^+ detected in the 10-MR channels by CO probing mean that a number of Si(OH)Al in the 10-MR channels are actually not activated. On the other hand, the Py study found the same number of Brønsted acid sites for catalysts 2 and 3. Therefore, the presence of K^+ must limit the Py diffusion in the 10-MR channels of catalyst 2, and the density of Si(OH)Al in the extremities of these channels must be higher for this sample compared to sample 3. The somewhat

lower acidity combined with the higher density of the Brønsted acid sites is therefore consistent with the lower MoBUFA selectivity.

Notably, in the gas-phase alkyl isomerisation of butene to isobutene, catalyst 5 also showed a very high selectivity, which was explained by a non-interconnected nanoreactor model in which the low density of active sites in the channels decreases the chance of successive reactions [15]. Although our system has been shown to undergo early pore blockage, high selectivity to MoBUFA can be explained by a similar model where the nanoreactors are limited to the channel extremities, consistent with the pore mouth hypothesis.

If we compare the NH_3-TPD curves recorded for our catalyst series, the maxima recorded for the second peak (corresponding to those sites strong enough to induce alkyl isomerisation) shift towards lower temperature (**Table 4.5**), and a negative correlation between these maxima and MoBUFA selectivities is found. This apparent contradiction with the IR study of CO adsorption/desorption can be explained by the fact that NH_3 is probing *all* acid sites. Since the Brønsted acid sites are heterogeneous [37] and their distribution in the various channels varies significantly between catalysts, TPD thus reflects better the relative amount of the strong acid sites in the 10-MR channels. Therefore, the selectivity of H-FER to MoBUFA depends not only on its specific channel dimensions and external/internal location of the acid sites, but also on its effective acidity.

4.5. Conclusions

The liquid-phase skeletal isomerisation of OA has been studied in the presence of different commercial protonated zeolite ferrierite (H-FER) catalyst materials. Despite four of the five having very similar Si/Al ratios, they show significant differences in activity, and selectivity towards the monomeric, BUFA and MoBUFA fractions. A number of complementary characterisation techniques have been used to assess their acidity in detail, including type, location, accessibility and strength. The initial activity was found to be related to the Brønsted acidity in the 10-MR channels. A low density of external acid sites enhances the selectivity to monomeric acids, while a high ratio of Brønsted to Lewis sites promotes the BUFA yield. MoBUFA selectivity was found to require few Brønsted acid sites of high strength in the 10-MR channel, reflected in a decrease of the effective acidity as seen by NH_3-TPD. Together, the results presented on activity and catalyst structure show that catalyst 4 is the best commercial catalyst for this application, and also provide insight into why its low external acidity and low density of strong Brønsted acidity in the 10-MR channels are beneficial for performance. Finally, the results presented provide detailed insights into the required characteristics in terms of acidity of an efficient OA isomerisation

catalyst. The relationships found between structure and activity may serve as guidelines for the synthesis of even more efficient catalysts.

Acknowledgements

Tiny Verhoeven (Eindhoven University of Technology) is gratefully acknowledged for carrying out the XPS analyses. Marjan Versluijs-Helder (Utrecht University) is thanked for performing the XRD and SEM analyses, and Arjan den Otter and Dr. Jinbao Gao (Utrecht University) for helping with the physisorption measurements. Fouad Soulimani and Dr. Hendrik van der Bij, both from Utrecht University, are thanked for support and advice in IR matters. Dr. Ara Muñoz-Murillo (Utrecht University) is acknowledged for performing the CO-IR analyses, and contributing to the related discussions. Ramon Oord (Utrecht University) is thanked for carrying out the NH_3-TPD measurements. Pascal Wijten (Utrecht University) is acknowledged for his assistance with the multi-autoclave operation. Tanja van Bergen-Brenkman (Croda) generously shared her knowledge and experience in OA alkyl isomerisation, and carried out a number of syntheses. Finally, Negar Rashidi and Marvin Burger, both from Croda, contributed by carrying out a number of syntheses and analyses.

References

[1] P. Granvallet, K.P. de Jong, A.G.T.G. Kortbeek, B. Kraushaar-Czarnetzki, H.H. Mooiweer, European Patent 0501577 (1992), to Shell.
[2] C.L. O'Young, R.J. Pellet, D.G. Casey, J.R. Ugolini, R.A. Sawaicki, J. Catal., 151 (1995) 758.
[3] B. de Ménorval, P. Ayrault, N.S. Gnep, M. Guisnet, Appl. Catal. A: General, 304 (2006) 1.
[4] P.A. Vaughan, Acta Crystallogr., 21 (1966), 983.
[5] T.M. Davis, C-Y. Chen, N. Žilková, D. Vitvaroná-Procházková, J. Čejka, S. Zones, J. Catal., 298 (2013) 84.
[6] F.R. Ribeiro, F. Alvarez, C. Henriques, F. Lemos, J.M. Lopes, M.F. Ribeiro, J. Mol. Catal. A: Chemical, 96 (1995) 245.
[7] S. van Donk, J.H. Bitter, K.P. de Jong, Appl. Catal. A: General, 212 (2001) 97.
[8] S-H. Lee, C-H. Shin, S.B. Hong, J. Catal., 223 (2004) 200.
[9] J. Houzvicka, V. Ponec, Appl. Catal. A: General, 145 (1996) 95.
[10] J. Houzvicka, J.G. Nienhuis, V. Ponec, Appl. Catal. A: General, 174 (1998) 207.
[11] G.D. Pirngruber, K. Seshan, J.A. Lercher, Micropor. Mesopor. Mater., 38 (2000) 221.
[12] V.L. Zholobenko, D.B. Lukyanov, J. Dwyer, J. Phys. Chem. B, 102 (1998) 2715.
[13] C. Márquez-Alvarez, A.B. Pinar, R. García, M. Grande-Casas, J. Pérez-Pariente, Top. Catal., 52 (2009) 1281.
[14] M. Trombetta, G, Busca, J. Catal., 187 (1999) 521.
[15] B. de Ménorval, P. Ayrault, N.S. Gnep, M. Guisnet, Catal. Lett., 98 (2004) 211.

[16] G. Onyestyák, Micropor. Mesopor. Mater., 104 (2007) 192.
[17] R. Rachwalik, M. Hunger, B. Sulikowski, Appl. Catal. A: General, 427-428 (2012) 98.
[18] H.L. Ngo, A. Nunez, W. Lin, T.A. Foglia, Eur. J. Lipid Sci. Technol., 108 (2007) 214.
[19] H.L. Ngo, R.O. Dunn, E. Hoh, Eur. J. Lipid Sci. Technol., 114 (2012) 213.
[20] Z.C. Zhang, M. Dery, S. Zhang, D. Steichen, J. Surf. Deterg., 7 (2004) 211.
[21] Helen L. Ngo, R. D. Ashby, A. Nunez, J. Am. Oil Chem. Soc., 89 (2012) 1885.
[22] J. Cason, W.R. Winans, J. Org. Chem., 15 (1949) 139.
[23] H. Wagner, R. Luther, T. Mang, Appl. Catal., A: General, 221 (2001) 429.
[24] D.V. Kinsman, J. Am. Oil Chem. Soc., 56 (1979) 823A.
[25] K.D. Haase, A.J. Heynen, N.L.M. Laane, Fat. Sci. Technol., 91 (1989) 350.
[26] H. L. Ngo, R.O. Dunn, B. Sharma, T.A. Foglia, Eur. J. Lipid Sci. Technol., 113 (2011) 180.
[27] R. Rachwalik, Z. Olejniczak, B. Sulikowski, Catal. Today, 101 (2005) 147.
[28] T.A. Isbell, R. Kleiman and B.A. Plattner, J. Am. Oil Chem. Soc., 71 (1994) 169.
[29] S. Storck, H. Bretinger, W. F. Maier, Appl. Catal., A: General, 174 (1998) 137.
[30] S. Zhang, Z.C. Zhang, Catal. Lett., 115 (2007) 114.
[31] T. Barzetti, E. Selli, D. Moscotti, L. Forni, J. Chem. Soc., Faraday Trans., 92 (1996) 1401.
[32] C.A. Emeis, J. Catal., 141 (1993) 347.
[33] B. Wichterlova, N. Zilkova, E. Uvarova, J. Cejka, P. Sarv, C. Paganini, J. A. Lercher, Appl. Catal. A: General, 182 (1999) 297.
[34] S. Bordiga, G. Turnes Palomino, C. Pazè, A. Zecchina, Micropor. Mesopor. Mater., 34 (2000) 67.
[35] K.I. Hadjiivanov, G.N. Vayssilov, in *Advances in Catalysis* (eds. B. Gates, H. Knözinger) Elsevier, Amsterdam, Vol. 47 (2002) pp 371.
[36] F. Kapteijn, J.A. Moulijn, R.A. van Santen, R. Wever, in *Catalysis: An Integrated Approach* (Eds. R.A. van Santen, P.W.N.M. van Leeuwen, J.A. Moulijn, B.A. Averill) Elsevier, Amsterdam, Vol. 123 (2000) pp 82.
[37] K. Chakarova, K. Hadjiivanov, Micropor. Mesopor. Mater., 177 (2013) 59.

Chapter 5

Summary, Concluding Remarks and Perspectives

5.1 Summary

Chapter 1 provides an introduction to oleochemistry and synthetic routes to branched fatty acids, and sets the background for this PhD research. The study is motivated by the need for better and more selective conversion processes in the alkyl isomerisation of fatty acids, and by the opportunity such improvements could bring in the broader utilisation of renewable and sustainable raw materials for the manufacture of consumer and industrial products.

Vegetable oils and animal fats have been used in industrial processes for over 150 years, however their utilisation has been dwarfed in the post-war chemical industry by hydrocarbon sources derived from crude oil and natural gas. As the world is faced with a dwindling supply of such mineral resources, there is growing interest to utilise plants, vegetables, wood and other renewable sources as raw materials for chemical building blocks. The additional benefit of the use of biomass-derived building blocks is the potential, when the products and materials are properly selected and converted, for a much-reduced CO_2 footprint compared to fossil-derived alternatives. Although the conversion technologies are still being developed in many cases, there are an increasing number of examples of platform chemicals now being derived from renewables on an industrial scale. The next phase, currently under development, is to combine the different technologies and raw materials on integrated “biorefinery” sites, in order to gain the economics, integration and scale from which the petrochemical industry benefits.

Fatty acids are the major raw materials of the modern oleochemical industry, and **Chapter 1** outlines the basic processes used in their manufacture: following hydrolysis of the crude vegetable oil or animal fat, a range of physical processes are used to purify and separate the fatty acids based on chain-length and/or melting point. Catalysis plays an important role in the derivatisation of these basic fatty acids; hydrogenation, amidation, amination, esterification and reduction to the alcohol are all industrially important catalytic processes.

Catalytic isomerisation (branching) of the (long) alkyl chains of hydrocarbons is widely performed in the petrochemical industry, as is the direct synthesis of such branched molecules. By contrast, examples of branching of fatty acids in the oleochemical industry are limited to the clay-catalysed polymerisation of unsaturated

fatty acids, where (mainly) methyl-branched fatty acids are formed as a co-product; however, it is difficult to steer the process to any significant degree towards higher yields of these branched acids. Following separation from the polymerised acids, hydrogenation and further purification, the complex mixture of isomers that is obtained, becomes the commercial product widely known as “isostearic acid”, henceforth referred to as ISAC.

ISAC holds a unique position in the oleochemical portfolio, due to its special combination of properties; low-temperature liquidity, thermal and oxidative stability, good biodegradability, lubricating and dispersing properties, amongst others. Major markets include lubricants and cosmetic products, in addition to a range of industrial applications. Despite these interesting properties and obvious potential, ISAC remains a relatively minor fatty acid product; the high costs of purification, and an inability to decouple its manufacture from that of the polymerised fatty acids, are certainly factors that limit the growth of this functionally versatile fatty acid.

The clay catalyst used in the co-production of ISAC is a montmorillonite material with interlayers of just the right depth to allow passage of the fatty acids onto the active sites, where the isomerisation takes place. The unconstrained carbocation intermediate, in addition to the desired rearrangement to the tertiary (branched) form, can also react freely with other unsaturated fatty acids to produce oligomerised fatty acids of 2 or 3 units, however. Modest selectivity improvements can be induced by controlling the swelling of the clay using water and cations, and by modifying the acidity of the clay, but the proportion of oligomerised fatty acids remains significant due to the unconstrained nature of the active site.

Zeolites, by contrast, contain active acid sites in channels with dimensional stability, potentially offering a constraining (shape-selective) mechanism by which to improve the selectivity of the branching reaction. Zeolites were studied as catalysts as early as the 1960’s for use in the petrochemical industry, and relevant industrially important transformations include the isomerisation of butene to isobutene and hydroisomerisation of linear alkanes (above C7); however, it was only in the 1990’s that researchers attempted to use zeolites for the branching of unsaturated fatty acids.

Early studies were based largely on extrapolations from results obtained in the petrochemical industry, and tended to favour the use of zeolites with medium to large pores/channels; water was also identified to be important for catalyst performance, although its function was not fully explained. Although some promising results were reported and accredited to the beneficial effects of crystal morphology modification and the introduction of mesopores, the high acidity and large channel sizes favoured in this early work in general led to unsatisfactorily high levels of by-products (e.g. lactones, polymerised acids, cracking products) and/or limited yields of the desired ISAC.

A significant breakthrough occurred in 2007, when Ngo and co-workers reported much higher yields and selectivities than previously achieved, using a protonated zeolite with the ferrierite framework (H-FER) [1]. Furthermore, they showed that addition of a bulky Lewis base (triphenylphosphine, TPP) enhanced selectivity to branched unsaturated fatty acids (BUFA). These new findings pointed to a shift in understanding of how the appropriate geometry and pore/channel size influence catalyst performance for his particular reaction. However, the zeolite was found to suffer from severe deactivation and to require regeneration treatment prior to re-use, in order to achieve economic viability.

Ferrierite belongs to the medium-pore zeolites, with two one-dimensional channels crossing perpendicularly to give 10-membered ring (MR) and 8-MR channels. This micropore system confers a number of catalytic properties specific to this zeolite compared to those previously tested. “Transition-state shape selectivity” is clearly a factor in inhibiting the oligomerisation, although more detailed insights are required to explain the exceptional yields and selectivities seen with this specific zeolite. This PhD Thesis aims to gain a detailed understanding of the structure - performance relationships displayed by H-FER in fatty acid isomerisation, by investigating two key topics: 1) the modes of and pathways to catalyst deactivation, and 2) the influence of key acidity parameters such as acid site density, accessibility and strength on catalyst performance.

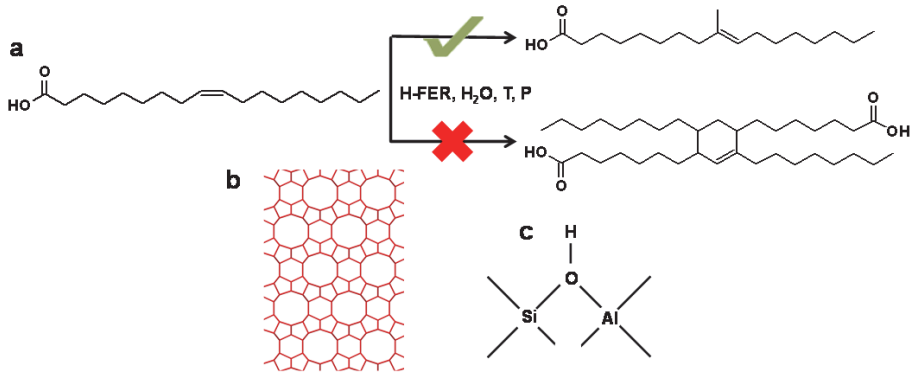

Figure 5.1: (a) Catalytic alkyl isomerisation of oleic acid over protonated ferrierite (H-FER), the reaction under study in this PhD Thesis; **(b)** framework of H-FER viewed along [001], showing the entrance of the medium 10-MR channels; **(c)** a zeolite Brønsted acid site, key to this reaction.

Chapter 2 focuses on the first major research topic and presents a detailed study of the liquid-phase skeletal isomerisation of oleic acid (OA) and its methyl ester (MO) in the presence and absence of TPP with commercial zeolite H-FER (with a Si/Al of 8.9), as catalyst material. The reactions have been carried out using a lab-scale batch reactor and conditions derived from Ngo and co-workers: 260 °C, 11 bar

and 5 wt% catalyst loading on OA [1]. Spent catalyst samples collected after catalytic testing have been analysed by a combination of analytical techniques, including UV-Vis and FT-IR spectroscopy. In addition, these materials have been submitted to HF dissolution, and the resulting carbonaceous extracts analysed by FT-IR, NMR and MS. The results confirm the superiority in activity and selectivity of the H-FER system, compared to the numerous zeolite types previously investigated. Addition of TPP to the reactant mixture further enhances the selectivity to BUFA, by binding reaction sites at the zeolite external surface where oligomerisation can occur.

A significant loss in conversion, observed in re-use experiments, indicated severe deactivation. While the FER framework was found to remain unaffected by the reaction, and little aluminium is leached, severe pore blockage was detected already at the moment the mixture reaches reaction temperature; this finding, coupled to the high selectivity, strongly suggests the importance a pore mouth mechanism must play in the catalytic conversion. The increased BUFA yields after addition of TPP support this model; the Lewis base selectively blocks non-specific surface reactions, and since the pores are already blocked at the onset of the reaction, only the pore mouths are left to provide the active sites for alkyl isomerisation.

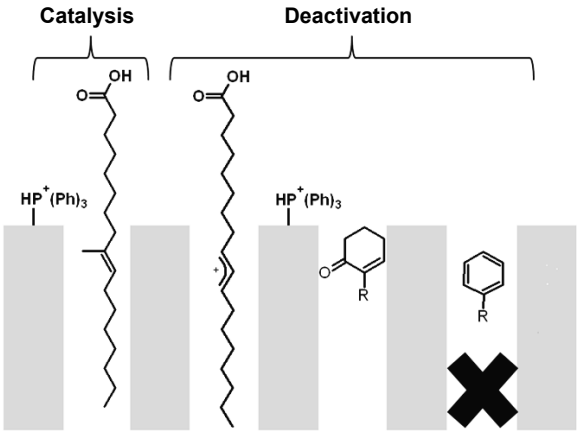

Figure 5.2: Overview of the blockage and poisoning process responsible for deactivation of H-FER during the alkyl isomerisation of OA, as investigated in Chapter 2.

Dodecylbenzene and other long chain alkylbenzenes were identified as the major “coke” constituents and are believed to be formed from OA via a cyclic conjugated ketone. In addition, (poly)enylic carbocations, formed through hydrogen transfer reactions between reactant species are held responsible for poisoning acid sites in the pore mouth and slowing down the skeletal isomerisation process. These (poly-)enylic species eventually undergo cyclisation, and are precursors to a very small amount of condensed aromatics. Higher levels of polyunsaturated acids in the

feedstock, i.e. oleic acid spiked with additional linoleic acid, enhance the level of carbonaceous deposits and the amount of condensed aromatics, supporting this explanation.

The elucidation of the mechanisms responsible for ferrierite deactivation and the related realisation that pore mouth catalysis leads to selectivity during skeletal isomerisation of OA provides valuable insights for the industrial development of this new and promising route to BUFA.

Pore mouth catalysis is a known, but still controversial model in zeolite catalysis. **Chapter 3** therefore seeks further evidence, by investigating the skeletal isomerisation of OA and elaidic acid (EA) over large zeolite ferrierite crystals (170 x 70 x 5 μm^3). Despite the very low surface area and pore mouth density, careful selection of the reaction conditions (i.e., slow stirring and long reaction time) enabled the catalysis of geometrical, positional and (to a minor extent) alkyl isomerisation, establishing the relevance of these model catalysts for commercial powdered zeolite ferrierite materials.

If catalysis is restricted to the pore mouth of the ferrierite, then an effect of surface area (and hence pore mouth number) on catalytic performance would be expected. This is indeed the case, as the model catalyst, with its significantly lower external non-basal surface area, reaches much lower conversion than the commercial ferrierite powders. The spent large zeolite crystals have subsequently been used to gain further evidence for the proposed model, by the powerful combination of microscopy and micro-spectroscopy techniques. Specifically, SEM measurements show that the catalyst morphology was conserved, and highlight two types of large crystals (thin and exfoliated platelets). Vis micro-spectroscopy enabled, by comparison with bulk Vis data, the detection of aromatic species and their localisation at the crystal edges. Confocal fluorescence microscopy also strongly suggested the coexistence of traces of polyenylic carbocations. Finally, polarisation-dependent fluorescence microscopy revealed that these carbonaceous species are, within all edges of the large H-FER crystals, aligned exclusively in the 10-MR channels. Mapping of the carbonaceous species in the model H-FER therefore provides evidence that the larger 10-MR channel pore mouths host the active sites for the skeletal isomerisation of OA and EA.

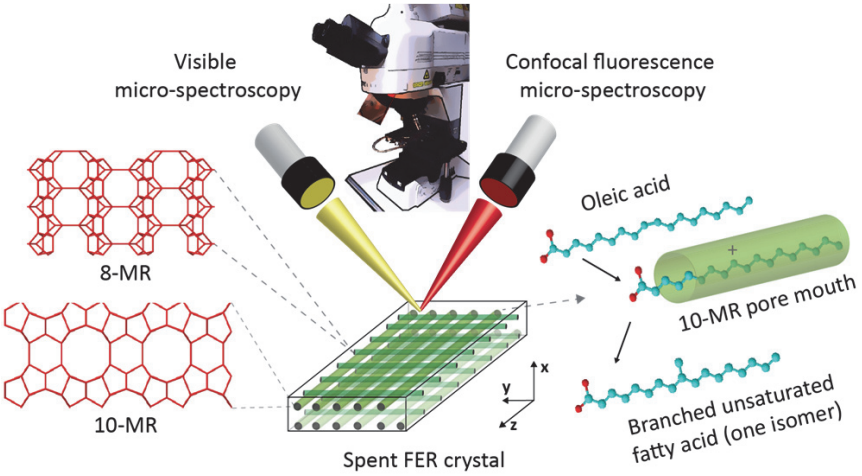

Figure 5.3: Schematic of the methodology based on the combination of Vis micro-spectroscopy and fluorescence microscopy, applied in Chapter 3 to confirm the pore mouth catalysis hypothesis for the alkyl isomerisation of OA.

Having established the link between the performance and properties of the H-FER framework in the alkyl isomerisation of OA, it is similarly important to understand the influence of acidity parameters (with a view to developing new and improved catalysts specifically tailored to this reaction), and this is the objective of **Chapter 4.** The skeletal isomerisation of OA has been studied using different commercial H-FER catalysts. Despite four of the five having very similar Si/Al ratios, they show significant differences in activity and selectivity towards the monomeric, BUFA and MoBUFA fractions. When comparing their morphology and textural properties, only their external surface areas were found to differ significantly, but without any clear correlation with their activity, as would be expected from the pore mouth catalysis model. Therefore, to understand the parameters at play, a number of complementary characterisation techniques have been used to assess the acidity characteristics of these materials in detail, including density, type, location, accessibility and strength.

The initial activity correlates with the Brønsted acidity in the 10-MR channels, as measured by adsorption/desorption of pyridine and IR; this result is consistent with the evidence for 10-MR channel pore mouth catalysis found in **Chapter 3**. XPS shows that, in general, a lower acidity in the outer crystallite layer enhances the selectivity to monomeric fatty acids. However, this method does not discriminate unconstrained, non-selective acid sites from selective ones located at the pore mouth. Based on the enhanced selectivity observed for isomerisation in presence of TPP, a method was developed to probe the density of non-selective acid sites in ferrierites of similar outer acidity by UV-Vis spectroscopy after TPP chemisorption. The lowest density of unconstrained external acid sites was found to correlate well

with the highest selectivity to monomeric fatty acids. The catalysts tested are characterised by a high ratio of Brønsted to Lewis sites, required for high BUFA yield. In addition, adsorption/desorption of CO followed by IR confirmed that *all* of these catalysts have 10-MR Brønsted acid sites of similar strength. High MoBUFA selectivity requires a lower effective acidity, i.e. fewer Brønsted acid sites in the 10-MR channels, as seen by NH_3-TPD.

Low external acidity, and low density of strong Brønsted acid sites in the 10-MR channels, are specific characteristics of the commercial zeolite H-FER "cp914c", which correspondingly gives the highest BUFA yield and selectivity to MoBUFA of the 4 catalysts tested with similar Si/Al. Evidently, the overall performance of the catalyst also depends on the synthesis route and/or the post-treatment applied. Detailed insights into the required characteristics in terms of acidity have been obtained, knowledge that can be used to guide the design of better OA alkyl isomerisation catalysts.

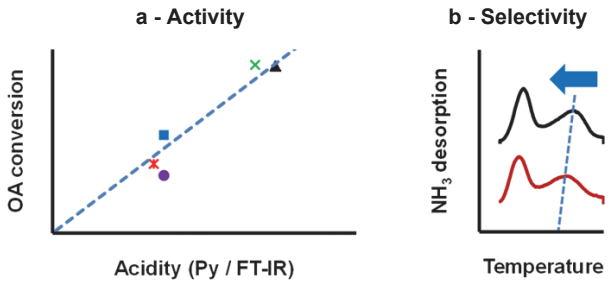

Figure 5.4: Key acidity parameters for the alkyl isomerisation of OA investigated in Chapter 4: **(a)** initial pore conversion correlates with Brønsted acidity in the 10-MR channels, as measured by pyridine adsorption/desorption, followed by FT-IR; **(b)** formation of MoBUFA is favoured by a lower effective acidity (fewer Brønsted acid sites), as measured by NH_3-TPD.

5.2 Concluding Remarks

The light alkyl branching of isostearic acid (ISAC) imparts a specific combination of physical properties and functionalities, giving it a unique position in the oleochemical portfolio. With its vegetable oil (or animal fat) origin, this special fatty acid has the potential to become a key building block in the expanding market for products and ingredients derived from renewable, sustainable resources. However, in order to achieve this goal, a much more cost-effective and selective route to alkyl isomerisation (branching) of unsaturated fatty acids is required.

Ferrierite, a medium pore zeolite, in its acid form has recently been found to give a step change improvement in both activity and selectivity to branching. The study of structure - performance relationships presented in this PhD Thesis, provides

insights into the underlying reasons for the exceptional properties of ferrierite for this reaction: in particular, the ideal size of its 10-membered ring (10-MR) channels, and the optimum strength of the Brønsted acid sites located in these channels.

Nevertheless, although all ferrierites give relatively good results compared to other frameworks, significant variations are seen in the performance of different zeolite H-FER, even those with very similar Si/Al ratio; in all cases, the location and density of the active site require modification in order to maximise both activity *and* selectivity to (mono-)branching. Specifically, elimination of non-constrained acid sites on the surface of the ferrierite crystallite, and careful control of the acid site density within the 10-MR channels, are essential to achieving the most selective catalyst. In conclusion, the performance of the H-FER can be further improved by modifying acidity via post-treatment and/or by controlling the acidity during synthesis.

Further, this study reveals some important intrinsic limitations of the ferrierite framework for the alkyl isomerisation of OA; the reaction is limited to the pore mouths of the 10-MR channels and, as a result, only a very small part of the zeolite surface is effectively used. This surprising finding implies there is considerable scope for the design of much more effective catalysts for this reaction.

Finally, this work illustrates the benefits of linking the properties of a catalyst at the bulk level to those of a single catalyst particle. Such an approach is well-suited to the study of zeolites, and hence the ferrierite used in this reaction, as they are ordered crystalline structures; the single particles give insights into e.g. location and orientation of reaction sites, which can then be extrapolated to what is seen in the bulk. Visualisation of spent model ferrierites by a number of microscopy/micro-spectroscopy techniques has hereby enabled the confirmation of the concept of pore mouth catalysis, restricted specifically to the larger zeolite channels. Furthermore, the combination with bulk spectroscopy has led to elucidation of the mechanism by which the remaining acid sites become poisoned, and hence a complete explanation of the severe deactivation observed with the bulk reactions.

These new findings provide the insights required to design much more cost-effective catalysts for alkyl-chain branching of fatty acids, a reaction which allows the production of functionally superior bio-based chemicals and ingredients, mirroring the established technology of alkyl chain branching of hydrocarbons in the mineral/petrochemical industry.

5.3 Perspectives

Ferrierite shows excellent potential as catalyst for the alkyl isomerisation of unsaturated fatty acids. Its framework of medium-sized channels with strong Brønsted acid sites plays a key role in the catalysis, and marks it out as an effective zeolite for this reaction. Nevertheless, significant shortcomings remain, and this PhD

Thesis indicates two main directions to explore, in order to further improve its performance. The first study should focus on further improving the selectivity to (mono-)branching, while the second study should address the activity, with potentially concomitant benefits for the stability. The ideal catalyst would allow these sometimes competing requirements to be reconciled.

In general, the contemporary "toolbox" available for catalyst design can be organised in different ways: "bottom-up" (or "assembly") strategies directly synthesise the structure, while "top-down" (or "demetallation") strategies start from an existing zeolite, and modify it in various ways. These approaches can be further divided into templating and non-templating methods, and can even be combined.

Based on the status of this research field and the knowledge gained in this PhD Thesis, the "top-down" approaches appear more realistic and cost-effective in the short-to-medium term. This conclusion is also reinforced by the significant research that has already been carried out on modification of ferrierites by the top-down approach, providing researchers with a solid foundation on which to build and develop new synthesis protocols. However, "bottom-up" approaches could be used to validate some of the insights in the structure-performance relationships gained in this PhD Thesis.

5.3.1. Selectivity to (Mono-)branching

Chapter 4 shows some significant differences in activity and selectivity for zeolites with similar Si/Al ratios related to the acidity location and density. As already mentioned, this suggests that the acidity can be optimised to further enhance (mono-)branching. A first strategy would be to control the effective acidity in the 10-MR channels through the synthetic route. If required, the outer surface of the crystals could be modified, in order to remove or quench any non-selective acidity.

In the absence of alkaline cations, the number of acid sites within the channels was found to be tunable by combining two structure directing agents (SDA), a small and a larger one [2-3]. For example, the relative amount of acid sites in the 10-MR channels of ferrierite could be increased from 10 to 36% by Pinar and co-workers by replacing pyrrolidine with 1-benzyl-1-methylpyrrolidinium and tetramethylammonium (BMP-TMA based template) [2,3] and even to 73% by Román-Leshkov et al. with hexamethyleneimine and TMA (HME-TMA based template) [3]. When the synthesis was performed using pyrrolidine in the presence of sodium cations, an acid site density of about 50% was measured in the 10-MR channel [2], significantly lower than ferrierites made without any organic SDA [4].

Synthesis in absence of organic template is simpler and more cost-effective, and therefore generally preferred in industrial applications. Despite this obvious advantage, zeolites made without organic SDA also show lower crystallinity and contain more non-selective sites, and therefore require post-synthesis modification

[5-6]. For example, a combination of steaming prior to exchange, followed by ammonium exchange and acid washing, has been found to be an effective post-treatment for ferrierites used in the isomerisation of butene to isobutene, giving final catalyst properties comparable to the more expensive templated alternatives [6].

5.3.2. Activity

Chapters 2 and 3 show that the reaction is limited to the 10-MR pore mouths, since the channels experience rapid blockage and poisoning from an early stage of the reaction. An obvious strategy is to increase the acid site density within the pore mouth of the 10-MR channels [2-3]; however, this would compromise the selectivity to (mono-)branching, and promote cracking reactions [7]. Alternatively, activity of the catalyst could be improved by increasing the density of pore mouths with enhanced access to active sites within the 10-MR channels, while preserving their strength; this would also have a beneficial effect on the deactivation.

Accessibility of the active acid sites of the zeolite has been a key focus of the literature, since diffusion limitation is intrinsically associated with the geometry of the micropore system. A number of strategies have thus been proposed to create auxiliary mesopores in the zeolites [8-10]. This effort has been motivated by two goals: to extend the use of zeolites to more bulky molecules, and to minimise secondary reactions leading to carbonaceous deposits and subsequently deactivation. These objectives are also relevant for the alkyl isomerisation of unsaturated fatty acid over ferrierite.

It is instructive to highlight some of the achievements in modification of ferrierites (mainly by the top-down approach) reported in the literature, which provide relevant starting points for future catalyst design for alkyl isomerisations.

Dealumination of ferrierite by oxalic acid results, in the gas-phase isomerisation of butene to isobutene, in a lower conversion, which correlates with the lower total number of acid sites. On the other hand, the higher selectivity to isobutene observed at low time-on-stream (TOS) is explained by the removal of non-selective external acid sites. Although the formation of mesopores is not mentioned, the treatment was found to lead to a larger external surface [11]. When applying dealumination by HCl to ferrierite used for the liquid-phase isomerisation of α-pinene, a significant increase in conversion (72 to 97%) has been observed, despite the lower Si/Al ratio. Evidence of mesopore formation (e.g. increase of external surface from 40 to 45 m^2/g) is only reported after dealumination under stronger conditions. The observed changes in product selectivity are instead explained by the increase of the Brønsted acid site strength [12].

Desilicated ferrierite has been successfully used for polyethylene pyrolysis [13]. After optimisation of the NaOH treatment, significant mesoporosity of both an inter- and intracrystalline nature was achieved (i.e. increase of the mesopore area by

a factor 3-4). This treatment is therefore much more effective than dealumination for the generation of mesoporosity, and in this work was confirmed to result in a faster conversion of the PE at lower temperature.

Delamination of ferrierite to give a material called ITQ-6 resulted in a further increase of the external surface (by a factor of ten). This nanosheet-based material is characterised by Brønsted and Lewis acid sites similar to those of the parent zeolite, but with greater accessibility (increased from 5 to 90%, based on 2,6-di-*tert*-butylpyridine adsorption/desorption followed by IR). The benefit of such a material is clearly reflected in the enhanced conversion measured for the cracking of 1,3,5-triisopropylbenzene [14]. However, the template used to synthesise the starting zeolite, and the ionic surfactant selected for the swelling step, are expensive. In addition, the significant increase of the external surface may also lead to a selectivity loss if it includes non-constrained acid sites.

5.3.3. Preliminary Results for the Alkyl Isomerisation of OA

Little has been reported on the effect of the above techniques on the efficiency of alkyl isomerisation of OA; only mass transfer limitations have been considered, by selection of specific molecular sieve materials with larger or even mesoporous channels. **Chapter 1** notes that increasing the pore size of the zeolite above 6 Å (e.g. zeolite Beta, BEA [15-16]) or using mesoporous sieves (MAS-5 [17-18]) has been shown to improve conversion, but at the expense of selectivity to the desired branched fatty acid. Alternatively, manipulation of the zeolite L morphology (LTL), to obtain flat crystals with smaller diffusion path, resulted in an increased OA conversion [19-20]. Both pieces of evidence support a strategy of improving accessibility to the active site, in a way that does not compromise the intermediate-state selectivity *at* the active site.

Building on the literature data described above, some preliminary experiments have been carried out using oxalic acid under strong conditions to dealuminate the outer surface of the ferrierite crystals. Catalytic testing (1.5 wt% H-FER on OA) has been carried out using a 15 mL multi-autoclave setup, following the procedure and conditions described in **Chapter 4**; the results obtained for the crude mixture composition and the H-FER before/after oxalic treatment are summarised in **Tables 5.1 and 5.2**, respectively. They show that by increasing the external surface and total pore volume (meso- and micropores) in a controlled way, a significant improvement in OA conversion from 74 to 87% is achieved after 3 h, without any increase of the oligomeric fraction (~10 wt%).

Table 5.1: Crude product analysis, for the skeletal isomerisation of OA at 260 °C over zeolite H-FER[a] (1.5 wt% loading), before and after treatment with oxalic acid (1 M, 75 °C, 24 and 48 h [11]).

Exp.	Catalyst	Reaction time (h)	Oligomer yields[b] (wt%)	BUFA yields[b] (wt%)	MoBUFA yields[b] (wt%)	Lactone yields[b] (wt%)	Conversion[b] (wt%)
1	2[c]	3	9.7	56	52	9.6	74
2	2_24h	3	10	58	53	7.9	81
3	2_48h	3	10	64	59	7.3	87

a: The reaction have been carried out using the 15 mL multi-autoclave setup and the procedure described in Chapter 4 (4.2.2).
b: The crude product has been determined using the equipment and methods given in Chapter 4 (4.2.2).
c: The parent H-FER used in this work is catalyst 2 in Chapter 4 (Table 4.2).

Table 5.2: Overview of textural properties based on N_2 physisorption of zeolite H-FER[a], before and after treatment with oxalic acid (1 M, 75 °C, 24 and 48 h [11]).

Catalyst	BET[a] Area (m^2/g)	S_E, External[a] area (m^2/g)	V_T,Total pore[a] volume(cm^3/g)	V_μ, Micropore[a] volume (cm^3/g)
2[b]	298	31	0.251	0.131
2_24h	319	47	0.268	0.134
2_48h	318	48	0.281	0.133

a: The equipment and methods used for the analyses of the zeolite samples are described in Chapter 4 (4.2.3).
b: The parent H-FER used in this work is catalyst 2 in Chapter 4 (Table 4.2).

These preliminary experimental results, together with the range of tools and techniques available for tailoring the detailed structure and acidity of the molecular sieve as outlined in literature, give reasons to be optimistic that significant further improvements are possible for the alkyl isomerisation of unsaturated fatty acids - and potentially other lipid-based raw materials. Such post-treated zeolites will further lower catalyst loading, and reduce deactivation rates; these are important conditions for the development of a sustainable and cost-effective process for ISAC production.

References

[1] H.L. Ngo, A. Nunez, W. Lin, T.A. Foglia, Eur. J. Lipid Sci. Technol., 108 (2007) 214.
[2] A.B. Pinar, C. Márquez-Álvarez, M. Grande-Casas, J. Pérez-Pariente, J. Catal., 263 (2009) 258.
[3] Y. Román-Leshkov, M. Moliner, M.E. Davis, J. Phys. Chem. C, 115 (2011) 1096.
[4] R.A. Rakoczy, M. Breuninger, M. Hunger, Y. Traa, J. Weitkamp, Chem. Eng. Technol., 25 (2002) 273.
[5] W. Xu, Y. Yin, S.L. Suib, J.C. Edwards, C. O'Young, J. Phys. Chem., 99 (1995) 9443.
[6] W. Xu, Y. Yin, S.L. Suib, J.C. Edwards, C. O'Young, J. Catal., 163 (1996) 232.
[7] B. de Ménorval, P. Ayrault, N.S. Gnep, M. Guisnet, Catal. Lett., 98 (2004) 211.
[8] S. van Donl, A.H. Hanssen, J.H. Bitter, K.P. de Jong, Catal. Rev., 45 (2003) 297.
[9] J. Pérez-Ramírez, C.H. Christensen, K. Egeblad, C.H. Christensen, J. Groen, Chem. Soc. Rev., 37 (2008) 2530.
[10] K. Möller, T. Bein, Chem. Soc. Rev., 42 (2013) 3689.
[11] B.S. Kwak, J. Sung, Catal. Lett., 53 (1998) 125.
[12] R. Rachwalik, Z. Olejniczak, J. Jiao, J. Huang, M. Hunger, B. Sulikowski, J. Catal., 252

(2007) 161.
[13] A. Bonilla, D. Baudouin, J. Pérez-Ramírez, J. Catal., 265 (2009) 170.
[14] A. Corma, U. Diaz, M.E. Domine, V. Fornés, J. Am. Chem. Soc., 122 (2000) 2804.
[15] S. Zhang, Z. Zhang, D. Steichen, US patent 6831184 (2004), to Akzo Nobel N.V.
[16] Z. Zhang, S. Zhang, US patent 7098353 (2006), to Akzo Nobel N.V.
[17] L.Ha, J.Mao, J. Zhou, Z.C. Zhang, S. Zhang, Appl. Catal. A: General, 356 (2009) 52.
[18] S. Zhang, Z. Zhang, European patent 1490171 (2004), to Akzo Nobel N.V.
[19] W.R. Hodgson, C.M. Lok, G. Roberts, W.T. Koetsier, European patent 0774451 (1997), to Unichema Chemie B.V.
[20] W.R. Hodgson, W.T. Koetsier, C.M. Lok, G. Roberts, US patent 5856539 (1999), to Unichema Chemie B.V.

Nederlandse Samenvatting

Hoofdstuk 1 geeft een inleiding in de oleochemie en de synthetische routes naar vertakte vetzuren, en schetst de achtergrond voor dit promotieonderzoek. De studie wordt ingegeven door de behoefte aan betere en selectievere processen voor de skeletisomerisatie van vetzuren, en de mogelijkheden die dergelijke verbeteringen kunnen opleveren voor breder gebruik van hernieuwbare en meer duurzame grondstoffen voor de productie van consumenten- en industriële producten.

Plantaardige oliën en dierlijke vetten worden al meer dan 150 jaar gebruikt in industriële processen, maar het gebruik ervan is in de naoorlogse chemische industrie overschaduwd door koolwaterstofbronnen zoals aardolie en aardgas. Omdat de wereld wordt geconfronteerd met een afnemend aanbod van dergelijke minerale hulpbronnen, is er groeiende belangstelling om planten, groenten, hout en andere hernieuwbare bronnen als grondstof voor chemische bouwstenen te gebruiken. Het bijkomend voordeel van het gebruik van bouwstenen afkomstig uit biomassa is in potentie een lagere CO_2-uitstoot in vergelijking met fossiele alternatieven, mits de producten en materialen zorgvuldig worden geselecteerd en omgezet. Hoewel de omzettingstechnologieën nog vaak in ontwikkeling zijn, komen er steeds meer voorbeelden van platformchemicaliën op industriële schaal die nu worden gewonnen uit hernieuwbare grondstoffen. De volgende fase, nu reeds in het beginstadium, is het combineren van de verschillende technologieën en grondstoffen tot geïntegreerde "bioraffinage" sites, teneinde de economie, integratie en schaalvoordelen te verkrijgen waar de petrochemische industrie al gebruik van maakt.

Vetzuren zijn de belangrijkste grondstoffen van de moderne oleochemische industrie en Hoofdstuk 1 schetst de fundamentele processen die onderdeel zijn van het productieproces: na de hydrolyse van de ruwe plantaardige olie of dierlijk vet, worden verschillende fysische processen gebruikt voor het zuiveren en scheiden van de vetzuren op basis van ketenlengte en/of smeltpunt. Katalyse speelt een belangrijke rol bij de derivatisering van deze basisvetzuren; hydrogenering, amidering, aminering, verestering en reductie tot alcohol zijn belangrijke katalytische processen voor de oleochemische industrie.

Katalytische isomerisatie (vertakking) van de (lange) alkylketens van koolwaterstoffen wordt wijdverbreid uitgevoerd in de petrochemische industrie, net zoals de directe synthese van dergelijke vertakte moleculen. Daarentegen zijn voorbeelden van vertakking van vetzuren in de oleochemische industrie beperkt tot de klei-gekatalyseerde polymerisatie van onverzadigde vetzuren, waarin (hoofdzakelijk) methyl-vertakte vetzuren worden gevormd als een co-product; het is

echter moeilijk om dit proces te sturen naar aanzienlijk hogere opbrengsten van deze vertakte zuren. Na scheiding van de gepolymeriseerde zuren van de oligomere hoofdcomponent, hydrogenering en verdere zuivering, wordt een complex mengsel van isomeren verkregen dat als handelsprodukt algemeen bekend staat als "isostearinezuur", hierna te noemen ISAC.

ISAC heeft een unieke positie in de oleochemische portefeuille, vanwege de bijzondere combinatie van eigenschappen; dit betreft onder andere lage temperatuur vloeibaarheid, thermische en oxidatieve stabiliteit, goede biologische afbreekbaarheid, smeer- en dispergerende eigenschappen. Belangrijke markten zijn smeermiddelen en cosmetische producten, en een scala aan industriële toepassingen. Ondanks deze interessante eigenschappen en duidelijk potentieel blijft de productie van ISAC relatief klein wat betreft volume; de hoge kosten van zuivering en de onmogelijkheid om de vervaardiging los te koppelen van die van gepolymeriseerde vetzuren zijn zeker factoren die de groei van dit functioneel veelzijdige vetzuur beperken.

De kleikatalysator die wordt gebruikt bij de productie van ISAC is een montmorilloniet met tussenlagen van precies de juiste diepte die het mogelijk maken dat de vetzuren op de actieve plaatsen komen, waar de isomerisatie plaatsvindt. Naast de gewenste omzetting naar de tertiaire (vertakte) vorm, kan het ongebonden carbokation-intermediair echter ook vrij reageren met andere onverzadigde vetzuren waarbij geoligomeriseerde vetzuren gevormd worden van twee of drie eenheden. Bescheiden verbeteringen in selectiviteit kunnen worden gerealiseerd door het regelen van de zwelling van de klei met water en kationen, en door aanpassing van de zuurtegraad van de klei, maar het aandeel van geoligomeriseerde vetzuren blijft hoog door de open structuur van de actieve plaats.

Zeolieten daarentegen bevatten actieve plaatsen in kanalen met dimensionele stabiliteit, met mogelijk een begrenzend (vormselectief) mechanisme, waarmee de selectiviteit van de vertakkingsreactie kan worden verbeterd. Zeolieten werden al onderzocht als katalysatoren in de jaren 60 voor de petrochemische industrie. Enkele relevante en voor de industrie belangrijke voorbeelden zijn de isomerisatie van buteen tot isobuteen en isomerisatie van lineaire alkanen (boven C7); het was echter pas in de jaren 90 dat onderzoekers geprobeerd hebben om zeolieten te gebruiken voor het maken van vertakte onverzadigde vetzuren.

Vroege studies zijn grotendeels gebaseerd op extrapolatie van resultaten verkregen in de petrochemische industrie, wat leidde tot de neiging om bij voorkeur zeolieten te gebruiken met middelgrote en grote poriën/kanalen; water werd ook geïdentificeerd als belangrijk factor voor de werking van de katalysator, hoewel de rol daarvan niet volledig kon worden verklaard. Hoewel enkele veelbelovende resultaten werden gerapporteerd en toegewezen aan de gunstige effecten van wijzigingen in kristalmorfologie en het aanbrengen van mesoporiën, leidde de hoge zuurtegraad en grote poriegroottes, die in dit vroege werk de voorkeur hadden, in het algemeen tot

onbevredigend hoge concentraties van nevenproducten (zoals lactonen, gepolymeriseerde zuren, kraakproducten) en/of beperkte opbrengsten van het gewenste ISAC.

Een belangrijke doorbraak deed zich voor in 2007, toen Ngo et al. veel hogere opbrengsten en selectiviteiten rapporteerden dan eerder waren gerealiseerd met behulp van een geprotoneerd zeoliet van het ferrieriet type (H-FER) [1]. Bovendien toonden ze aan dat toevoeging van een Lewisbase (trifenylfosfine, TPP) van voldoende grootte de selectiviteit verbeterde voor vertakte onverzadigde vetzuren (BUFA). Deze nieuwe vinding zorgde voor een verandering van opvatting over hoe de juiste geometrie en porie- en kanaalgrootte van invloed zijn op de werking van de katalysator voor zijn specifieke reactie. De zeoliet bleek echter ernstig te deactiveren waardoor uitgebreide opwerking vóór hergebruik vereist is om het proces rendabel te laten zijn.

Ferrieriet is een zeoliet met middelgrote poriën met twee loodrecht kruisende ééndimensionale kanalen met een 10-voudige ringstructuur en 8-voudige ringstructuren (MR). Dit microporiesysteem leidt tot een aantal unieke katalytische eigenschappen vergeleken met de eerder geteste zeolieten. Selectiviteit door beperking van de ruimtelijke vorm van de overgangstoestand, is een factor in het remmen van de oligomerisatie, hoewel meer gedetailleerd inzicht nodig is om de uitzonderlijke opbrengsten en selectiviteiten te verklaren die gezien zijn met deze specifieke katalysator. Dit proefschrift heeft tot doel een gedetailleerd inzicht te verkrijgen in de correlatie tussen structuur en de prestaties van H-FER in vetzuurisomerisatie, door twee belangrijke onderwerpen te onderzoeken: 1) de manieren van en routes naar katalysatordeactivering, en 2) de invloed van de belangrijkste zuurtegraadparameters zoals dichtheid, toegankelijkheid en sterkte van zure sites op katalysatoractiviteit.

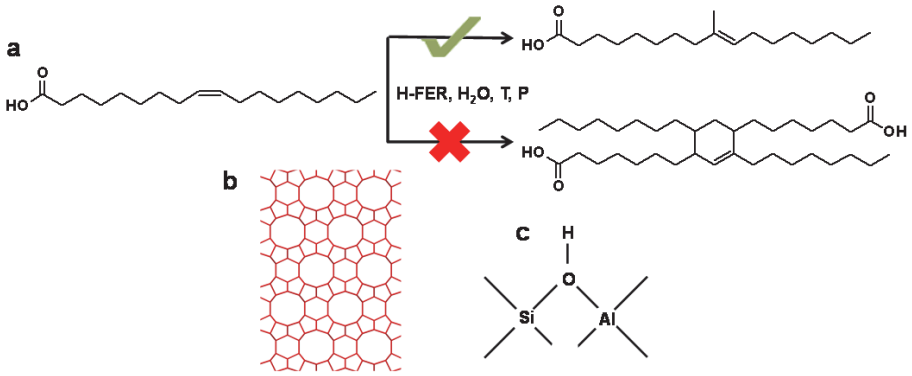

Figuur 1: (a) Katalytische skeletisomerisatie van oliezuur in geprotoneerd ferrieriet (H-FER), de reactie die in dit proefschrift is bestudeerd; **(b)** framework van H-FER gezien langs de [001] richting, waardoor de ingang van de middelgrote 10-MR kanalen zichtbaar wordt; **(c)** Brønsted zure sites in H-Fer, belangrijk voor deze reactie.

Hoofdstuk 2 richt zich op het eerste grote onderzoeksonderwerp en presenteert een gedetailleerde studie van de ketenisomerisatie van oliezuur (OA) en zijn methylester (MO) in de vloeistoffase en in aanwezigheid en afwezigheid van TPP met de commerciële zeoliet H-FER (met een Si/Al verhouding van 8.9) als katalysatormateriaal. De reacties werden uitgevoerd met een laboratoriumschaal-batchreactor en condities die zijn afgeleid van het werk van Ngo et al.: 260 ° C, 11 bar en 5 gew% katalysatorbelading met OA [1]. Gebruikte katalysatormonsters werden na het katalytisch testen verzameld en geanalyseerd met een combinatie van analytische technieken, waaronder UV-Vis en FT-IR spectroscopie. Daarnaast zijn deze materialen opgelost in HF en de resulterende koolstofhoudende extracten geanalyseerd met FT-IR, NMR en MS. De resultaten bevestigen de superioriteit in activiteit en selectiviteit van het H-FER systeem, in vergelijking met de vele zeolieten die voorheen zijn onderzocht. Toevoeging van TPP aan het reactiemengsel verbetert de selectiviteit naar BUFA door binding aan reactieplaatsen op het buitenoppervlak van het zeoliet waar oligomerisatie kan optreden.

Een significant verlies in omzetting, waargenomen in hergebruikexperimenten, wees op ernstige deactivering. Terwijl bleek dat de FER structuur werd aangetast door de reactie en slechts weinig aluminium word verloren in de vloeistof, werd een ernstige blokkering van de poriën al op het moment dat het mengsel de reactietemperatuur bereikt; deze bevinding, gekoppeld aan de hoge selectiviteit, wijst sterk op de belangrijke rol die een zogenoemd poriemond-mechanisme moet spelen in de katalytische omzetting. De toegenomen BUFA opbrengst na toevoeging van TPP ondersteunt dit model; de Lewisbase blokkeert selectief niet-specifieke oppervlaktereacties, en aangezien de poriën reeds bij het begin van de reactie geblokkeerd raken, verschaffen alleen de poriemonden de actieve plaatsen voor skeletisomerisatie.

Dodecylbenzeen en andere langketenige alkylbenzenen werden geïdentificeerd als de belangrijkste “cokes” bestanddelen en worden verondersteld te worden gevormd uit OA via een cyclisch geconjugeerd keton. Verder worden (meervoudig) geconjugeerde carbokationen, ontstaan uit waterstofoverdrachtreacties tussen reactanten, verdacht van de vergiftiging van de zure sites in de poriemond en vertraging van het ketenisomerisatieproces. Deze (meervoudig) geconjugeerde componenten ondergaan uiteindelijk cyclisatie, en zijn de voorlopers van een zeer kleine hoeveelheid gecondenseerde aromaten. Hogere concentratie van polyonverzadigde vetzuren in de voeding, dat wil zeggen oliezuur verrijkt met extra linolzuur, zorgen voor meer koolstofhoudende afzettingen en gecondenseerde aromaten, wat in overeenstemming met deze uitleg is.

De opheldering van de mechanismen die verantwoordelijk zijn voor ferrierietdeactivering en het daarmee verband houdende besef dat poriemondkatalyse leidt tot selectiviteit tijdens ketenisomerisatie van OA, biedt

waardevolle inzichten voor de verdere industriële ontwikkeling van deze nieuwe en veelbelovende route naar BUFA.

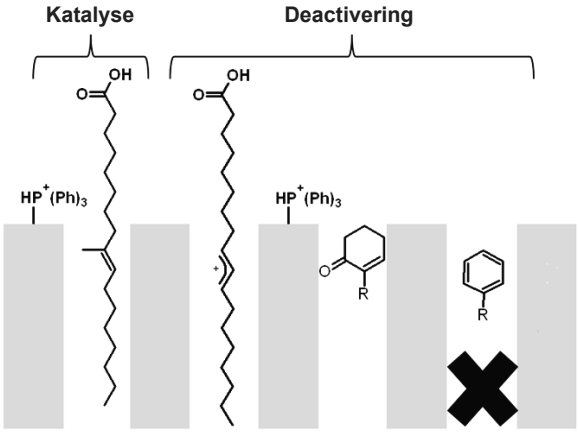

Figuur 2: Overzicht van het verstoppings- en vergiftigingsproces verantwoordelijk voor de deactivering van H-FER tijdens skeletisomerisatie van OA, zoals onderzocht in Hoofdstuk 2.

Poriemondkatalyse is een gekend, maar nog steeds controversieel model in zeolietkatalyse. In **Hoofdstuk 3** wordt daarom verder bewijs hiervoor gezocht, door het onderzoeken van de ketenisomerisatie van OA en elaidinezuur (EA), het transisomeer van OA, over grote ferrierietkristallen. Ondanks het zeer beperkte externe oppervlak en lage poriemonddichtheid, maakten een zorgvuldige selectie van de reactieomstandigheden (dat wil zeggen, langzaam roeren en lange reactietijd) de katalyse mogelijk van isomerisatie van de alkylgeometrie, positie en (in mindere mate) substitutie. Hiermee werd de relevantie van deze model katalysatoren voor de commerciële, poedervormige ferrierietmaterialen aangetoond.

De zeer lage conversie geconstateerd bij de modelkatalysator vergeleken met commerciële ferrierietpoeders, zoals verwacht vanwege het veel lagere externe oppervlak van de eerstgenoemde, ondersteunt feitelijk de hypothese van poriemondkatalyse. De gebruikte grootte zeolietkristallen (170 x 70 x 5 μm^3) zijn vervolgens bestudeerd m.b.v. een krachtige combinatie van microscopie- en micro-spectroscopietechnieken. SEM metingen laten zien dat de katalysatormorfologie behouden blijft en dat het materiaal uit twee typen grote kristallen bestaat (dunne en geschilferde plaatjes). Vis micro-spectroscopie maakte het mogelijk, door vergelijking met bulk Vis data, aromatische verbindingen te detecteren en lokaliseren op de randen van de kristallen. Confocale fluorescentiemicroscopie leverde sterke aanwijzigingen voor de coëxistentie van sporen van meervoudig geconjugeerde carbokationen. Tenslotte toonde polarisatie-afhankelijke fluorescentiemicroscopie dat deze koolstofhoudende materialen, in alle randen van de grote H-FER kristallen, uitsluitend opgelijnd zijn op een lijn komen in de 10-MR kanalen. Het in kaart

brengen van de koolstofhoudende materialen in de H-Fer modelmaterialen leverde zo het bewijs dat de grotere poriemonden in de 10-MR kannalen de actieve plaatsen bevatten voor de ketenisomerisatie van OA en EA.

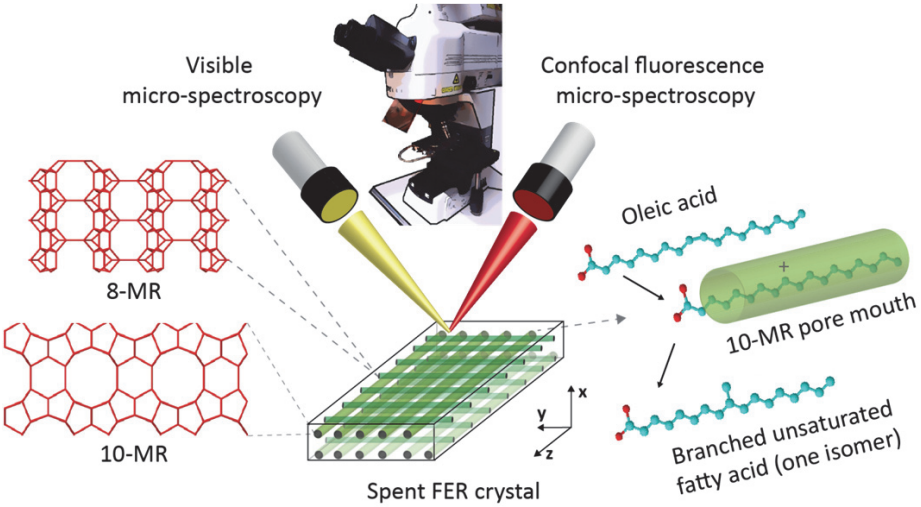

Figuur 3: Schematische voorstelling van de methodologie die gebaseerd is op de combinatie van Vis micro-spectroscopie en fluorescentiemicroscopie, toegepast hoofdstuk 3 om de hypothese van poriemondkatalyse voor skeletisomerisatie van OA te bevestigen.

Nu het verband is aangetoond tussen de prestaties en eigenschappen van het H-FER kristal grootte vorm in de skeletisomerisatie van OA is het eveneens van belang te begrijpen wat de invloed is van de zuurtegraadparameters (met het oog op de ontwikkeling van nieuwe en verbeterde katalysatoren voor deze reactie), en dit is de doelstelling van **Hoofdstuk 4**. De ketenisomerisatie van OA werd onderzocht met verschillende commerciële H-FER katalysatoren. Hoewel vier van de vijf een vergelijkbare Si/Al-verhoudingen hebben, vertonen ze significante verschillen in activiteit en selectiviteit voor de monomere, BUFA en MoBUFA fracties. Bij het vergelijken van hun morfologie en textuureigenschappen, bleken alleen hun uitwendige oppervlakken aanzienlijk te verschillen, maar zonder duidelijke correlatie met hun activiteit, zoals zou worden verwacht op basis van het poriemondkatalysemodel. Om de parameters die van belang zijn te begrijpen, is een aantal aanvullende karakterisatietechnieken gebruikt om de zure eigenschappen van deze materialen in detail in kaart te brengen, zoals dichtheid, type, locatie, toegankelijkheid en sterkte.

De aanvankelijke activiteit blijkt verband te houden met de Brønsted-zuurtegraad in de 10-MR kanalen, zoals gemeten door adsorptie/desorptie van pyridine en IR. Dit resultaat is consistent met het bewijs voor katalyse in de 10-MR kanaalporiemond (Hoofdstuk 3). Uit XPS metingen blijkt in het algemeen dat een

lagere zuurtegraad op/in de buitenste laag van het materiaal zorgt voor hogere selectiviteit naar monomere vetzuren. Echter, deze methode maakt geen onderscheid tussen vrije, externe niet-selectieve zure plaatsen en de selectieve zure plaatsen die zich bevinden in de poriemond. Op grond van de verbeterde selectiviteit waargenomen voor isomerisatie in aanwezigheid van TPP, werd een methode ontwikkeld op basis van UV-Vis spectroscopie na TPP chemisorptie, om de dichtheid van de niet-selectieve zure plaatsen in ferrierieten te onderzoeken die een vergelijkebare externe zuurtegraad hebben. De laagste dichtheid van vrije externe zure sites bleek goed te correleren met de hoogste selectiviteit voor monomere vetzuren. De geteste katalysatoren worden gekenmerkt door een hoge verhouding van Brønsted- tot Lewiszuren, vereist voor hoge BUFA yield. Daarnaast bevestigden metingen van adsorptie/desorptie van CO gevolgd door IR dat *al* deze katalysatoren 10-MR Brønstedzure plaatsen hebben van vergelijkbare sterkte. Hoge MoBUFA selectiviteit vereist een lagere zuurheid, dat wil zegen minder Brønstedzure plaatsen in de 10-MR kanalen, hetgeen tot uiting komt in een lagere effectieve zuurtegraad zoals gezien wordt met NH_3-TPD.

De lage externe zuurtegraad en lage dichtheid van sterke Brønsted zure sites in de 10-MR kanalen, zijn dus de specifieke kenmerken van de commerciële zeoliet H-FER "cp914c", die zorgen voor de hoogste BUFA opbrengst en selectiviteit voor MoBUFA in vergelijking met de katalysatoren met soortgelijke Si/Al die zijn getest. Uiteraard hangt de algehele prestatie van de katalysator ook af van de syntheseroute en/of nabehandeling die is toegepast. Het gedetailleerde inzicht in de gewenste kenmerken m.b.t. zuurtegraad dat is verkregen, kan nu worden gebruikt voor het ontwerp van betere OA skeletisomerisatiekatalysatoren.

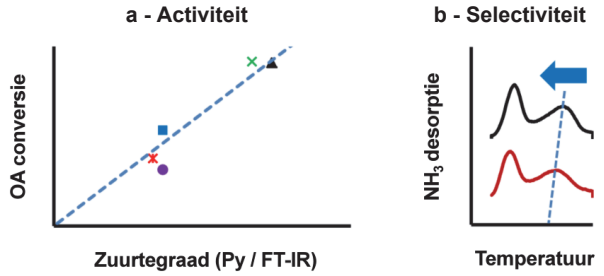

Figuur 4: Belangrijke zuurtegraadparameters voor de skeletisomerisatie van OA zoals onderzocht in Hoofdstuk 4: **(a)** het verband tussen initiële porieconversie en Brønstedzuurtegraad in de 10-MR kanalen, zoals gemeten met pyridine adsorptie/desorptie, gevolgd door FT-IR; **(b)** de vorming van MoBUFA wordt bevorderd door een lagere effectieve zuurtegraad (minder Brønstedzure plaatsen), zoals gemeten met NH_3-TPD.

Referenties

[1] H.L. Ngo, A. Nunez, W. Lin, T.A. Foglia, Eur. J. Lipid Sci. Technol., 108 (2007) 214.

List of Abbreviations

AlPO	Aluminophosphate
BET	Brunauer-Emmett-Teller
BMP	1-Benzyl-1-methylpyrrolidinium
BUFA	Branched-chain Unsaturated Fatty Acids
CCD	Charge-Coupled Device
CO-IR	Carbone monoxide adsorption/desorption followed by Fourier-transform Infrared spectroscopy
DEPT NMR	Distortionless Enhancement by Polarization Transfer - Nuclear Magnetic Resonance
DR	Diffuse Reflectance spectroscopy
EELS	Electron Energy Loss Spectroscopy
EFAl	Extra-Framework Aluminium
EMCCD	Electron-Multiplying Charge-Coupled Device
EU	European Union
ETO	Ethanol To Olefin
FER	Ferrierite
Exp.	Experiment
FID	Flamme Ionisation Detection
FT-IR	Fourier-Transform Infrared spectroscopy
ICP-MS	Inductively Coupled Plasma with Mass Spectrometry detection
GC	Gas Chromatography
GC-MS	Gas Chromatography with Mass Spectrometry detection
GCxGC	Two-dimensional Gas Chromatography
ISAC	Isostearic Acid
HT-GC	High-Temperature Gas Chromatography
H-FER	Protonated form of ferrierite
HME	Hexamethyleneimine

MAS NMR	Magic Angle Spinning Nuclear Magnetic Resonance
MO	Methyl Oleate
MoBUFA	Mono-Branched-chain Unsaturated Fatty Acids
MOD	Model catalyst
MR	Membered Ring
MTO	Methanol To Olefin
NA	Numerical Aperture
NH_3-TPD	Ammonia Temperature-Programmed Desorption
NMR	Nuclear Magnetic Resonance
OA	Oleic Acid
P	Pressure
Py	Pyridine
Py-IR	Pyridine adsorption/desorption followed by Fourier-transform Infrared spectroscopy
SAPO	Silicon-substituted Aluminophosphate
SDA	Structure Directing Agent
STEM	Scanning Transmission Electron Microscopy
T	Temperature
TCD	Thermal Conductivity Detector
TGA	Thermogravimetry Analyses
TMA	Tetramethylammonium
TOF-MS	Time-Of-Flight-Mass Spectrometry
TOS	Time-On-Stream
TPP	Triphenylphosphine
USA	United States of America
UV-Vis	Ultraviolet-Visible spectroscopy
Vis	Visible spectroscopy
XPS	X-ray Photoelectron Spectroscopy
ZSM	Zeolite Socony Mobil

List of Publications and Presentations

Publications on which this thesis is based

“Skeletal Isomerisation of Oleic Acid over Ferrierite in the Presence and Absence of Triphenylphosphine: Pore Mouth Catalysis and Related Deactivation Mechanisms”,
S.C.C. Wiedemann, J.A. Stewart, F. Soulimani, T. van Bergen-Brenkman, S. Langelaar, B. Wels, P. de Peinder, P.C.A. Bruijnincx, B.M. Weckhuysen, J. Catal., 316 (2014) 24-35 (DOI:10.1016/j.jcat.2014.04.018).

“Skeletal Isomerisation of Oleic Acid over Ferrierite: Influence of Acid Site Number, Accessibility and Strength on Activity and Selectivity”,
S.C.C. Wiedemann, A. Muñoz-Murillo, R. Oord, T. van Bergen-Brenkman, B. Wels, P.C.A. Bruijnincx, B.M. Weckhuysen, J. Catal., 329 (2015) 195-205 (DOI:10.1016/j.jcat.2015.05.013).

“Isostearic Acid, a Unique Fatty Acid with Great Potential”,
S.C.C. Wiedemann, P.C.A. Bruijnincx, B.M. Weckhuysen, in *Chemicals and fuels from bio-based building blocks* (eds. F. Cavani, F. Basile, S. Albonetti, A. Gandini) Wiley-VCH, Weinheim, accepted for publication.

“Large Ferrierite Crystals as Models for Catalyst Deactivation during Skeletal Isomerization of Oleic Acid: Evidence for Pore Mouth Catalysis”,
S.C.C. Wiedemann, Z. Ristanović, G.T. Whiting, V.R.R. Marthala, J. Kärger, J. Weitkamp, B. Wels, P.C. A. Bruijnincx and B.M. Weckhuysen, accepted for publication in Chem. Eur. J.

Other publications

Emission spectroscopy
“Excited Species from a Pulsed Discharge in Helium at One Atmosphere Pressure”,
W.E. Wentworth, Y. Qin, S. Wiedemann, S.D. Stearns, J. Madabushi, Appl. Spectrosc., 49 (1995) 1282-1298.

NIR spectroscopy
"Developing a robust sampling and measuring unit for at-line NIR analysis of esters",

S.C.C Wiedemann, W.G. Hansen, V.A.L. Wortel and J.W.J. Gielen, J. Near Infrared Spec., 5 (1997) 149-156.

"Information Depth of Vis-NIR Light in Polyethylene Films Using Transmission and Reflectance Measurements",
W. Haanstra, W.G. Hansen, M.J.G. Huys, B.J. Kip, P. Palmen, J. Roumen, M. Snieder, T. Van De Weerdhof, S.C.C Wiedemann, V.A.L. Wortel, Appl. Spectrosc., 52 (1998) 863-868.

"NIR Calibration in Practice"
S.C.C. Wiedemann, W.G. Hansen, M. Snieder, Analusis, 26 (1998) M38-M43.

"Tolerance of Near Infrared Calibrations to Temperature Variations; A Practical Evaluation",
W.G. Hansen, S.C.C. Wiedemann, M. Snieder and V.A.L. Wortel, J. Near Infrared Spec., 8 (2000) 125-132.

"Optimising Multivariate Calibration by Robustness Criteria",
V.A.L. Wortel, W.G. Hansen and S.C.C. Wiedemann, J. Near Infrared Spec., 9 (2001) 141-151.

Electronic nose
"Evaluation and Optimisation of an Electronic Nose",
W.G. Hansen and S.C.C. Wiedemann, in *Electronic Noses & Sensor Array Based Systems - Design & applications - Proceedings of the 5th International Symposium on Olfaction and the Electronic Nose* (eds. W.J. Hurst), Technomic Publishing Company, Lancaster (1999) pp 131-144.

"Optimisation of an Electronic Nose for Glycerine Discrimination using the Taguchi Principle",
W.G. Hansen, S.C.C. Wiedemann, H. van der Bol, V.A.L. Wortel, in *Electronic Noses and Olfaction 2000 - Proceedings of the 7th International Symposium on Olfaction and Electronic Noses*, (eds. J.W. Gardner, K.C. Persaud), Institute of Physics Publishing, Bristol (2000) pp 133-140.

Elemental analysis
"Direct Analysis of Ca, P, and Fe in Oleochemicals by Inductively Coupled Plasma MS",
S.C.C. Wiedemann, H. Abbes, W.G. Hansen, J. Am. Oil Chem. Soc., 81 (2004) 437-440.

Process simulation
"Diabatic distillation process. Part I: numerical simulation and optimization",
A. Ramadane, S. Wiedemann, T. Cachot, R. Rivero, P. Le Goff, in *Récents Progrès en Génie des Procédés - Procédés de Séparation* (1991), Vol. 5, pp 257-262.

Oral Presentations

"Insights into Deactivation of Ferrierites during Oleic Acid Isomerisation"
S.C.C. Wiedemann, J.A. Stewart, F. Soulimani, T. van Bergen-Brenkman, S. Langelaar, B. Wels, P.C.A. Bruijnincx, B.M. Weckhuysen, NCCC XIV, Noordwijkerhout, The Netherlands, March 2013.

"Insights into Deactivation of Ferrierites during Oleic Acid Isomerisation"
S.C.C. Wiedemann, J.A. Stewart, F. Soulimani, T. van Bergen-Brenkman, S. Langelaar, B. Wels, P.C.A. Bruijnincx, B.M. Weckhuysen, IRDG, Teijin Aramid B.V, Arnhem, The Netherlands, April 2013.

"Skeletal Isomerisation of Oleic Acid over Ferrierite: Pore Mouth Catalysis and Related Deactivation Mechanisms"
S.C.C. Wiedemann, J.A. Stewart, F. Soulimani, T. van Bergen-Brenkman, S. Langelaar, B. Wels, P. de Peinder, P.C.A. Bruijnincx, B.M. Weckhuysen, 7th Workshop on Fats and Oils as Renewable Feedstock for the Chemical Industry, Karlsruhe, Germany, March 2014.

"Skeletal Isomerisation of Oleic Acid over Ferrierite: Influence of Acidity on Performance"
S.C.C. Wiedemann, A. Muñoz-Murillo, R. Oord, T. van Bergen-Brenkman, B. Wels, P.C.A. Bruijnincx, B.M. Weckhuysen, 8th Workshop on Fats and Oils as Renewable Feedstock for the Chemical Industry, Karlsruhe, Germany, March 2015.

Poster presentations

"Large Ferrierite Crystals as Models for Catalyst Deactivation during Skeletal Isomerization of Oleic Acid"
S.C.C. Wiedemann, Z. Ristanović, J. Weitkamp, B. Wels, P.C. A. Bruijnincx and B.M. Weckhuysen, NCCC XV, Noordwijkerhout, The Netherlands, March 2014.

“Skeletal Isomerisation of Oleic Acid over Ferrierite: Pore Mouth Catalysis and Related Deactivation Mechanisms”
S.C.C. Wiedemann, J.A. Stewart, F. Soulimani, T. van Bergen-Brenkman, S. Langelaar, B. Wels, P. de Peinder, P.C.A. Bruijnincx, B.M. Weckhuysen, FEZA 2014 Poster workshop, Sustainable solutions: biomass-related catalysis, Leipzig, Germany, September 2014.

Acknowledgements

When I first started this PhD, I was looking for new horizons and challenges, having over the course of my career realised that industrial science and chemistry were (and are) my real passion. Almost five years later, I can confirm that the hoped-for challenges were forthcoming! But the experience has been much richer than I could have imagined, due to the inspiration and support received from colleagues and friends during these years. Although many people contributed to this PhD at various points in time, I would like to say a special “merci” to those who have been most closely associated with this project:

Dear Bert, thank you for having the courage and vision to take on this project, and with such wholehearted commitment. The collective knowledge and expertise of your group in the fields of catalysis and spectroscopy was a constant source of comfort and inspiration. You were able to stand back from the nitty-gritty details, and keep the research pointing in the right direction. Your scientific network was a fantastic asset, especially in obtaining assistance in some highly specialised areas that would be difficult and time-consuming to source from scratch. I was always conscious of a gentle pressure keeping the momentum going and, despite your hectic and continent-hopping schedule, you made the time available when needed.

Dear Pieter, you played a key role in helping me with the many technical challenges in the project, and in teaching me to think in a more structured way. I have worked for 20 years in oleochemistry, and thought that I had ‘got the hang of it’, but you regularly surprised me with the depth and scope of your insights. Your questions and comments during the biomass meetings gave me a broader view on biomass catalysis, which was refreshing and inspiring. Thank you for your time, dedication and patience when working on the publications; through your corrections, edits and comments, I learned so much about how to write clearly and concisely, which is a skill that will serve me well for the rest of my career - for that I am extremely grateful.

Going back to the very conception of the project, I also would like to thank Wei Hansen (my former manager during the Unichema/Uniqema days) for originally suggesting the idea of a PhD to me. I am also grateful to Peter de Peinder and Tom Visser; Peter for organising the IRDG and stimulating the contact between academia and industry, and Tom for initiating the first discussions with Bert.

A very special thanks to David Parker and Eric Philipse (both formerly of Croda) for supporting the PhD proposal within Croda. Since David's retirement, Mick Green has taken over as Vice President Research & Technology - Performance Technologies and Industrial Chemicals, and continues to sign the cheques! Thank you all for your trust and support, I am proud to be part of a company with such vision and generosity.

Dear Bas, you joined Croda after the start of my PhD project, but have consistently supported it, and provided insightful feedback on the papers. You always made time for my many questions, despite your busy schedule and frequent business trips hopping between the Netherlands and UK!

Dear Robert Jan, thank you for demonstrating your trust in me, and for helping me to combine it with my "day job". You showed genuine interest in my progress, and helped me with the difficult task of producing the Dutch language summary!

Utrecht University was my "second office" for almost 5 years, and I have many people to thank there for the support they provided, both in the project and in making my association with the University such a richly rewarding experience.

I would like to start with the "unsung heroes" of the lab, the technical support team:
Fouad, as well as the fantastic support you gave me on all issues related to IR, I will especially remember your master classes in pellet-making!
Marjan, for the beautiful images that you made of both the large and small crystals, which were real works of art and displayed your wonderful photographer's eye;
Ad and Ad, Oscar, for all your work to get the oven up and running for the large crystal studies;
Pascal, for your patient training and help with the multi-reactor, it was a pleasure to work with and learn from you!

Dymph and Monique, for your assistance with the administration around my PhD, and for making my integration into the University department as smooth as possible.

Although my family and working life did not often allow me to take part in the social events, I would like to thank all Utrecht colleagues for warmly accepting me and making me feel part of the team: Annelie, Ara, Arjen, Carlo, Christoph, Clare, Daniël, Davide, Dilek, Davide, Dimitrie, Evelien, Fang, Fernando, Fiona, Frank, Gareth, Helena, Hirsa, Homer, Ilona, Ines, Inge, Javi, Jinbao, Joe, Joris, Jovana, JX, Katinka, Lisette, Marianna, Marjolein, Marleen, Matt, Mozaffar, Peter H., Qinyun, Rafael, Ramon, Robin, Rogier, Roy, Sankar, Shanmugam, Selvedin, Suzanne, Tamara, Thomas, Tomas, Upakul, Wenhao, Zafer and Zoran.

A special mention goes to my workplace neighbours who always welcomed me despite my irregular and sometimes unscheduled appearances! Peter M., Jesper, Hendrik, Marte and Jessi; my co-participants at the CatPrep2014: Nazila, Peter B., Petra and Wang; and of course the “French connection”: Jamal and Sandra.

Several Utrecht colleagues collaborated with me on specific parts of the thesis, and contributed to the related publications. All brought valuable insights to the thesis, and enriched both my personal understanding of the science as well as the quality and depth of the work: Joe and Ines (Chapter 2), Zoran and Gareth (Chapter 3) and Ara and Ramon (Chapter 4). Thank you all for giving your valuable time, knowledge and expertise so generously!

The research also benefited from several external collaborations and contacts. Chapter 3 would not have been possible without the large ferrierite crystals; I would therefore like to thank Prof. dr. Jörg Kärger (Leipzig), Dr. Reddy Marthala (Erlangen) and Prof. dr. Jens Weitkamp (Stuttgart) for this valuable contribution to the project.

Croda gave generous financial support, but also provided the use of experimental facilities at Gouda. I was privileged to work with so many knowledgeable colleagues there, who assisted with the experimental work and shared their knowledge, insights and expertise with me during the PhD. Special thanks go to the following:

Tanja, for sharing the wealth of practical knowledge and experience that you have, both in general laboratory practice and in the specific OA alkyl isomerisation reaction.
Tanja, Peter G. and Negar, for the many syntheses that you have carried out on my behalf - only when I got access to the “multi-reactor” could I reach the level of practical efficiency that you achieved in the first two years!
Marvin, Stephan and Wim, for your assistance with various analytical aspects of the project, as well as for the interest you showed in the work.
Hans R. and Hans V. for helpful comments, suggestions and insights on the introductory text.
Lia and Paulina my office mates, for your kindness, support and understanding.

Dear Henkjan, we have worked together for many years, running analytical projects together for businesses around the world, and it was always a positive, memorable and enjoyable experience. It was therefore a great comfort to me to know that you would be around when I started the PhD. You have been my “right hand man” at Gouda, and helped me many times when I was in Utrecht and unexpected issues arose at work. I could always count on your support, and this has been a hugely important factor in juggling the priorities and deadlines between study and work.

Besides Utrecht and Gouda, there was a bit of time for family life in Rotterdam! We tried to keep all the many activities of the children (and husband!) going during these years, and this was only possible due to the kindness and support of our friends and family. A very big “merci” to:

Wessel for his encouragement, and for providing the inspiration of someone who already successfully combines a career in TNO and academia;
Lynn for helping many times with the football runs;
Waika for the encouraging chats we had at the school gates each Wednesday;
Juliette for her beautiful flute CDs, that accompanied and inspired me on my late-night writing sessions!

Edward and Francois, for putting up with your part-time mum; sorry for all the times I was late home after school, for the half-weekends and for bringing my laptop on family holidays; I will do my best to make this up, starting with a ‘proper’ summer holiday in 2016 (your choice of location)!

Papa et Maman, “merci” for taking the boys during the school holidays, and crossing France to look after them at our place when Peter and I were away for work reasons. Maman, the wonderful school lunches and dinners that you always made for the boys are now the reference (!). Papa, we were super-impressed at your efforts in learning some Dutch, in order to help the boys with their football training!

Peter, a few lines are not enough to express my gratitude for the support and encouragement you have provided over these last years. You took over the childcare and home responsibilities when needed, and your ‘English humour’ helped me to get through some challenging moments, and allowed me to keep a sense of perspective. A very special thank you for reviving the ‘branched fatty acids’ topic at Croda, following your attendance at the 2008 AOCS meeting in Cincinnati - the discussions that followed formed the embryo of this PhD. I could not have hoped for a better topic, and with it we have finally broken the ‘jinx’ of unfinished PhD’s on my side of the family! Are you ready for the next episode in our lives…?

Sophie

Curriculum Vitae

Sophie Wiedemann was born in Paris, France on the 4th of October 1966. In 1992, she graduated in Chemistry and Chemical Engineering from CPE (École Supérieure de Chimie Physique Électronique de Lyon). This was followed by a period of study at the University of Houston under Prof. Wayne Wentworth, where she worked on the development of a universal detector for gas chromatography. This research led to her first publication and the award of a Master of Science degree in Physical Chemistry.

On her return to France in 1994, Sophie briefly joined the thermochemistry department within INSA (Institut National de Science Appliquées) in Lyon as a Research Assistant, conducting a study of sorbitol polymorphism by differential scanning calorimetry (DSC) and X-ray diffraction under Prof. Pierre Claudy for the company Roquette Frère.

Then in 1995, she came to Gouda in the Netherlands and took a position as Scientist within Unichema, a major European producer of oleochemicals and a company within the Unilever group. In 1997, ICI purchased Unichema from Unilever, and combined it with their lubricants and surfactants division under a new name, Uniqema. In this period, Sophie developed a wide range of new analytical tools and techniques for the company, in the fields of olfactometry ("electronic nose"), thermal analysis (DSC, thermogravimetry), spectroscopy (near infrared, NIR) and elemental analysis (ICP-MS). She published and presented her work on a regular basis, and developed a specialisation in NIR where she presented at international conferences. Her work in the field of NIR contributed to the development of the technique worldwide within the company. In 2006, Croda, a UK-based speciality chemicals manufacturer, purchased Uniqema: Sophie continued her role there as Analytical Scientist, taking on responsibility for the characterisation of Gouda products in support of their registration for REACH.

In January 2011, with the generous financial support of Croda, she started her PhD under the supervision of Prof. Bert Weckhuysen and Dr. Pieter Bruijnincx in the Inorganic Chemistry and Catalysis group of the Debye Institute at Utrecht University. The fruits of this research have been published in scientific journals and as a book chapter, and presented at several international conferences. The chapters of this PhD Thesis are based on the aforementioned publications and presentations.